

**Modeling Cold-Formed Steel Screw Connections with an Insulation
Layer Using Finite Element Analysis**

by

Zane Frederick Witt

A Report Submitted to the Faculty of the
Milwaukee School of Engineering
In Partial Fulfillment of the
Requirements for the Degree of
Master of Science in Structural Engineering

Milwaukee, Wisconsin

June 2015

Abstract

This study focused on creating a model using finite element analysis to accurately predict the maximum force, maximum displacement, and failure mode of a cold-formed steel screw connection with an insulation layer. These connections use cold-formed steel studs, a layer of rigid insulation and a metal sheathing panel with a screw connecting all three layers. The analysis includes geometric and material nonlinearities. To determine the accuracy of the model, the predicted maximum force, maximum displacement and failure mode were compared to previously completed tests of screw connection. The results show that the finite element model can predict the force and displacement for connections using thin studs and panels with some degree of accuracy. For connections using thicker studs and metal sheathing panels, the model predicted failure at very low force and displacement when compared to the test results.

Acknowledgments

This project would not have been possible without contributions from many people. These people were willing to put forth the time and effort in order to help me complete this capstone project, and I sincerely appreciate all their support.

Anthony Leonardelli set the foundation for much of the work found in this project. Anthony was more than willing to help me understand previously completed work and provided insight to make this project more efficient. Pat Lynch at MBA Steel was extremely helpful when materials were needed for testing. Justin Tracey helped a great deal with the testing involved in this project. From material acquisition to the test method, Justin was more than willing to provide a helping hand. I'd also like to thank the members of my committee, Dr. Davis and Dr. Huttelmaier for their willingness to help.

This project would not have been possible without my advisor, Dr. Stahl. Stahl. Your patience through the tedious troubleshooting of the model and guidance throughout the development were vital to the completion of this project. I thank you for all the time you sacrificed over the course of this project.

Lastly, I'd like thank my family for their constant support throughout my academic career. Mom and Dad, Grandma and Grandpa, Uncle and Aunt Jody, this report is dedicated to you all.

Table of Contents

List of Figures	6
List of Tables	10
Nomenclature	11
Section 1 - Project Information	15
1.1 Background	15
1.2 Objectives	16
Section 2 - Literature Review	18
2.1 Forest Products Laboratory Research (2012)	18
2.2 American Iron and Steel Institute (2012).....	21
2.3 Gao (2011)	27
2.4 Leonardelli, Stahl, Moen (2014).....	29
Section 3 - Developing the Model	32
3.1 Connection Model.....	32
3.1.1 Nodes, Elements and Degrees of Freedom	32
3.1.2 Screw Element and Geometric Nonlinearity	34
3.1.3 Plate Element and Material Nonlinearity.....	37
3.2 Insulation Stiffness Testing.....	42
3.2.1 Initial Panel Testing	42
3.2.2 Washer Testing	49

3.2.3 CFS Stud Testing	53
3.3 Mathcad Implementation	59
3.3.1 Geometric Nonlinearity Verification	69
3.3.2 Load-Controlled Model	70
3.3.3 Displacement-Controlled Model.....	72
Section 4 - Using the Model	73
4.1 Calibrating the Model	73
4.1.1 Adjustments to <i>Roark's</i> Moment Capacity.....	75
4.2 Simulation of P- Δ Responses.....	78
4.3 Strength Prediction of Connection.....	82
Section 5 - Recommendations	85
References.....	87
Appendix A: Mathcad Worksheet	91

List of Figures

Figure 1: Screw Connection without Insulation Layer (right) Compared to Screw Connection with Insulation Layer (left).....	15
Figure 2: Table 7 in FPL 469.....	19
Figure 3: FPL 469 Ultimate Load versus Insulation Thickness.	20
Figure 4: Variables Used in AISI Failure Mode Equations.....	22
Figure 5: AISI S905 Failure Modes.....	25
Figure 6: The “Washer Effect” Seen in the Rigid Board Insulation.....	28
Figure 7: Rigid Polyisocyanurate Board Insulation Stress versus Strain Plot.....	28
Figure 8: Leonardelli Test Specimen.....	30
Figure 9: Leonardelli Load versus Displacement Plot.....	31
Figure 10: Leonardelli Test Setup.....	33
Figure 11: Screw Connection Model (Elements Numbers Circled, Degrees of Freedom not Circled).	34
Figure 12: Nonzero Displacement Screw Connection Model (Elements Numbers Circled, Degrees of Freedom not Circled).....	34
Figure 13: Corotational Element Formulation Definitions.....	36
Figure 14: Bending Deformation Zone of the Metal Sheathing Panel.	38
Figure 15: Case 20 in Table 11.2 of <i>Roark’s Formulas for Stress and Strain</i>	39
Figure 16: Elastic-Perfectly Plastic Relationship for Rotational Plates.....	40
Figure 17: Rotational Plate Stiffness Equation Plot.	41
Figure 18: Rotational Plate Moment Equation Plot.....	41
Figure 19: Insulation Test Setup.....	43

Figure 20: Insulation Test Frame.....	44
Figure 21: Frame Clamped onto Load Cell Channel.....	44
Figure 22: Load versus Displacement Plot for 25-Gauge Panel.....	45
Figure 23: Load versus Displacement Plot for 16-Gauge Panel.....	46
Figure 24: Modified Load versus Displacement Plot and Trendlines for the 25-Gauge Panel.....	47
Figure 25: Modified Load versus Displacement Plot and Trendlines for the 16-Gauge Panel.....	47
Figure 26: Modified Load versus Displacement Plot with Linear Stiffness for 25-Gauge Panel.....	48
Figure 27: Modified Load versus Displacement Plot with Linear Stiffness for 16-Gauge Panel.....	49
Figure 28: Washer Testing Setup.....	50
Figure 29: 1-inch Washer Load versus Displacement Plot.....	51
Figure 30: 1.5-inch Washer Load versus Displacement Plot.....	52
Figure 31: 2-inch Washer Load versus Displacement Plot.....	52
Figure 32: Crushed Insulation Member after Completed Washer Test.	53
Figure 33: Test Setup for CFS Insulation Testing.	54
Figure 34: 25-Gauge Panel, 1-inch Insulation Stud Load versus Displacement Plot (1.5-inch Flange).	55
Figure 35: 25-Gauge Panel, 1-inch Insulation Load versus Displacement Plot with Exponential Curve (1.5-inch Flange).....	56

Figure 36: 16-Gauge Panel, 1-inch Insulation Load versus Displacement Plot with Exponential Curve (1.5-inch Flange).....	56
Figure 37: 25-Gauge Panel, 2-inch Insulation Load versus Displacement Plot with Exponential Curve (1.5-inch Flange).....	57
Figure 38: 16-Gauge Panel, 2-inch Insulation Load versus Displacement Plot with Exponential Curve (1.5-inch Flange).....	57
Figure 39: 25-Gauge Panel, 2-inch Insulation Load versus Displacement Plot with Exponential Curve (2.5-inch Flange).....	58
Figure 40: Cantilever Beam Location Vector Example.....	60
Figure 41: Frame Element Stiffness Matrix Programmed Function.....	61
Figure 42: "Zero_Matrix" Programmed Equation.	61
Figure 43: Global Matrix Assembly Programmed Function.	62
Figure 44: Element Displacement Vector Function.....	62
Figure 45: Element Forces Function for the CFS Stud.....	63
Figure 46: Element Forces Function for the Panel.	64
Figure 47: Element Forces Function for the Insulation Strut.	65
Figure 48: Element Forces Function for the Screw.	66
Figure 49: Stiffness Function for the CFS Stud.....	67
Figure 50: Stiffness Function for the Panel.	68
Figure 51: Stiffness Function for the Insulation Strut.	68
Figure 52: Stiffness Function for the Screw.	69
Figure 53: Visual Analysis Verification Model for the Base Iteration (Top) and the First Iteration (Bottom).	70

Figure 54: Load-Controlled Analysis Load versus Displacement Graph.	71
Figure 55: Load versus Displacement Graph with Area of Non-Convergence Circled. ..	72
Figure 56: Moment-Rotation Relationship with RPS_{factor}	76
Figure 57: Load versus Displacement Plot Showing EPF and RPS_{factor} Effects.....	78
Figure 58: Load versus Displacement Plot for Connection Type 13.....	79
Figure 59: Load versus Displacement Plot for Connection Type 23.....	80
Figure 60: Load versus Displacement Plot for Connection Type 26.....	81
Figure 61: Load versus Displacement Plot for Connection Type 30.....	81
Figure 62: Load versus Displacement Plot for Connection Type 52.....	82

List of Tables

Table 1: Modified Insulation Stiffness.	48
Table 2: Connection Types and Material Properties.....	74
Table 3: Grabber Construction Products Screw Properties.	75
Table 4: EPF by Connection Type.....	77
Table 5: Failure Modes for Each Connection Type.....	84

Nomenclature

Symbols

a	Plate elements; Radius of plate bending zone
A	Element area used in frame element stiffness matrix
b	Plate elements; Radius of trunnion
d	Nominal screw diameter
d_h	Screw head diameter or hex washer head integral washer diameter
d_w	Steel washer diameter
d'_w	Effective pull-over resistance diameter
E	Modulus of elasticity (29,500 ksi for CFS)
F	Global force vector in finite element analysis
F	Yield model; force
f_e	Geometric nonlinearity; element forces in local coordinates
f_e	Geometric nonlinearity; element forces in global coordinates
F_{u1}	Tensile strength of member in contact with screw head or washer
F_{u2}	Tensile strength of member not in contact with screw head or washer
I	Moment of inertia used in frame element stiffness matrix
k	Element stiffness matrix used in finite element analysis
K	Global stiffness matrix used in finite element analysis
k_o	Plate elements; rotational plate initial elastic stiffness
L	Element length used in frame element stiffness matrix
M or $M(\theta)$	Plate elements; moment at given angle of rotation
M_y	Plate elements; yield moment of plates
M_p	Plate elements; plastic moment of plates

P or P_c	Force in insulation strut
P_{ns}	Nominal shear strength [resistance] of sheet per screw
P_{not}	Nominal pull-out strength [resistance] of sheet per screw
P_{nov}	Nominal pull-over strength [resistance] of sheet per screw
P_{ss}	Nominal shear strength [resistance] of screw as reported by manufacturer or determined by independent laboratory testing
P_{ts}	Nominal tension strength [resistance] of screw as reported by manufacturer or determined by independent laboratory testing
Q	Required shear strength
T	Element transformation matrix used in finite element analysis
T	Required tension strength in AISI equation
t	Thickness of stud or panel in plate stiffness calculations
t_1	Thickness of member in contact with screw head or washer
t_2	Thickness of member not in contact with screw head or washer
t_c	Lesser of depth of penetration and thickness t_2
t_{insul}	Thickness of insulation layer
t_{panel}	Thickness of sheathing panel
U	Global displacement vector in finite element analysis
u_e	Geometric nonlinearity; element displacement in new local coordinates
U_{new}	Geometric nonlinearity; new displacement vector found at each iteration
W	Work
α	Geometric nonlinearity; the rigid body rotation at each iteration
α	Plate elements; output value from <i>Roark's</i> table

β	Geometric nonlinearity; final angle of element in iteration (current angle) with respect to horizontal axis
β	Plate elements; output value from <i>Roark's</i> table
β_0	Geometric nonlinearity; initial angle of element in iteration (previous angle) with respect to horizontal axis
$\Delta\theta$ or $\bar{\theta}$	Geometric nonlinearity; the rotation of the element at a node in local coordinates
θ	Geometric nonlinearity; the rotation of the element in global coordinate with respect to original position
θ	Plate elements; angle of rotation
ΔP	Geometric nonlinearity; unbalanced force vector
ΔU	Geometric nonlinearity; displacement increment vector
Δx	Geometric nonlinearity; element node disp. in horizontal direction (local)
Δy	Geometric nonlinearity; element node disp. in vertical direction (local)
Σf_e	Geometric nonlinearity; total of internal forces, ignores support loads (reactions)
σ_y	Yield stress of stud or panel
Φ	ASD safety factor
Ω	LRFD Safety Factor

Abbreviations

AISI	American Iron and Steel Institute
ASD	Allowable Stress Design

CFS	Cold-Formed Steel
DOF	Degree(s) of Freedom
EPF	Exponential Power Factor
FEA	Finite Element Analysis
FPL	Forest Products Laboratory
LRFD	Load and Resistance Factor Design
LVDT	Linear Variable Displacement Transducer
MSST	Master of Science in Structural Engineering
RPS_{factor}	Rotational Plate Stiffness Factor
XPS	Extruded Polystyrene

Section 1 - Project Information

1.1 Background

The increasing concern for the environment has encouraged building designers and constructors to develop more efficient buildings. This includes designing the building envelope to be more efficient, which has added extra amounts of insulation on the perimeter of the building. In cold-formed steel (CFS) construction, this insulation is placed between the CFS studs and the sheathing on the exterior of the building, as shown in Figure 1.

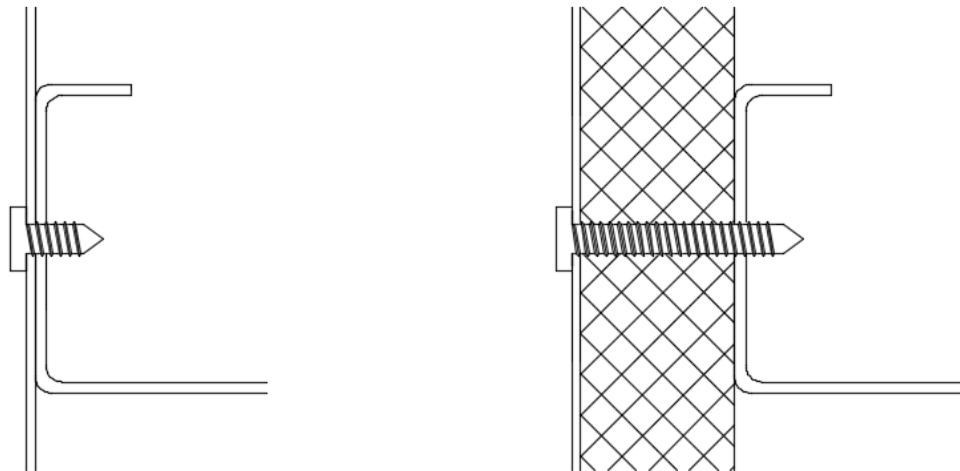


Figure 1: Screw Connection without Insulation Layer (right) Compared to Screw Connection with Insulation Layer (left).

The American Iron and Steel Institute (AISI) *North American Specification for the Design of Cold-Formed Steel Structural Members* provisions for screw connections does not address connections that have a layer of insulation between the connected members [1]. Because of this, connections with a layer of insulation cannot be properly

designed. The gap caused by the rigid insulation layer causes strength and stiffness reduction in the connections [2].

1.2 Objectives

The purpose of this project was to predict the load versus displacement relationship of a screw connection between a CFS stud and sheathing with an insulation layer. In order to predict the non-linear stiffness of the CFS screw connection, it was modeled using a finite element analysis approach. Some members had non-linear stiffness representing yielding or crushing in the actual connection.

The primary goal of this study was to find a load versus displacement relationship for a shear force applied at the sheathing layer on the screw connection. Load versus displacement data collected by Leonardelli [3] were used to determine if the model created in this study is accurate. Connection specimens analyzed with the model matched those of Leonardelli. Screws used were #10, #12, #14; sheathing layers were CFS panels with thicknesses of 0.0180 inch and 0.0565 inch (25 gauge and 16 gauge ignoring zinc coating); CFS studs were 600S200-97, 600S200-68, and 600S200-43; insulation was extruded polystyrene insulation board (XPS) with thicknesses of 1 inch, 2 inch and 4 inch [3].

Failure modes were incorporated into the finite element model; when one of the failure modes was reached the simulation was stopped. The identified failure modes were: combined shear and pull-out, combined shear and pull-over, combined shear and tension in the screw [1], and tensile stress in the screw. The failure mode discovered for

each specimen was also compared to the failure mode indicated in the testing by Leonardelli.

Section 2 - Literature Review

2.1 Forest Products Laboratory Research (2012)

Research performed at Forest Products Laboratory (FPL) [4, 5] has produced an accurate method for determining the strength of dowel connections in wood. This method includes connections with a layer of insulation between members. The research also looked into wood studs with metal sheathing similar to what would be seen in the cold-formed screw connection. The report also addressed load versus displacement relationships in the dowel connection. However, this relationship was based on test data, not the yield model.

This model assumes that the joint does not fail due to insufficient spacing or end distances at loads below the fastener yield. The model ignores friction between the layers because it is difficult to find the friction force in the connection; in some cases, there is no friction force.

The method used to derive the yield model is virtual displacement, and the system is assumed to be plastic. Using virtual displacement, strain energy is found for the nail bending and wood embedment. The total strain energy is equal to external work done. Work (W) is equal to force (F) times distance, so using the virtual displacement method, the external work is equal to the force times one unit ($W=F*1$). The work is then minimized, in order to get the ultimate force.

The wood yield model also addresses an insulation layer, as shown in Figure 2. In the wood connections, the yield load is greatly decreased by having an intermediate layer of insulation.

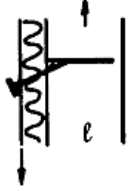
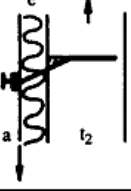
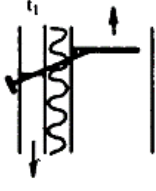
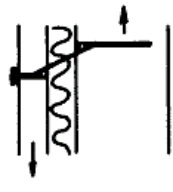
Mode of failure number	Failure geometry	Number of nail yield points	Yield load F_u (lb)	Failure mode determinants
3.3A		1	$F_u = f_e \sqrt{e^2 + 2\gamma} - e$	Theoretical length of nail: $\ell = \sqrt{e^2 + 2\gamma} + 2\sqrt{\gamma}$
3.4A		2	$F_u = f_e \left[\sqrt{e^2 + 4\gamma} - e \right]$	Theoretical length of nail: $\ell = \sqrt{e^2 + 4\gamma} + 2\sqrt{\gamma} + a$
3.3B		1	$F_u = \frac{f_e}{3} \left[2\sqrt{t_1^2 + et_1 + e^2 + 3\gamma} - (t_1 + 2e) \right]$	Thickness conditions: $\frac{\sqrt{e^2 + 4\gamma} - e}{2} < t_1 < \frac{\sqrt{e^2 + 8\gamma} - e + 4\sqrt{\gamma}}{2}$ Theoretical length of nail: $\ell = \frac{2t_1 + e}{3} + \frac{2}{3}\sqrt{t_1^2 + et_1 + e^2 + 3\gamma} + 2\sqrt{\gamma}$
3.4B		2	$F_u = \frac{f_e}{2} \left[\sqrt{e^2 + 8\gamma} - e \right]$	Thickness conditions: $t_1 \geq \frac{\sqrt{e^2 + 8\gamma} - e + 4\sqrt{\gamma}}{2}$ Theoretical length of nail: $\ell = \sqrt{e^2 + 8\gamma} + 4\sqrt{\gamma}$

Figure 2: Table 7 in FPL 469 [4].

The nomenclature in Figure 2 is as follows:

F_u = Yield load (lbs),

f_e = Wood embedment strength (lbs/in),

e = Insulation layer thickness (in),

a = Thickness of cleat under nail head (in),

M_y = Yield moment of nail (lbs-in),

$\gamma = M_y/f_e$.

The FPL report featured a plot showing the ultimate load of the connection versus the insulation thickness, shown in Figure 3. In the yield model, the ultimate load of the connection follows the curve of a negative exponential with respect to the insulation thickness. It is reasonable for the CFS stud connection to follow the behavior of the yield model; the ultimate strength will decrease less as the insulation stiffness increases.

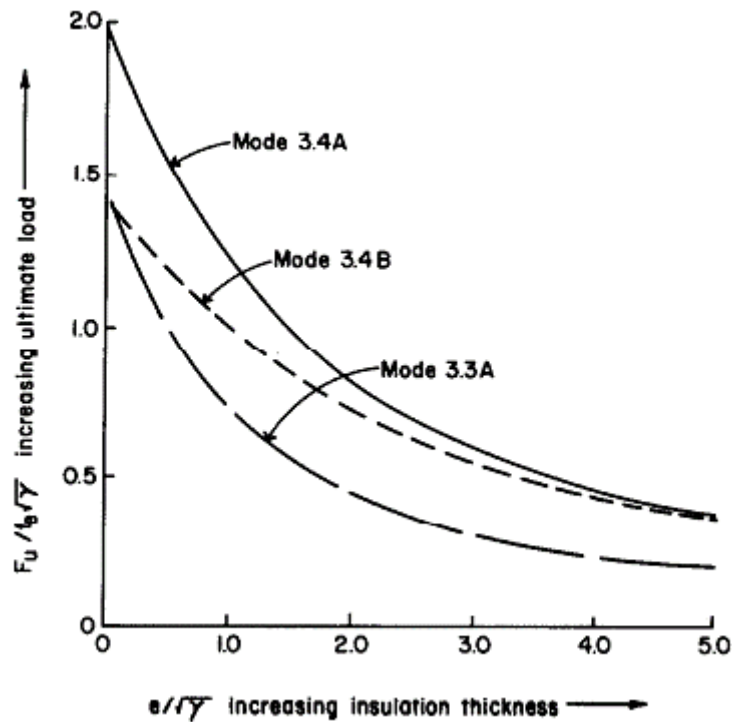


Figure 3: FPL 469 Ultimate Load versus Insulation Thickness [4].

The wood yield model was originally thought to have a more direct application to the cold-formed steel model. After researching the yield model, it was determined that the information may be helpful, but there is no direct application to CFS framing with an insulation layer. In the yield model, the stud and sheathing are controlled by bearing,

where in the CFS connection sheathing and stud are expected to act as rotational elements. The failure modes in the yield model focus on dowel failure, which are also studied in the CFS connection, but the other failure modes (combined shear and pull-out/pull-over) are not similar to those found in the yield model. The wood connection also assumes plastic behavior but the finite element model for the CFS connection includes elastic and plastic behavior.

Key assumptions that helped with the development of the CFS finite element model are the idea that friction between members is ignored and that the connection will not fail due to insufficient spacing. Friction will be ignored because it is difficult to determine what stiffness is added due to any friction between members. Spacing requirements are ignored in this study because the finite element model looks at a single connection, not a group of multiple screws connecting the sheathing to the CFS stud.

2.2 American Iron and Steel Institute (2012)

The current provision for screw connections in CFS does not address connection with a rigid insulation layer. The provisions for screw connection are found in the AISI *North American Specification*, Section E4. Although there are no provisions for connections with an insulation layer, the failure modes described for screw connections can be applied in the finite element model. Three specific failure modes are applied in the finite element model: Combined Shear and Pull-Over (E4.5.1), Combined Shear and Pull-Out (E4.5.2), and Combined Shear and Tension in Screws (E4.5.3) [1]. Each equation has a strength reduction factor that depends on whether the design is Allowable Stress Design [ASD] (Ω) or Load and Resistance Factor Design [LRFD] (Φ). This study looks at the

actual failure of the CFS screw connection so the safety factor will be ignored when implementing these failure modes in the model. Figure 4 shows some of the variables used in the AISI provisions for screw connections. Variables with the subscript “1” are properties of the sheathing panel and variables with the subscript “2” are properties of the CFS stud.

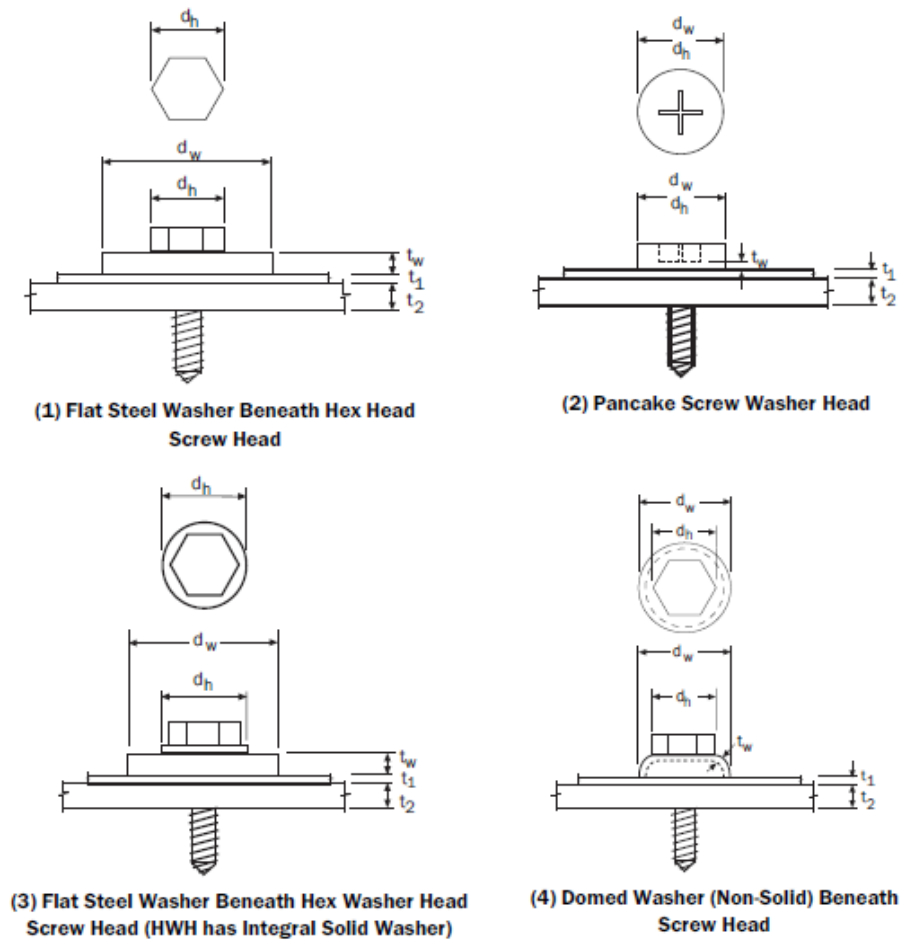


Figure 4: Variables Used in AISI Failure Mode Equations [1].

Combined shear and pull-over occurs when the sheathing panel (t_1) is thin relative to the stud wall thickness (t_2). If the screw head or washer diameter (d_w) used in the

connection is large, pull-over will be prevented. Testing completed at West Virginia University shows that if the washer diameter exceeds 0.75 inch pull-over is prevented [1]. Equations (1), (2) and (3) are the AISI equations for combined shear and pull-over [1]. In the *North American Specification*, Equations (1), (2) and (3) are numbered (Eq. E4.5.1.2-1), (Eq. E4.5.1.2-2) and (Eq. E4.5.1.2-3), respectively. Because pull-over focuses on the sheathing panel, the equations for the nominal shear and tension strength utilize the ultimate strength of the panel (F_{u1}). Equations (1), (2) and (3) are:

$$Q / P_{ns} + 0.71 T / P_{nov} \leq 1.10, \quad (1)$$

$$P_{ns} = 2.7 t_1 d F_{u1}, \quad (2)$$

$$P_{nov} = 1.5 t_1 d_w F_{u1} . \quad (3)$$

The nomenclature for Equations (1), (2) and (3) is:

d = Nominal screw diameter,

d_w = Steel washer diameter,

F_{u1} = Tensile strength of member in contact with screw head or washer,

P_{nov} = Nominal pull-over strength [resistance] of sheet per screw,

P_{ns} = Nominal shear strength [resistance] of sheet per screw,

Q = Shear force on the screw,

T = Tension force on the screw,

t_1 = Thickness of member in contact with screw head or washer.

The AISI provisions for combined shear and pull-out are based on tearing and tilting failure modes found as separate equations earlier in the screw connection

provisions and illustrated in Figure 5. This failure mode occurs when the CFS stud wall thickness (t_2) is approximately the same or less than the sheathing panel thickness (t_1) [1]. Unlike pull-over, pull-out focuses on the CFS stud so the ultimate strength of the stud is used to find the nominal shear and tension strength. Equations (4), (5) and (6) are the *North American Specification* equations for combined shear and pull-out. Equations (4), (5) and (6) are numbered by AISI as (Eq. E4.5.2.1-1), (Eq. E4.5.2.1-2) and (Eq. E4.5.2.1-3), respectively:

$$Q / P_{ns} + T / P_{not} \leq 1.15, \quad (4)$$

$$P_{ns} = 4.2 (t_2^3 d)^{1/2} F_{u2}, \quad (5)$$

$$P_{not} = 0.85 t_c d F_{u2}. \quad (6)$$

The nomenclature for Equations (4), (5) and (6) is as follows:

d = Nominal screw diameter,

F_{u2} = Tensile strength of member not in contact with screw head or washer,

P_{not} = Nominal pull-out strength [resistance] of sheet per screw,

P_{ns} = Nominal shear strength [resistance] of sheet per screw,

Q = Shear force on the screw,

T = Tension force on the screw,

t_2 = Thickness of member not in contact with screw head or washer,

t_c = Lesser of depth of penetration and thickness t_2 .

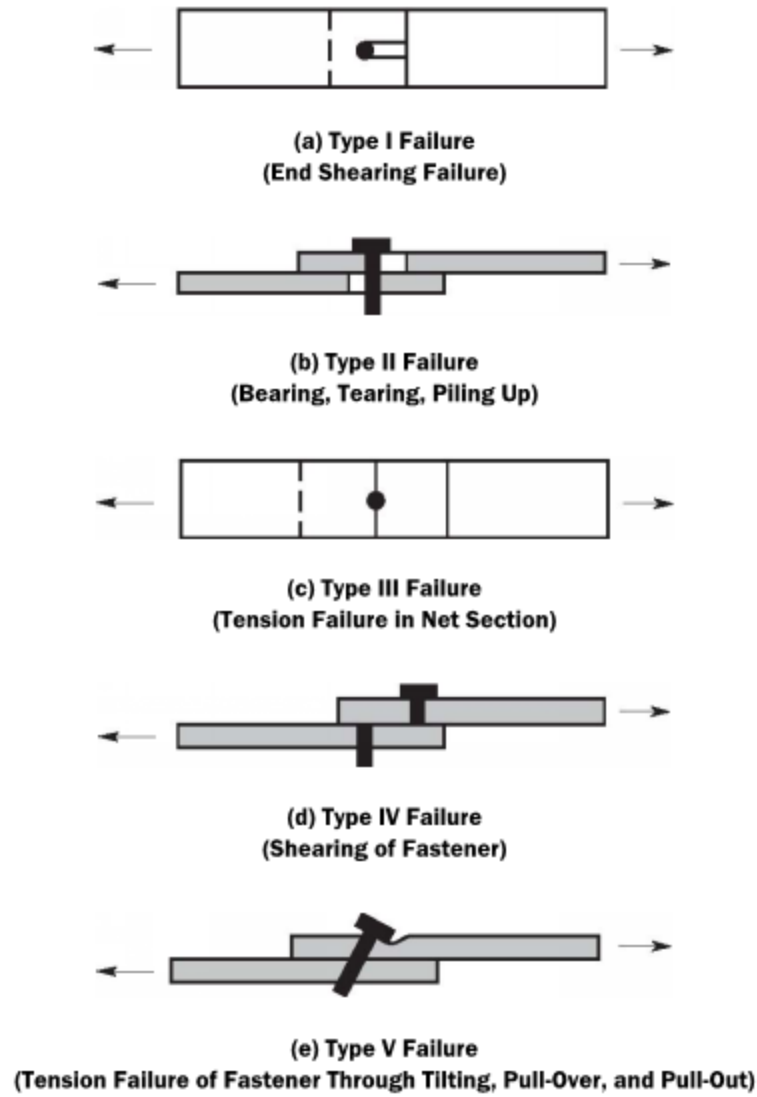


Figure 5: AISI S905 Failure Modes [6].

Combined shear and tension of the screw itself has a separate equation. The equation is simply a combination of the AISI nominal screw shear force and nominal screw tension force. The ultimate forces for the screws are published by manufacturer or found in independent testing [1]. Equation (7) is the AISI equation (Eq. E4.5.3.1-1):

$$Q / P_{ss} + T / P_{ts} \leq 1.3 . \quad (7)$$

The nomenclature for Equation (7) is as follows:

P_{ss} = Nominal shear strength [resistance] of screw as reported by manufacturer or determined by independent laboratory testing,

P_{ts} = Nominal tension strength [resistance] of screw as reported by manufacturer or determined by independent laboratory testing,

Q = Shear force on the screw,

T = Tension force on the screw.

The provisions provided by the AISI for the failure modes above have limits on connection properties such as panel thicknesses, ultimate strengths, and screw size. These limits are based on the test programs that were used to develop the equations. For example, the tests performed for combined shear and pull-over had limited sheathing panel thicknesses so it can only be proven that the equations provided work for the limited range of thicknesses [1]. The limits on connection properties also show that certain failure modes will not occur if the connection geometry does not meet the limits. For example, pull-out will not occur if the CFS is too thick ($t_2 > 0.0724$ inches) or has a very high ultimate strength ($F_{u2} > 121$ ksi) [1]. For this study, it was assumed that these equations are not limited so they could be applied to each specimen type.

The equations provided by the AISI provisions are able to calculate failure for three of the four failure modes. The fourth failure mode, which is not in the AISI provisions, is combined bending and tension in the screw. This allows for a failure load to be found in the finite element model, at which point the analysis will stop. Predicted

failure modes will be compared to Leonardelli test data; depending on the results, the AISI provisions may have to be modified to more accurately predict failure.

2.3 Gao (2011)

Gao [7] performed testing to determine the flexural capacity of cold-formed steel members found in roof and wall construction, primarily Z-sections and C-sections. The focus of the testing was to find the capacity of the members when the sheathing was subjected to negative pressure due to wind. The tests performed also looked into the effect of rigid board insulation on the flexural capacity of the steel members.

When studying rotational restraint of members with a layer of rigid board insulation between a girt and metal panel, Gao found that the insulation creates a “washer effect” to increase pull-over capacity [6]. In the “washer effect”, the connection acts as if there is a large washer under the screw head. This spreads the fastener force and decreases deformation in the panel. The “washer effect” of the insulation can be seen in Figure 6.

The insulation used in the study by Gao was 50.8 mm (2.0 inch) thick Dow Thermax. Dow Thermax is a glass-fiber reinforced polyisocyanurate foam insulation laminated between 1 mil aluminum foil on both sides. Gao describe the insulation as being stiff until the cell wall of the rigid board insulation buckled, then the stiffness is lowered as the air voids in the insulation are compressed. Testing showed a stiffness of 6.70 MPa (972 psi), with a yield stress of 0.154 MPa (22.3 psi). In the plastic range, the stiffness decreased to 0.0689 MPa (9.99 psi). Figure 7 shows the observed tri-linear behavior of the insulation; initially having a stiff response, then less stiff response as voids are compressed, and then stiffer response after most of the voids have been compressed [7].

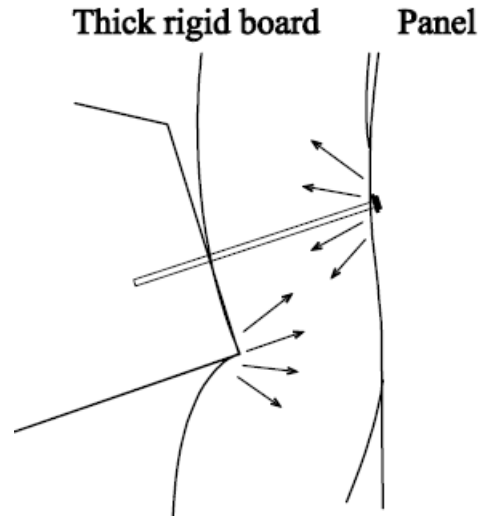


Figure 6: The “Washer Effect” Seen in the Rigid Board Insulation [7].

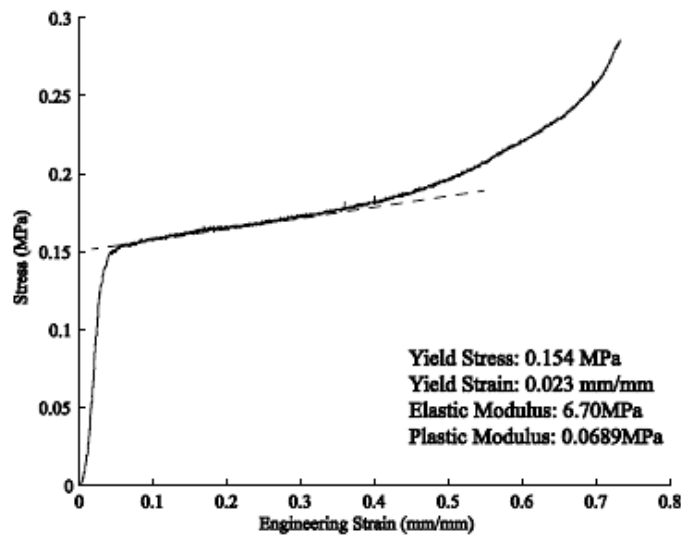


Figure 7: Rigid Polyisocyanurate Board Insulation Stress versus Strain Plot [7].

The rigid board insulation information provided by Gao is applicable to this study because it gives an expectation for the behavior of the insulation. The insulation used in the Gao testing does not match that used by Leonardelli [3] or by this study. This study

will have its own insulation stiffness testing, but the properties provided by Gao will be used for comparison.

2.4 Leonardelli, Stahl, Moen (2014)

Leonardelli, Stahl, and Moen [2, 3] conducted shear tests to explore the effect of rigid board insulation, steel sheet thickness, and screw diameter on CFS screw connection strength and behavior. This test program was used to understand the shear behavior of screw connections with an insulation gap between the CFS stud and CFS sheathing panel and to explore how the AISI provisions could be modified to accommodate a connection with rigid insulation. Test results from this study showed that connections with rigid board insulation of one inch or more had a considerable reduction in connection capacity.

The testing program was limited to screw connections with a layer of extruded polystyrene (XPS) insulation board between standard CFS structural studs and sheet metal panels with a single screw. Variables not addressed included insulation compressive strength, framing member flange width, orientation of framing member with respect to load direction, and screw head/washer diameter. A sketch of Leonardelli's test setup can be seen in Figure 8. Testing examined four variables: insulation thickness, base thickness (stud), panel thickness, and screw diameter.

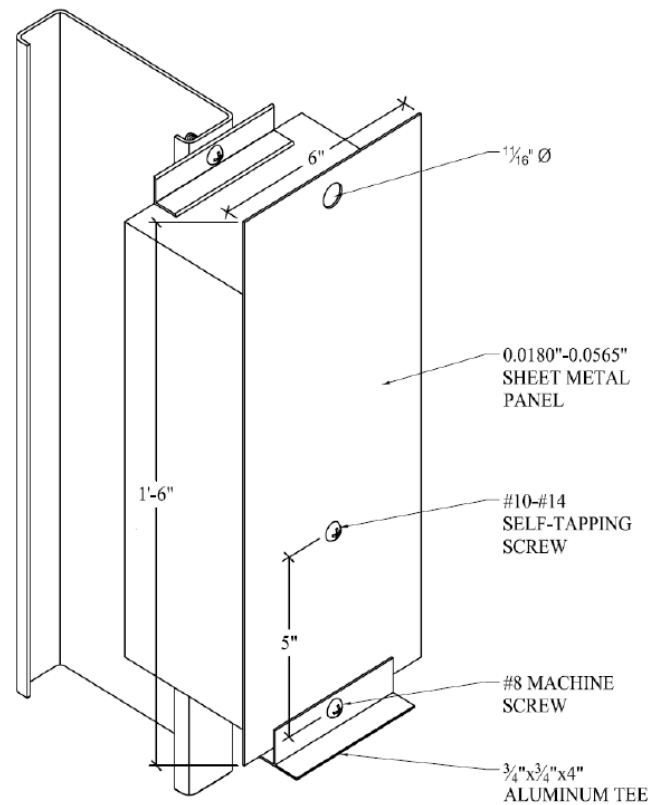


Figure 8: Leonardelli Test Specimen [2].

Multiple tests were conducted by Leonardelli to study the variables in the CFS screw connection. The final load versus displacement plot for all connection specimens can be seen in Figure 9. This displacement plot and the data used in the plot will be compared to the load and displacement output from the finite element model. Unlike the yield model [4, 5], the connections with an insulation layer demonstrate a consistent reduction of strength regardless of the insulation thickness.

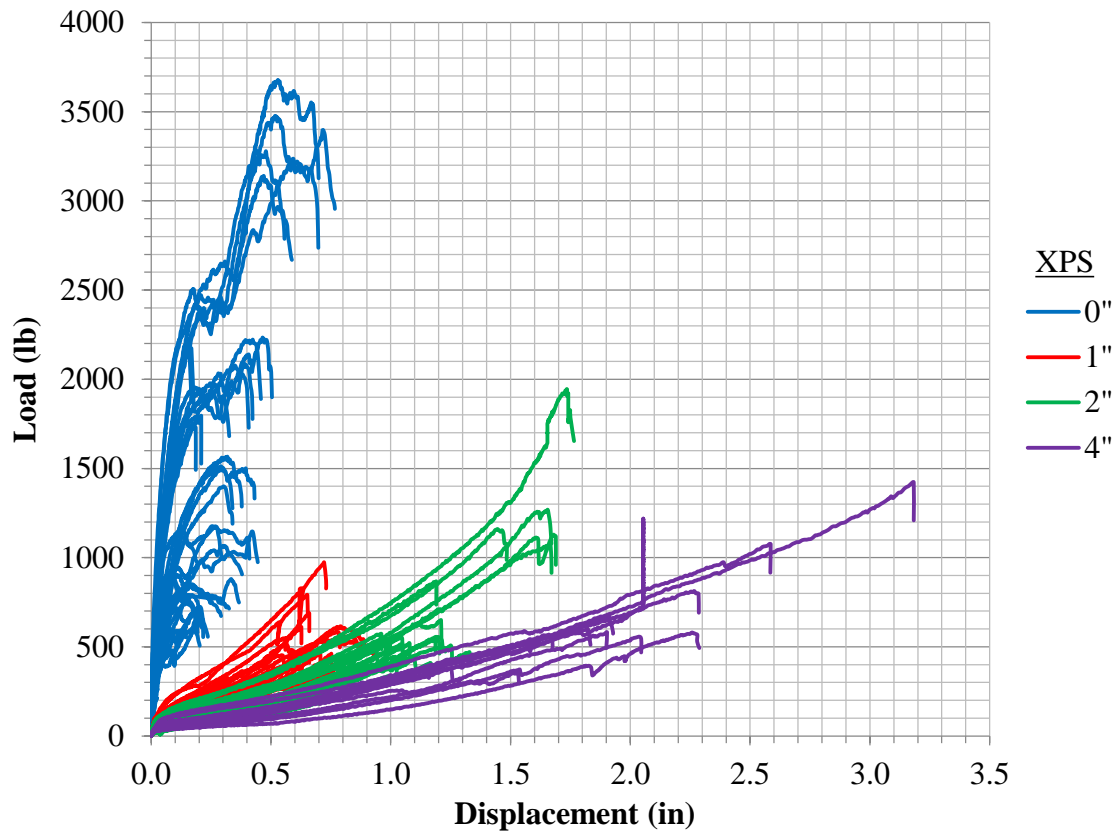


Figure 9: Leonardelli Load versus Displacement Plot [3].

This study expands on the work presented by Leonardelli *et al.* The objective for this study is to create a finite element model which can match the data found by the Leonardelli testing. The stiffness prediction given by Leonardelli encompasses a relatively small amount of connection types. By creating a mechanics based model of the test specimen, a wider range of specimens can be used. In this study, test data from Leonardelli was used to validate the predictions made with the finite element model.

Section 3 - Developing the Model

3.1 Connection Model

3.1.1 Nodes, Elements and Degrees of Freedom

A finite element model was created with four elements to match the test specimen used in the study by Leonardelli [3]. These elements are the CFS stud (element 1), the screw (element 2), the CFS sheathing panel (element 3), and the insulation layer (element 4). Element 4 is a bar element (i.e. it carries axial force only) used to model the compression strut formed in the insulation. Elements 1 and 3 are rotational elements used to model the small regions of the CFS stud wall and CFS sheathing panel that rotate out of plane due to the moment at the end of the screw. Element 2 is the screw and is modeled as a frame element. Figure 10 is a photo taken of the test setup in the study by Leonardelli [3] and Figure 11 is a sketch of the finite element model used in this study. The element numbers in Figure 11 are circled.

Global degrees of freedom (DOF) are shown in Figure 11. Degree of freedom 1 represents the rotation of the stud wall away from the deforming zone around the screw; this rotation is assumed to be zero. Degrees of freedom 2 and 3 are the horizontal and vertical displacements of the screw at the stud; these are assumed to be zero. Degree of freedom 4 is the rotation at the end of the screw at the stud. The rotation at DOF 4 differs from the rotation at DOF 1 because of the deformation of the stud wall due to the bending moment at the end of the screw. Degree of freedom 5 is the horizontal displacement at the screw head. This displacement is not necessarily zero, because as the vertical displacement becomes large the head end of the screw approximately traces a circular arc. As this occurs, DOF 5 will move into the insulation layer, activating the insulation

compression strut (element 4). Degree of freedom 6 is the vertical displacement at the screw head, which is the primary displacement of the connection. Degree of freedom 7 is similar to DOF 4; it is the rotation of the screw at the sheathing panel. Degree of freedom 8 is the rotation of the sheathing panel away from the screw, which is assumed to be zero. Degree of freedom 9 is the horizontal displacement of the insulation strut at the CFS stud; this is assumed to be zero.

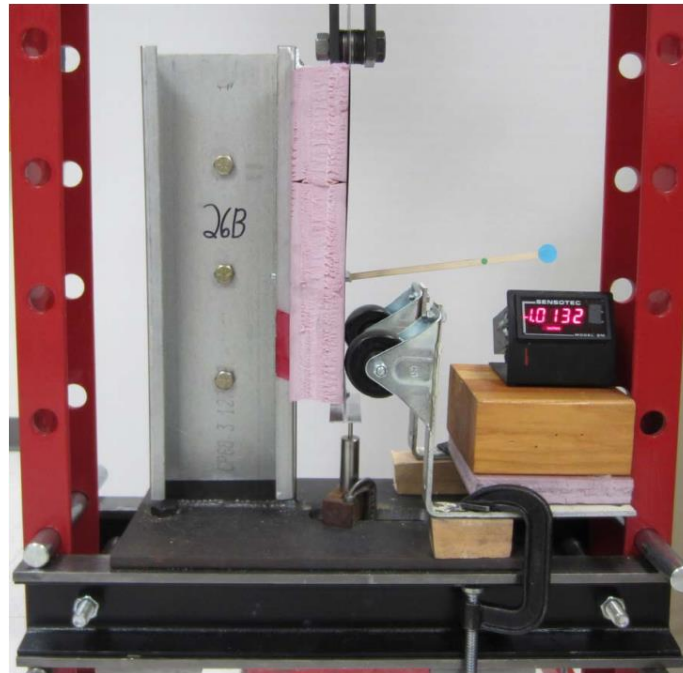


Figure 10: Leonardelli Test Setup [3].

Enforcing the known zero displacement leaves four DOF whose displacement is not known. These DOF are 4, 5, 6, and 7 shown in green in Figure 11 and re-numbered as active DOF 1, 2, 3 and 4 in Figure 12.

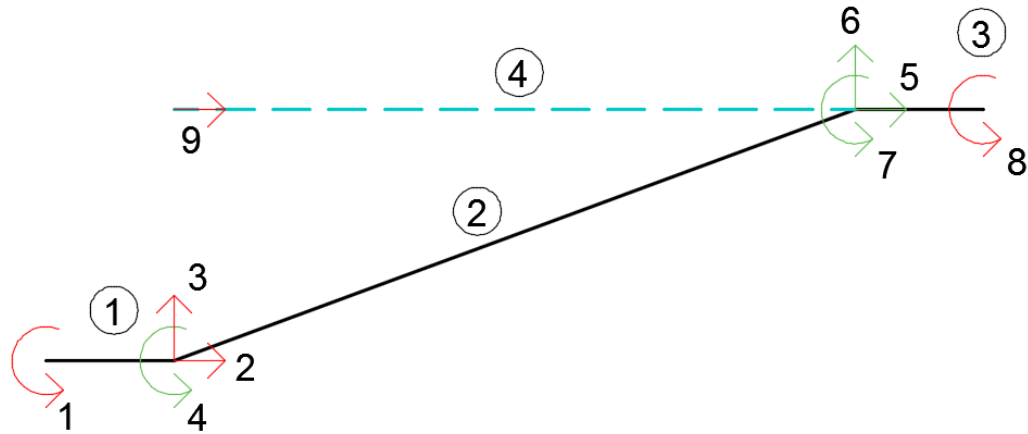


Figure 11: Screw Connection Model (Elements Numbers Circled, Degrees of Freedom not Circled).

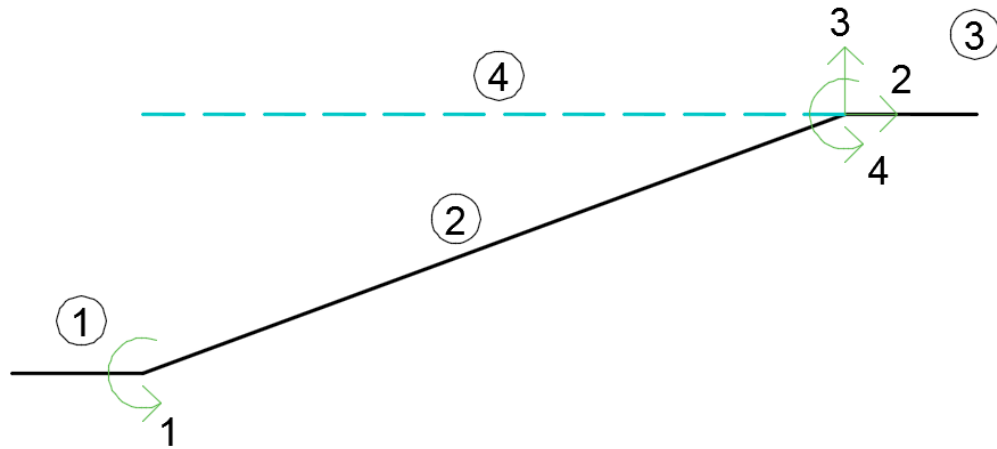


Figure 12: Nonzero Displacement Screw Connection Model (Elements Numbers Circled, Degrees of Freedom not Circled).

3.1.2 Screw Element and Geometric Nonlinearity

Geometric nonlinearity was incorporated into the model so the analysis could include the large displacements reported by Leonardelli [3]. An iterative procedure was developed using a corotational formulation [8] for the screw element. This approach allows for large displacements and large rigid-body rotations as long as the element

curvatures and strains are small. In the corotational formulation, the element local coordinate system (x_l and y_l in Figure 13) rotate with the element as the structure deforms.

To start the iterative procedure, initial global displacements are needed. This can be found in an initial analysis (used for load-controlled analysis) or initial displacements can be inserted directly (displacement-controlled analysis). From the initial global displacements, the element displacements are found. Next, the original angle of the element, (β_o) , is subtracted from the current angle of the element, (β) , to find the rigid body rotation, (α) . For horizontal elements β_o is zero, and if there is no vertical displacement at either node β is zero. The new length of the element is determined using the element displacements. The element is then analyzed at both nodes. The first node's horizontal and vertical displacements in the local coordinate system are equal to zero. The node's rotation in the local coordinate system, $(\bar{\theta})$, is equal to the node's global rotation at that node, (θ) , minus the rigid body rotational, (α) . This process is repeated for the second node, except the axial displacement is equal to the new length of the element minus the original length of the element. Once both nodes have been analyzed, the new displacements are combined to create a new local displacement vector for the element. From this new local displacement vector (u_e), local element forces (f'_e) are found by multiplying the element stiffness matrix (k) by the new displacements. These new forces are then rotated into global coordinates using a transformation matrix depending on the orientation. See Figure 13 for a visual representation of these variables.

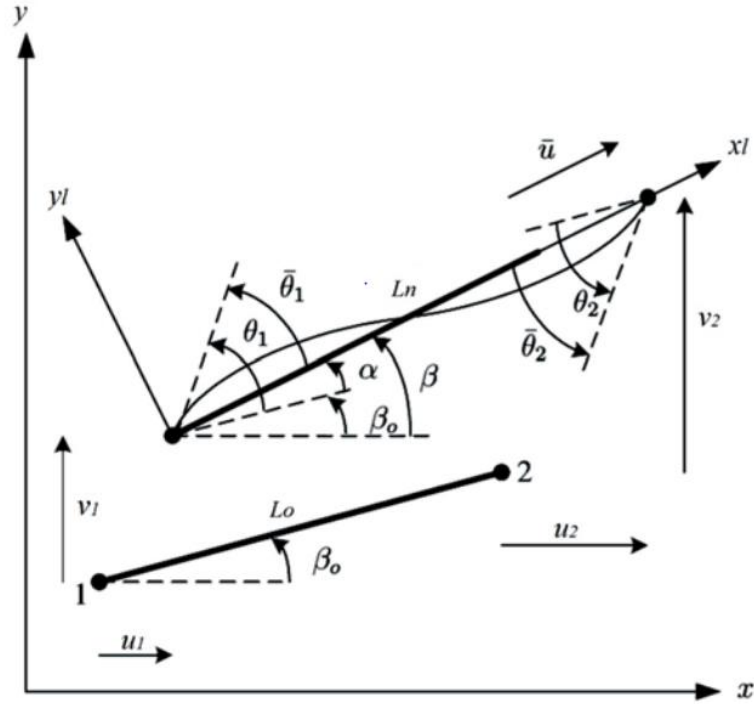


Figure 13: Corotational Element Formulation Definitions [9].

For load-controlled analysis, an initial analysis is conducted using typical finite element analysis. This process includes creating an element stiffness matrix (k) for each element, combining those stiffnesses, and eliminating those stiffness terms that correspond to DOF that are supports (creating reduced stiffness matrix, K). This reduced stiffness matrix is then inverted and multiplied by the load vector (F) to get the global displacements (U). Equations (8) and (9) are the basic equations representing this concept:

$$F = K U, \quad (8)$$

$$U = K^{-1} F. \quad (9)$$

After each element has been analyzed and element forces have been found, the element forces can be combined at each node to create a global element force vector (Σf_e). The global element force vector is then subtracted from the original force vector (F) to find the unbalanced force vector (ΔP). The inverse of the global stiffness matrix is then multiplied by ΔP to find the displacement increment vector (ΔU). The displacements increment is then added to the previous displacements to form a new displacement vector at each iteration (U_{new}). Equations (10), (11) and (12) show this procedure. This process is repeated until the displacement value differences are negligible:

$$\Delta P = F - \Sigma f_e, \quad (10)$$

$$\Delta U = K^{-1} \Delta P, \quad (11)$$

$$U_{new} = U + \Delta U. \quad (12)$$

The analysis for this study used the Newton-Raphson [10] approach to iterate toward equilibrium. The structure stiffness matrix was updated for each iteration based on the new displacement vector found at the previous iteration. It is worth noting that for the screw element the element stiffness matrix in local coordinates does not change, only the transformation matrix (T) based on the new geometry at each iteration.

3.1.3 Plate Element and Material Nonlinearity

The plate elements represent a zone of bending deformation found in the CFS stud flange wall and the sheathing panel. The deformation is caused by the moment at the ends of the screw. In this study, these bending zones in the flange wall and panel are

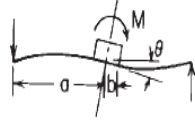
idealized as circular plates with concentrated moments applied at the center. *Roark's Formulas for Stress and Strain* was used to find the initial elastic stiffness and yield moment of the circular plates [11]. An example of a panel showing the bending deformation is found in Figure 14.



Figure 14: Bending Deformation Zone of the Metal Sheathing Panel [3].

The rotational elements were determined to be most similar to *Roark's* Case 20b: Central couple on an annular plate with a simply supported outer edge (trunnion loading), with the trunnion fixed to the plate. The trunnion would be a small cylindrical protrusion created by drilling the screw into the members. Case 20 in Table 11.2 of *Roark's* can be seen in Figure 15.

20. Central couple on an annular plate with a simply supported outer edge (trunnion loading)



(Note: For eccentric trunnions loaded with vertical loads, couples, and pressure on the plate, see Refs. 86 and 87)

20a. Trunnion simply supported to plate. For $\nu = 0.3$

$$\theta = \frac{\alpha M}{Et^3}, \quad \tau_{\max} = \tau_{rt} = \frac{\lambda M}{at^2} \text{ at } r = b \text{ at } 90^\circ \text{ to the plane of } M$$

$$\sigma_{\max} = \sigma_t = \frac{\gamma M}{at^2} \text{ at } r = b \text{ in the plane of } M$$

b/a	0.10	0.15	0.20	0.25	0.30	0.40	0.50	0.60	0.70	0.80
λ	9.475	6.256	4.630	3.643	2.976	2.128	1.609	1.260	1.011	0.827
γ	12.317	8.133	6.019	4.735	3.869	2.766	2.092	1.638	1.314	1.075
α	2.624	2.256	1.985	1.766	1.577	1.257	0.984	0.743	0.528	0.333

20b. Trunnion fixed to the plate

$$\theta = \frac{\alpha M}{Et^3}, \quad (\sigma_r)_{\max} = \frac{\beta M}{at^2} \text{ at } r = b \text{ in the plane of } M$$

b/a	0.10	0.15	0.20	0.25	0.30	0.40	0.50	0.60	0.70	0.80
β	9.478	6.252	4.621	3.625	2.947	2.062	1.489	1.067	0.731	0.449
α	1.403	1.058	0.820	0.641	0.500	0.301	0.169	0.084	0.035	0.010

Figure 15: Case 20 in Table 11.2 of *Roark's Formulas for Stress and Strain* [10].

The rotational elements' initial elastic stiffness (k_o) and yield moment (M_y) are calculated by Equation (13) and Equation (14), respectively. These come from the moment-rotation relationship shown in Case 20b in Figure 15. The variable “a” is the radius of the plate bending area, and the variable “b” is the radius of the trunnion. For the CFS stud and panel, the b/a ratio was estimated from photographs (Figure 14, for example) of failed connection specimens from the study by Leonardelli [3]. The values for α and β were interpolated from the table if the b/a ratio did not match one of the values in the table. The variable “t” is the thickness of the stud or plate. Thus:

$$k_o = E t^3 / \alpha, \quad (13)$$

$$M_y = \sigma_y a t / \beta. \quad (14)$$

The flange of the CFS stud and the sheathing panel (both rotational elements), were considered for material nonlinearity. It was assumed that the elements were elastic-perfectly plastic and produced a moment versus rotation plot like that shown in Figure 16.

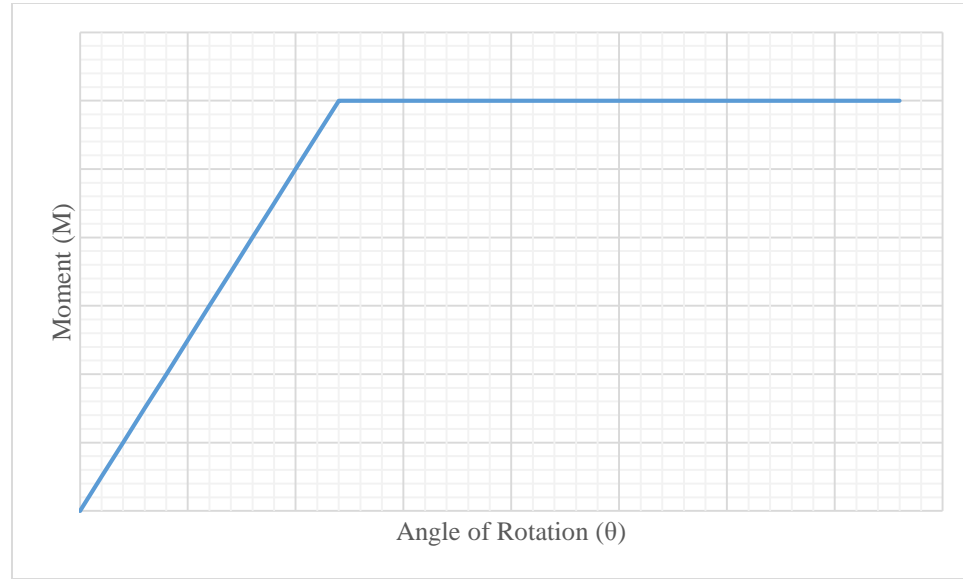


Figure 16: Elastic-Perfectly Plastic Relationship for Rotational Plates.

To get a curve for the elastic plastic relationship, an exponential function was used because of the known shape produced from it. The stiffness equation was first set up as $k = k_0 e^{-A\theta}$. The moment at any rotation is the integral of the stiffness equation, producing $M = -k_0(1/A)e^{-A\theta} + C$. To solve for constants A and C , boundary conditions were set so that at large rotation, the moment should be equal to the yield moment (M_y), and at no rotation, the moment should be equal to zero. These boundary conditions produce Equation (15) and (16):

$$k=k_o*e^{-(k_o/M_y)*\theta}, \quad (15)$$

$$M=-M_y * e^{-(k_o/M_y)*\theta} + M_y. \quad (16)$$

Example plots of the stiffness and moment equations are shown in Figure 17 and 18.

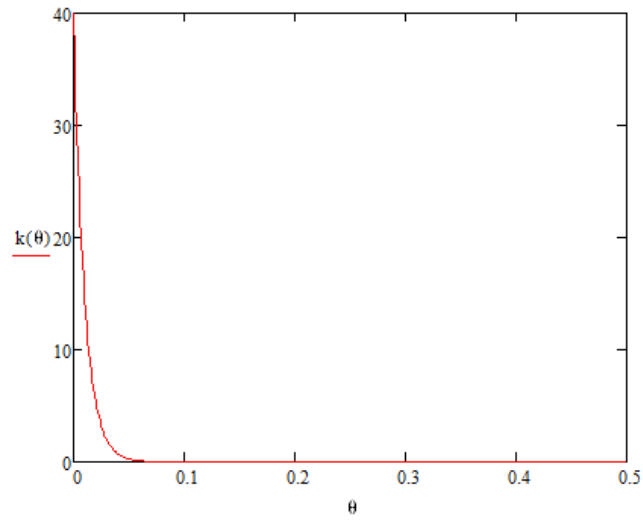


Figure 17: Rotational Plate Stiffness Equation Plot.

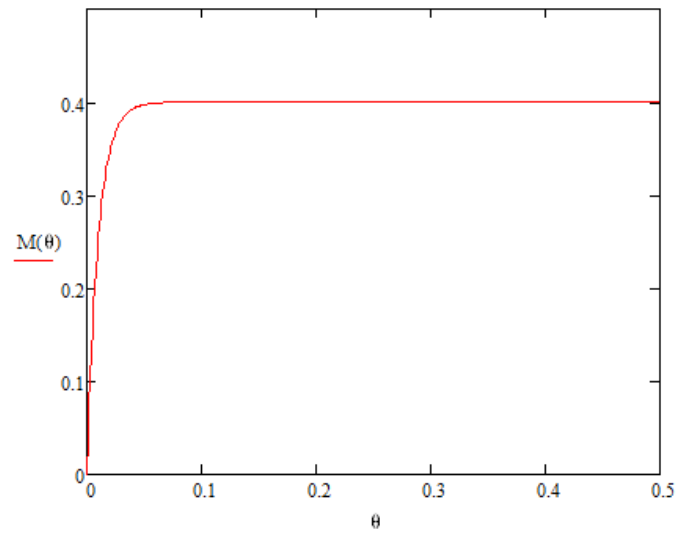


Figure 18: Rotational Plate Moment Equation Plot.

3.2 Insulation Stiffness Testing

3.2.1 Initial Panel Testing

With no reference value to use for the insulation strut stiffness, testing was done to determine a stiffness value. Tests were performed with 16-gauge and 25-gauge panels, and insulation thickness of 1 inch, 2 inches, and 4 inches. The sizes of the panels and insulation were limited to 6-inch by 6-inch squares because the panels were 6 inches wide when received from MBA Steel. Insulation and panel specimens matched those used by Leonardelli [3]. The insulation board was Owens Corning Foamular 150 Extruded Polystyrene (XPS) Rigid Foam Insulation, which has a minimum compressive strength of 15 psi. Insulation boards were either 1 inch or 2 inches thick. To make the 4-inch insulation layer, two layers of the 2-inch insulation board were used. The CFS panels were ASTM 1003 (ASTM 2013) designation ST50H ($F_y=50$ ksi, $F_u=65$ ksi). The panel thicknesses were 0.0180 inches (25 gauge) and 0.0565 inches (16 gauge). Before testing, the thickness of each panel types were measured. The 16 gauge matched the thickness published by Leonardelli but the 25 gauge did not. The measured thickness for the 25-gauge panel was 0.0240 inches. It is believed that Leonardelli listed the thickness of the steel only and ignored the zinc coating used to galvanize the panel. According to the *AISI North American Specification*, gauge thickness is an obsolete method of specifying sheet steel thickness [1]. With no way to find the thickness of the 25-gauge panel without the zinc coating, the measured thickness of 0.0240 inches was used in this study.

The test setup is shown in Figure 19. Initial testing was conducted to determine if the test method and setup would be acceptable. During initial testing, no frame was used below the steel panel. With no frame being used, the steel panel buckled while

compressing the insulation. This result is not realistic; plate buckling did not appear in actual metal sheathing.

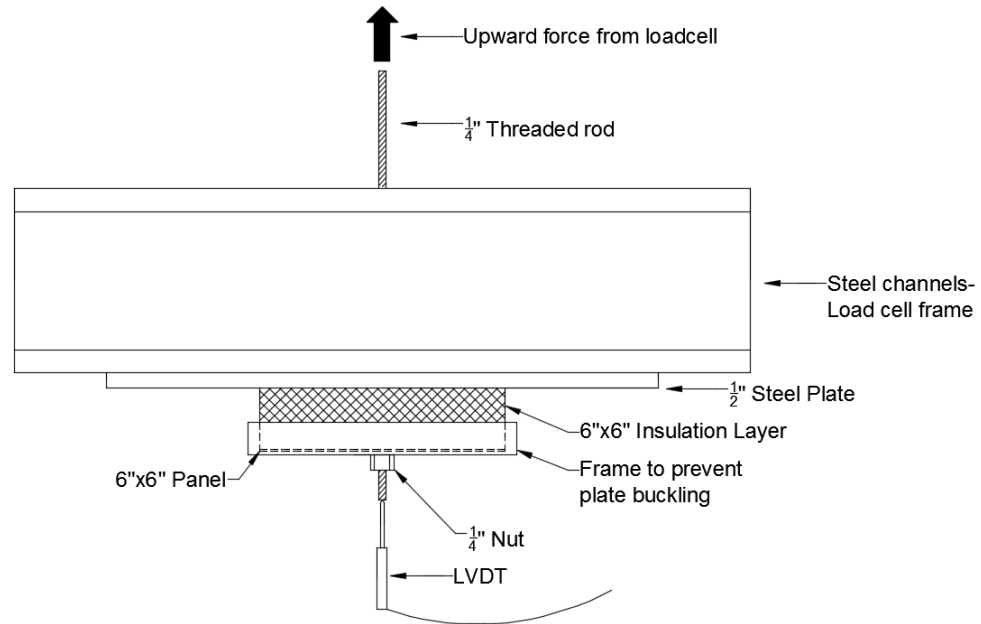


Figure 19: Insulation Test Setup.

In order to try to prevent plate buckling, a steel frame was used. This frame can be seen in Figure 20, and as shown in Figure 21. It was clamped to the channels of the test frame, beneath the panel. The clamps were tightened until all edges of the 6-inch by 6-inch panel were touching the frame. The frame was not tightened past that point to avoid introducing compressive stress into the insulation before testing began.



Figure 20: Insulation Test Frame.



Figure 21: Frame Clamped onto Load Cell Channel.

Test data were originally plotted based on the thickness of the insulation. The data showed that the insulation stiffness was not dependent on the insulation thickness but on

the thickness of the panel. Figures 22 and 23 show the load versus displacement relationship for the insulation based on panel thickness. The frame was able to prevent plate buckling until the displacement read by the Linear Variable Displacement Transducer (LVDT) was around 0.3 inches. At that point, the plate buckled and the load versus displacement relationship changed.

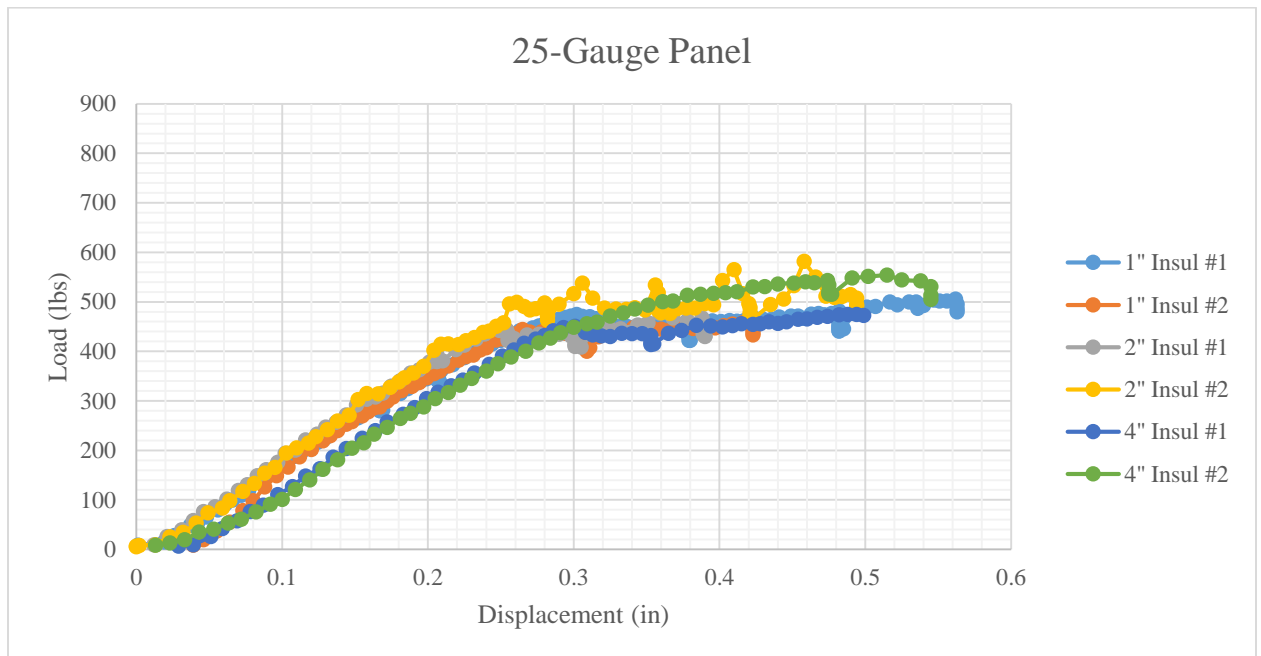


Figure 22: Load versus Displacement Plot for 25-Gauge Panel.

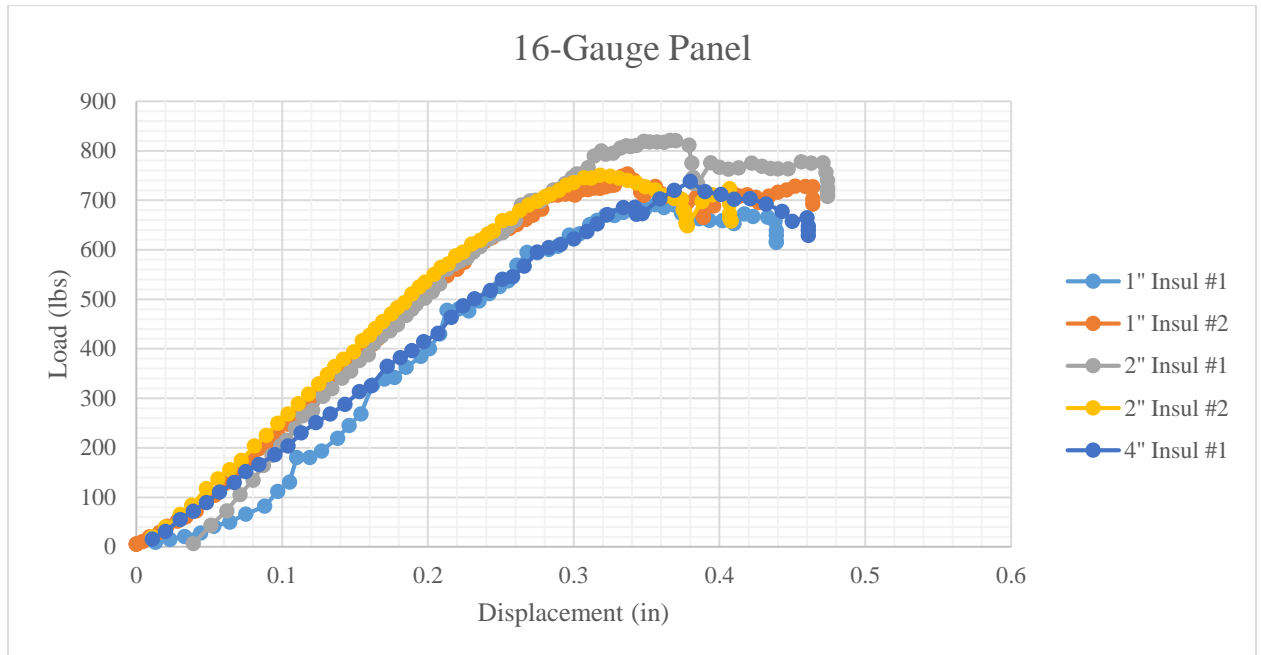


Figure 23: Load versus Displacement Plot for 16-Gauge Panel.

Because plate buckling did not occur in the real connections, the load and displacement values were ignored after the plate had buckled. A linear trendline was created for each trial (ignoring the post-buckling behavior). The slopes of the trendlines were averaged based on the panel thickness, and that average value was used as the insulation stiffness (since the derivative of a load versus displacement equation is the stiffness). Table 1 shows the slope of each trendline and the average value for each panel. The test data show that the stiffness was dependent on the panel used, not on the insulation thickness. The values for stiffness are 1.8 kips per inch for the 25-gauge panel (0.0180 inch) and 2.43 kips per inch for the 16-gauge panel (0.0565 inch). Modified load versus displacement plots and trendlines for both panels can be found in Figure 24 and Figure 25.

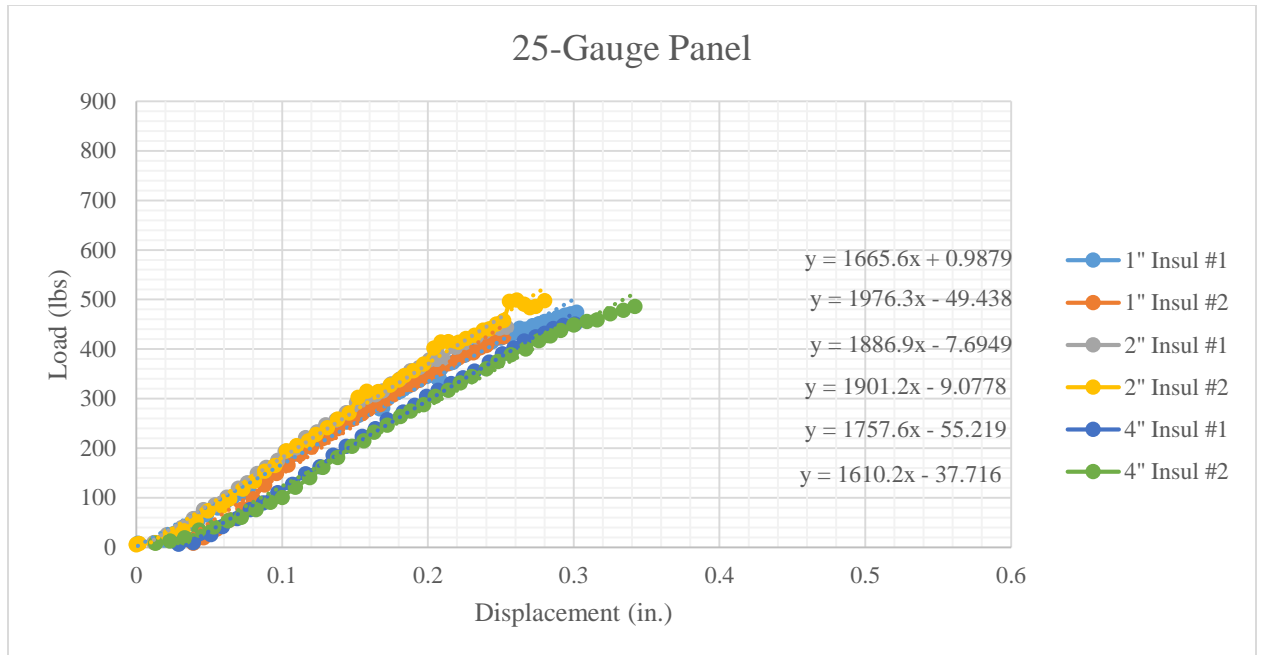


Figure 24: Modified Load versus Displacement Plot and Trendlines for the 25-Gauge Panel.

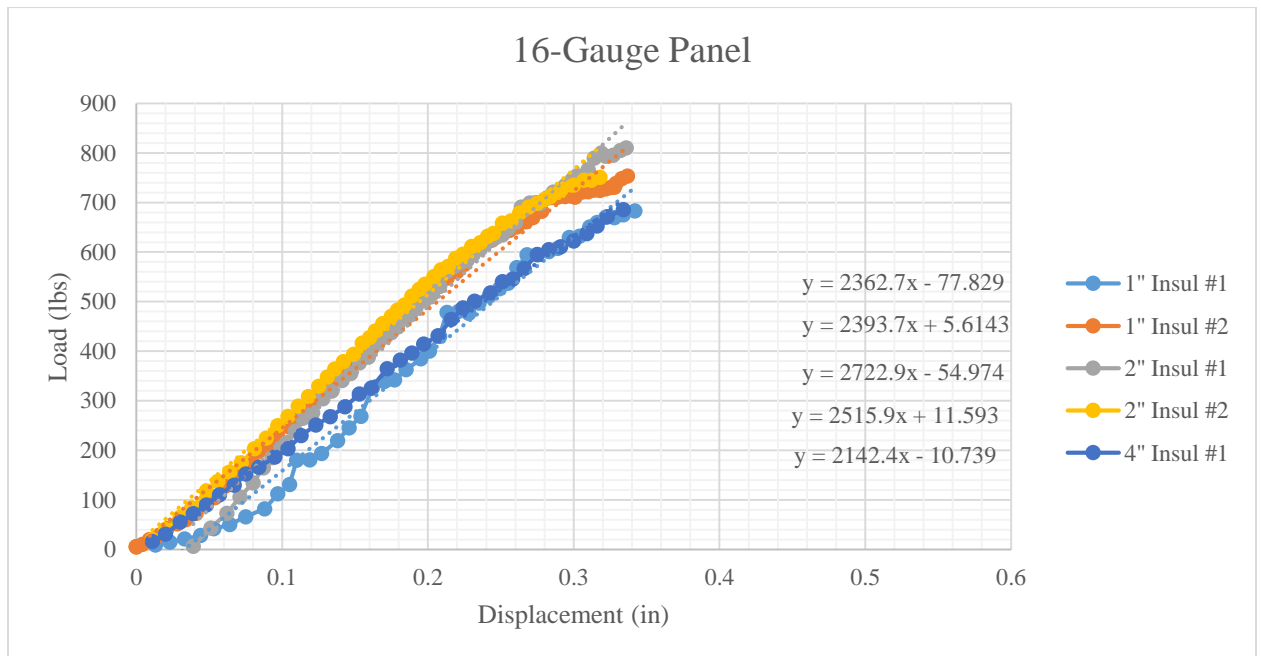
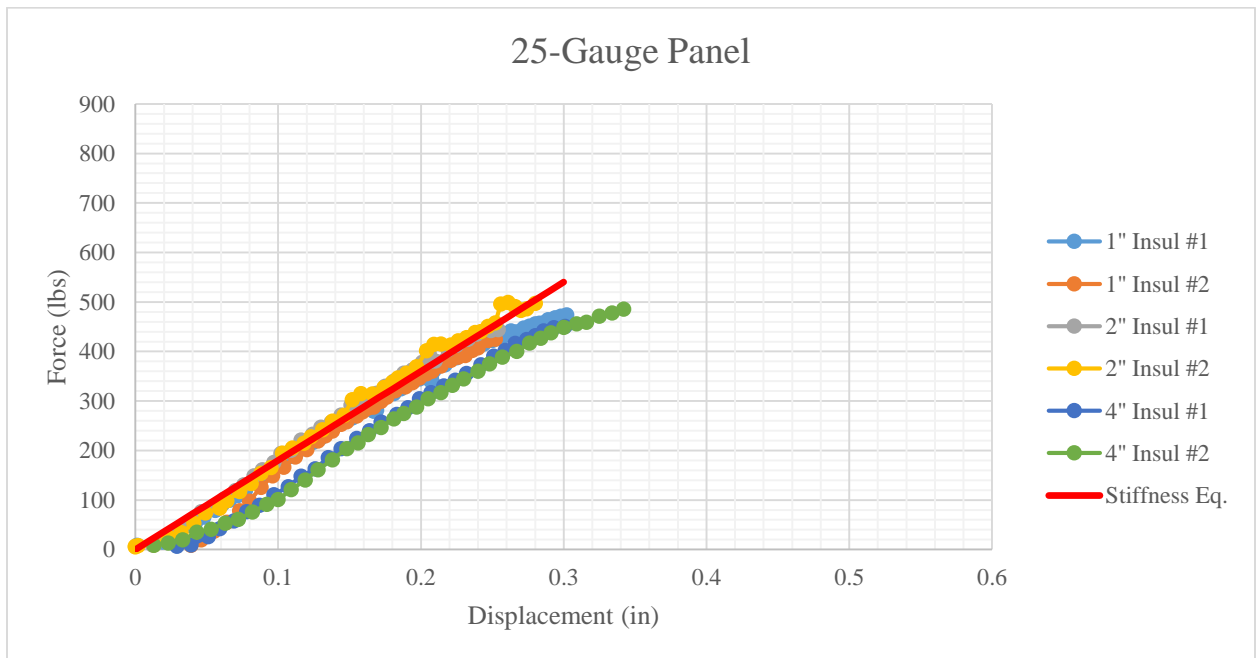


Figure 25: Modified Load versus Displacement Plot and Trendlines for the 16-Gauge Panel.

Table 1: Modified Insulation Stiffness.

	25-gauge panel stiffness (#/in.)	16-gauge panel stiffness (#/in.)
1 in. insulation trial #1	1665	2365
1 in. insulation trial #2	1975	2395
2 in. insulation trial #1	1885	2725
2 in. insulation trial #2	1900	2515
4 in. insulation trial #1	1760	2140
4 in. insulation trial #2	1610	-
Average	1800	2430

Figures 26 and 27 show the modified data along with a line representing the linear stiffness found from averaging the trendline slopes. The stiffness values are 1800 lbs/in for the 25-gauge panel and 2430 lbs/in for the 16-gauge panel. Because these linearized ranges only extend to approximately 0.3 inches and the insulation compressions observed by Leonardelli [3] were larger, it was determined more testing must be done.

**Figure 26: Modified Load versus Displacement Plot with Linear Stiffness for 25-Gauge Panel.**

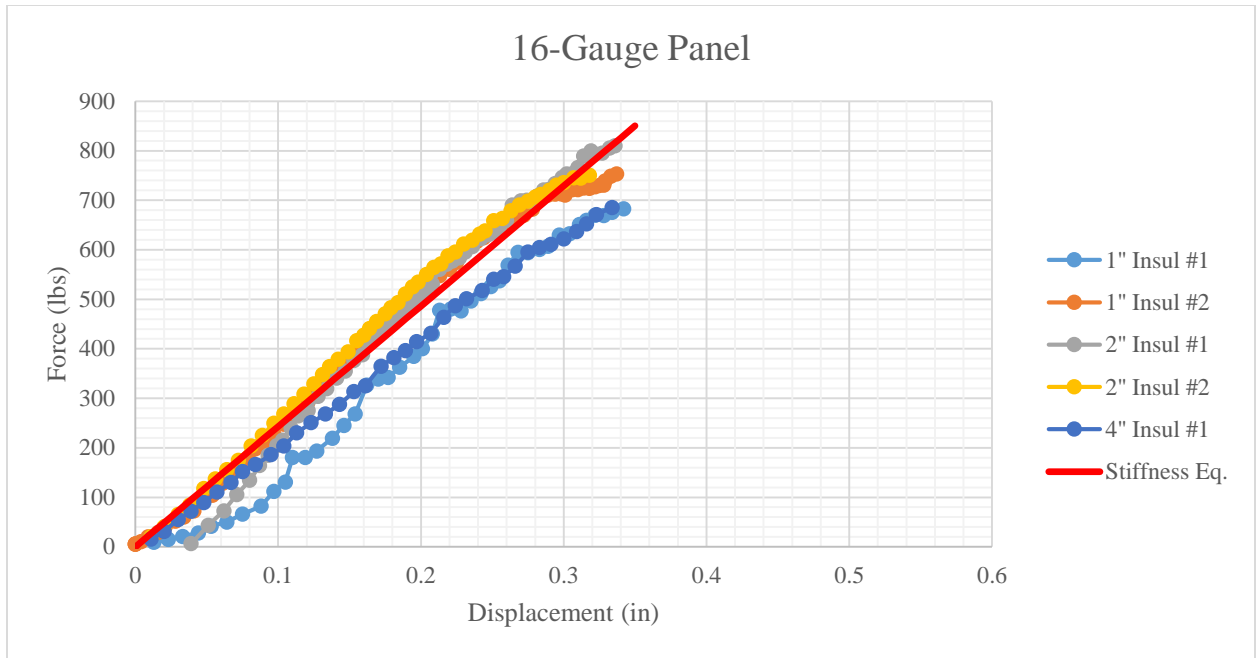


Figure 27: Modified Load versus Displacement Plot with Linear Stiffness for 16-Gauge Panel.

3.2.2 Washer Testing

Washer testing was done in order to determine whether the bilinear relationship found in the initial panel testing was caused by plate buckling or by insulation properties. The tests were performed with the same basic setup, except the panel was replaced by a washer and there was no insulation test frame. Figure 28 shows the washer in place of the panel.



Figure 28: Washer Testing Setup.

Three different sized washers were used in the tests: 1-inch diameter, 1.5-inch diameter, 2-inch diameter. By using different sized washers, the results would demonstrate the effect that bearing area had on the insulation stiffness. Only two insulation thicknesses were used, 1-inch and 2-inches. The different thicknesses would confirm that the insulation stiffness was not dependent on its thickness. Each washer was tested a total of four times, twice with 1" insulation and twice with 2" insulation.

Washer tests results were grouped together by washer size to show that the insulation stiffness was not dependent on the insulation thickness. The load versus displacement plots created for the 1-inch, 1.5-inch and 2-inch washer can be seen in Figure 29, 30 and 31, respectively. Unlike the panel testing, the bilinear relationship produced in these plots were due to an initial insulation stiffness, then a reduced stiffness

when the insulation began to get crushed, demonstrating the cell wall behavior discussed by Gao [7]. Figure 32 shows a test specimen after insulation crushing. The results show no difference in the stiffness of the two thicknesses until the 1-inch insulation is compressed to where the material densifies and the stiffness increases.

Results show that the stiffness varies based on the bearing area. Once determined, it was confirmed that previous test data for insulation stiffness would not be sufficient. The previous testing focused on the effect of the panel on the stiffness, but ignored that the insulation would bear against a 600S200 cold-formed stud. The area on the stud is significantly less than the full area of the insulation.

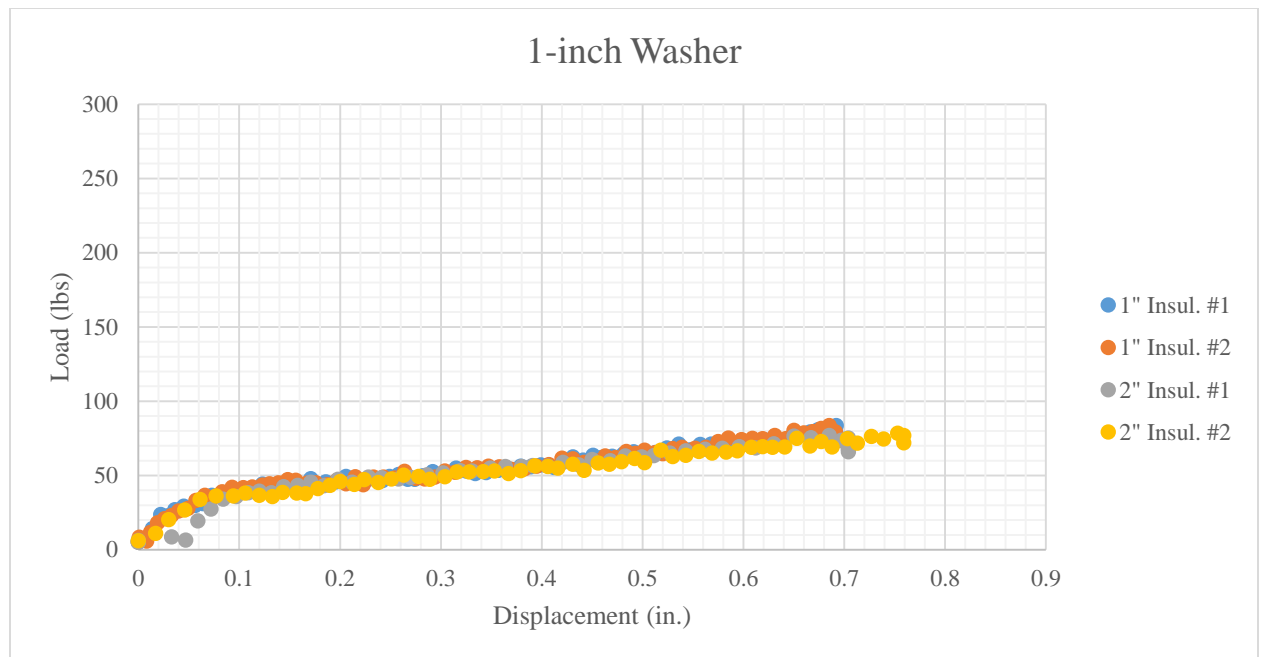


Figure 29: 1-inch Washer Load versus Displacement Plot.

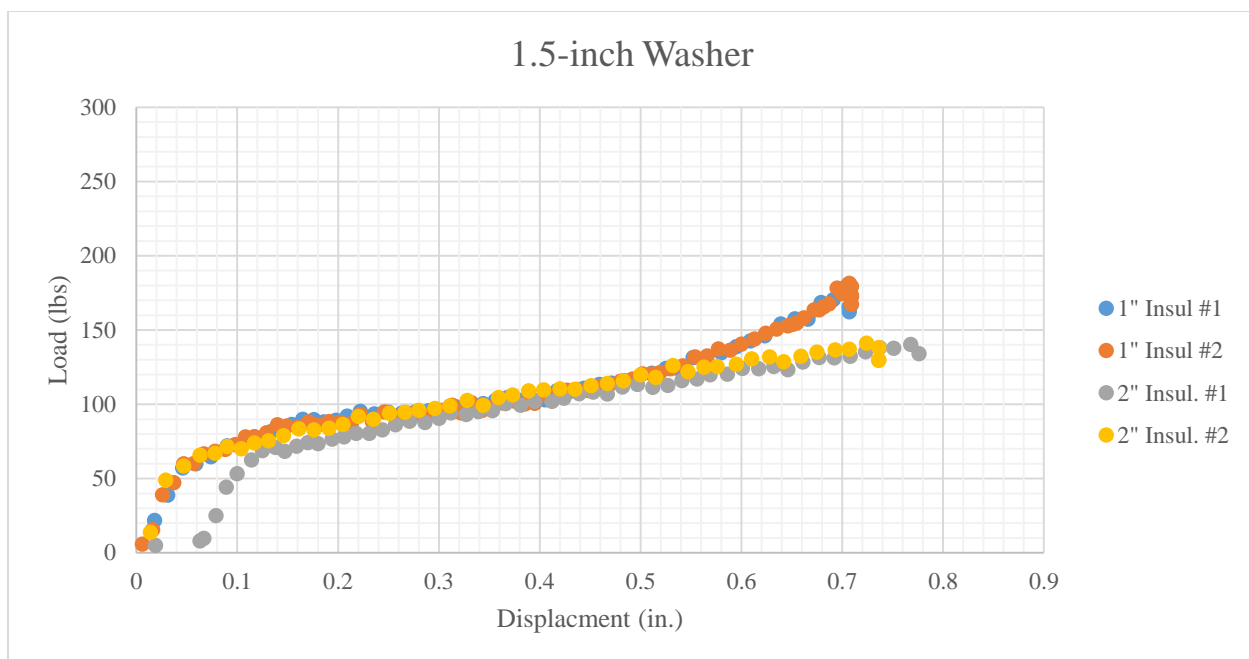


Figure 30: 1.5-inch Washer Load versus Displacement Plot.

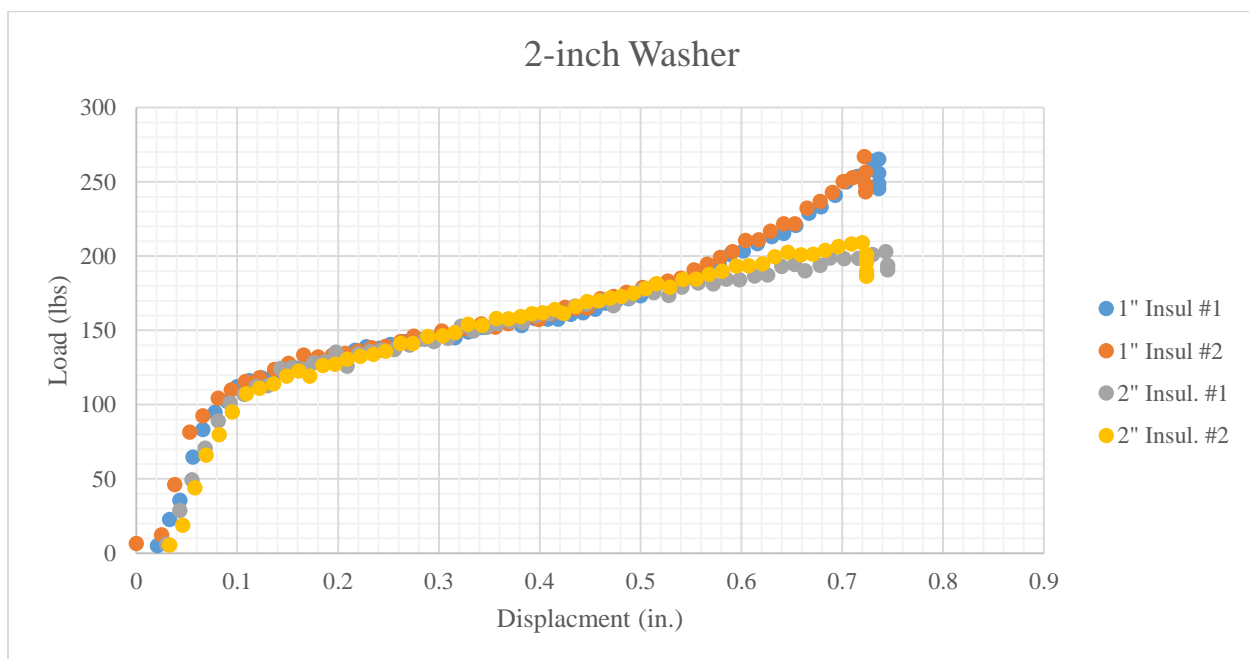


Figure 31: 2-inch Washer Load versus Displacement Plot.



Figure 32: Crushed Insulation Member after Completed Washer Test.

3.2.3 CFS Stud Testing

Further testing was required in order to account for the smaller bearing area of the 600S200 stud. The test program followed the previous tests, except a CFS stud was placed between the ½-inch steel plate and the insulation. This modification to the test setup can be seen in Figure 33. Placing the LVDT at the bottom of the rod was no longer acceptable due to slight deformation in the stud during the compression of the insulation, causing the rod to bend slightly and lose contact with the LVDT. To solve this problem, the LVDT was placed above the load cell.

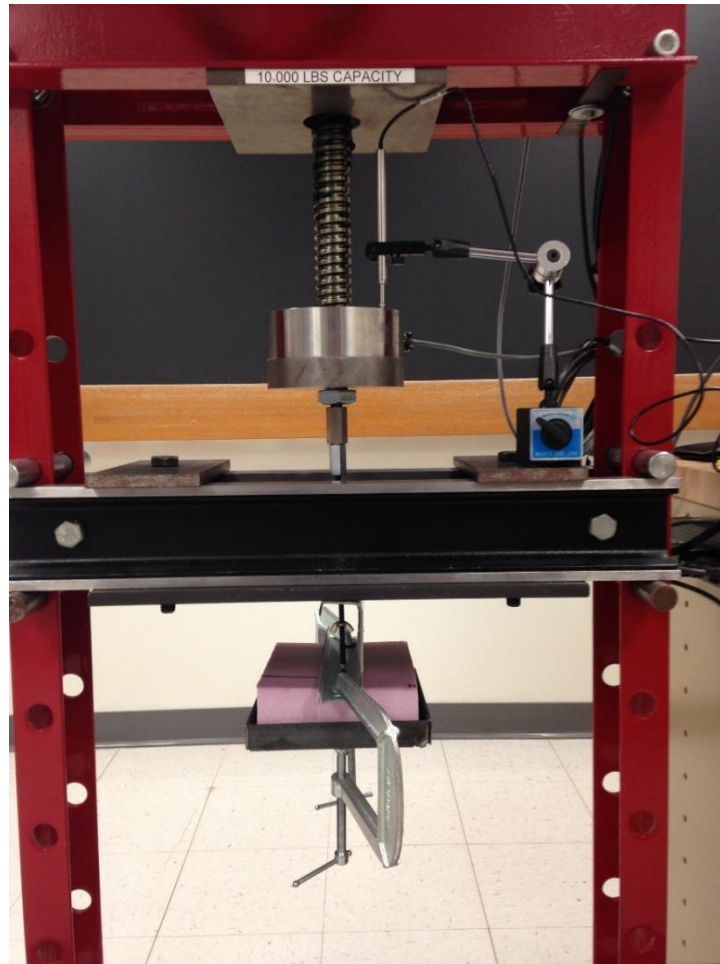


Figure 33: Test Setup for CFS Insulation Testing.

Testing was limited to CFS studs with flange widths of 1.5 inches and 2.5 inches; no CFS studs with a 2-inch flange width were available to match the 600S200 used in testing by Leonardelli [3]. During testing, the stud with the 2.5-inch flange was subject to significant web deformation, causing results to be inaccurate. Limited data were collected from the 2.5-inch stud. Figure 34 shows two of the load versus displacement plots for the 1.5-inch stud.

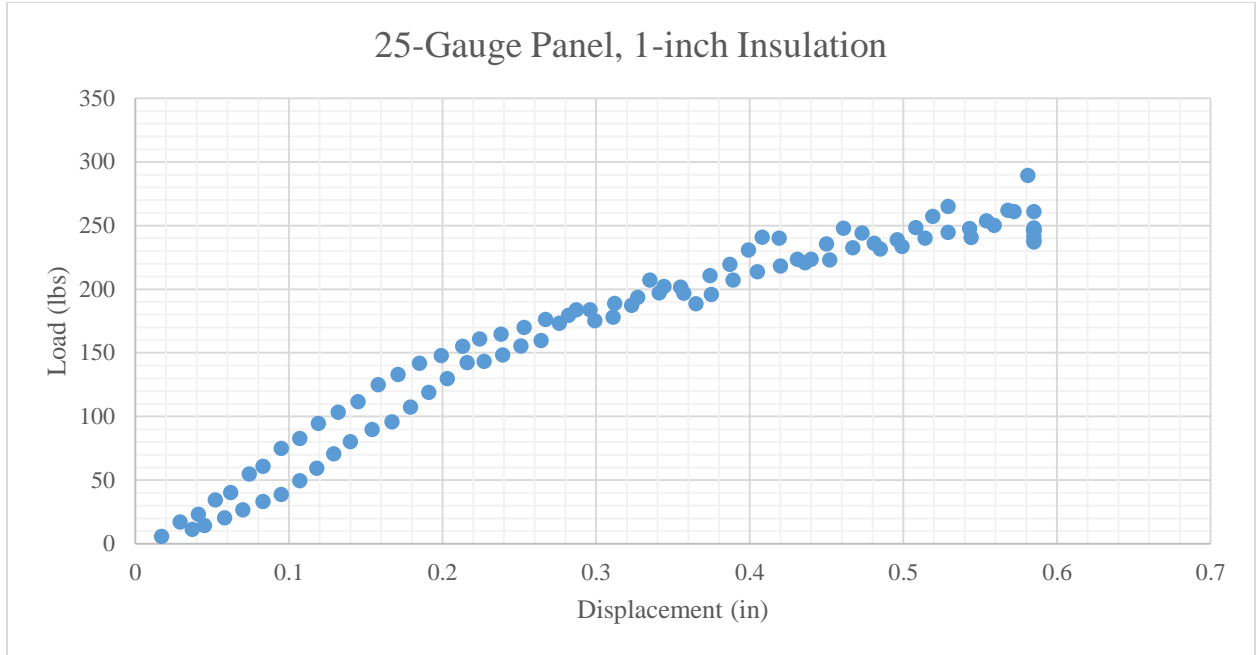


Figure 34: 25-Gauge Panel, 1-inch Insulation Stud Load versus Displacement Plot (1.5-inch Flange).

Each setup displayed similar nonlinear behavior as that shown in Figure 34. It was decided that an exponential equation would be developed to represent the nonlinear behavior. Because of the limited scope of these tests, this equation would be limited to using the thickness of the panel and the thickness of the insulation as variables. There was no formal regression analysis performed for the equation; it was simply fit to the load versus displacement plots. Equation (17) is the exponential equation, which was created for the 1.5-inch stud:

$$P = (-500 t_{\text{insul}} e^{-60 t_{\text{panel}} \Delta} + 500 t_{\text{insul}}) / t_{\text{insul}}^{0.85} . \quad (17)$$

Using Equation (17) on each of the load versus displacement plots for the 1.5-inch CFS stud created Figure 35 through Figure 38. Unlike previous testing, this round of tests showed a slight dependence on insulation thickness as indicated in Equation (17).

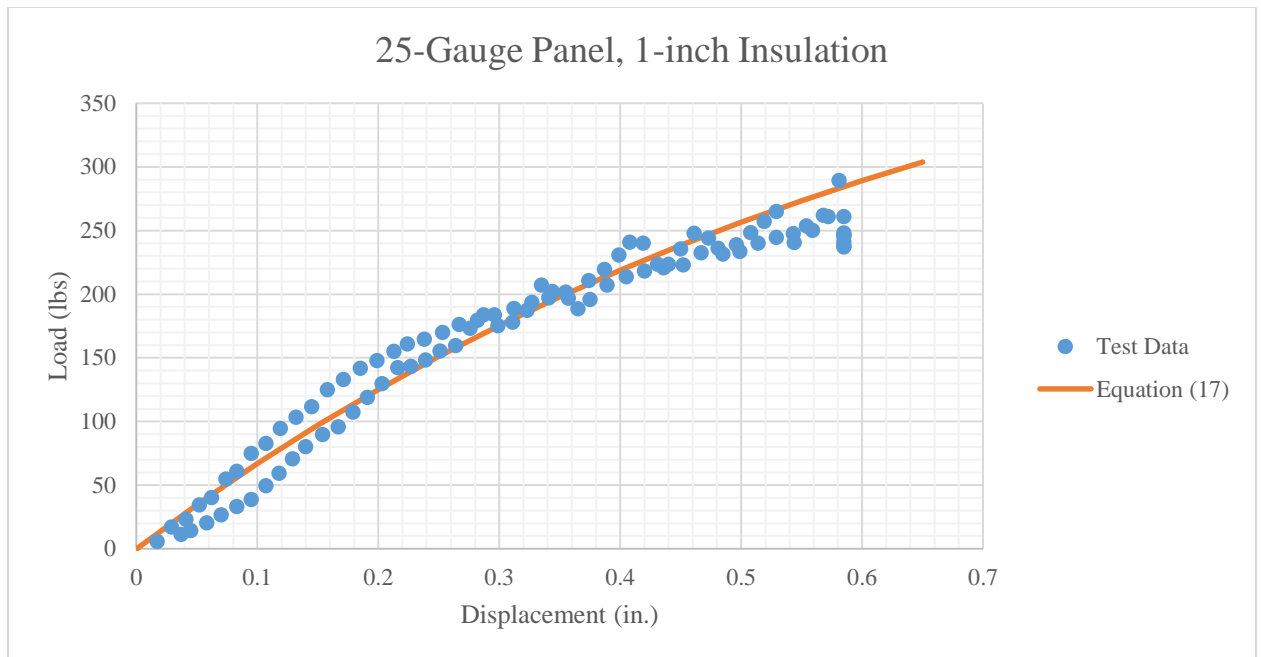


Figure 35: 25-Gauge Panel, 1-inch Insulation Load versus Displacement Plot with Exponential Curve (1.5-inch Flange).

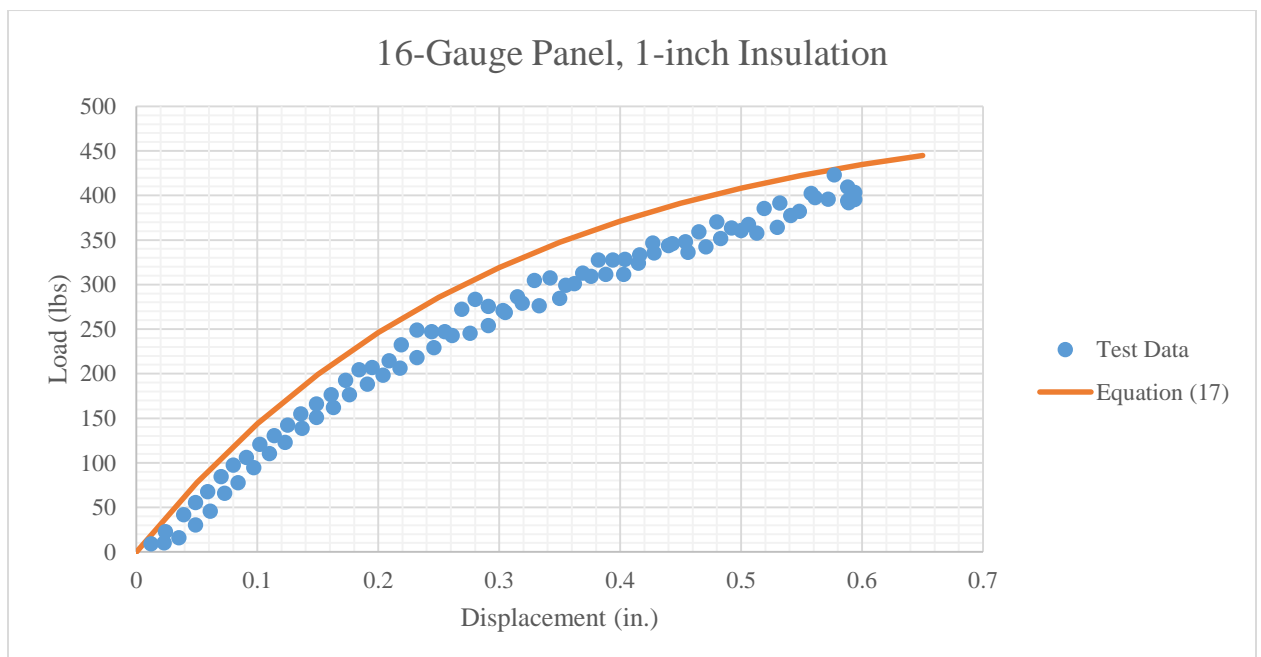


Figure 36: 16-Gauge Panel, 1-inch Insulation Load versus Displacement Plot with Exponential Curve (1.5-inch Flange).

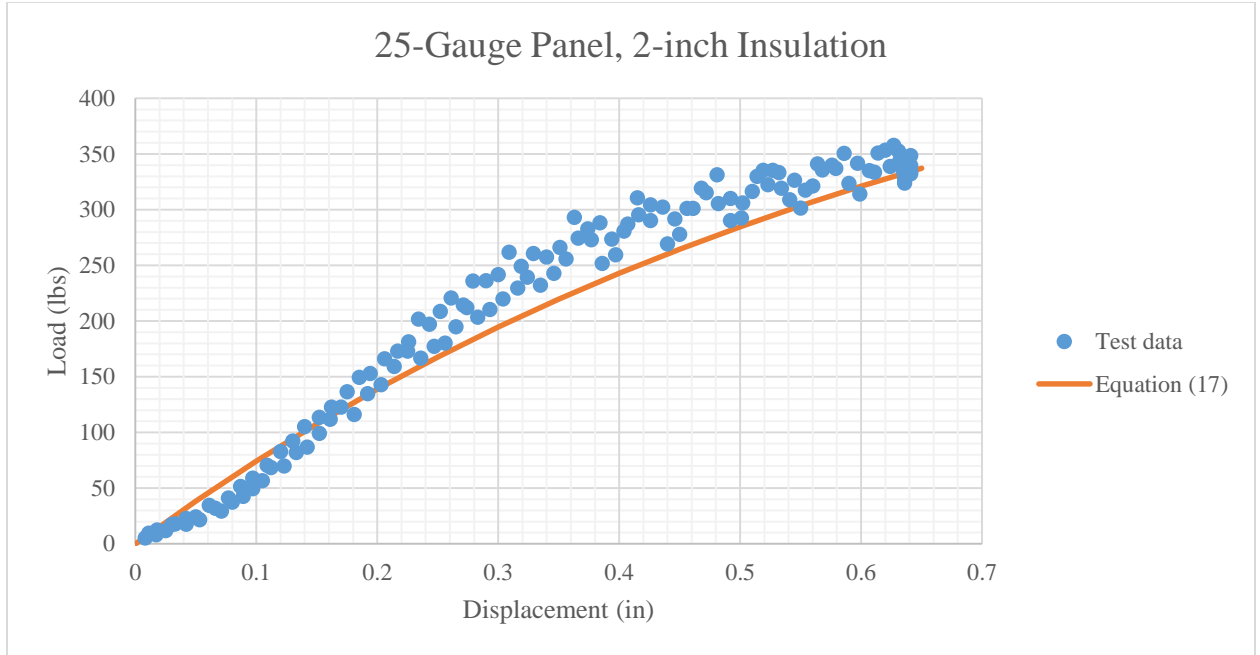


Figure 37: 25-Gauge Panel, 2-inch Insulation Load versus Displacement Plot with Exponential Curve (1.5-inch Flange).

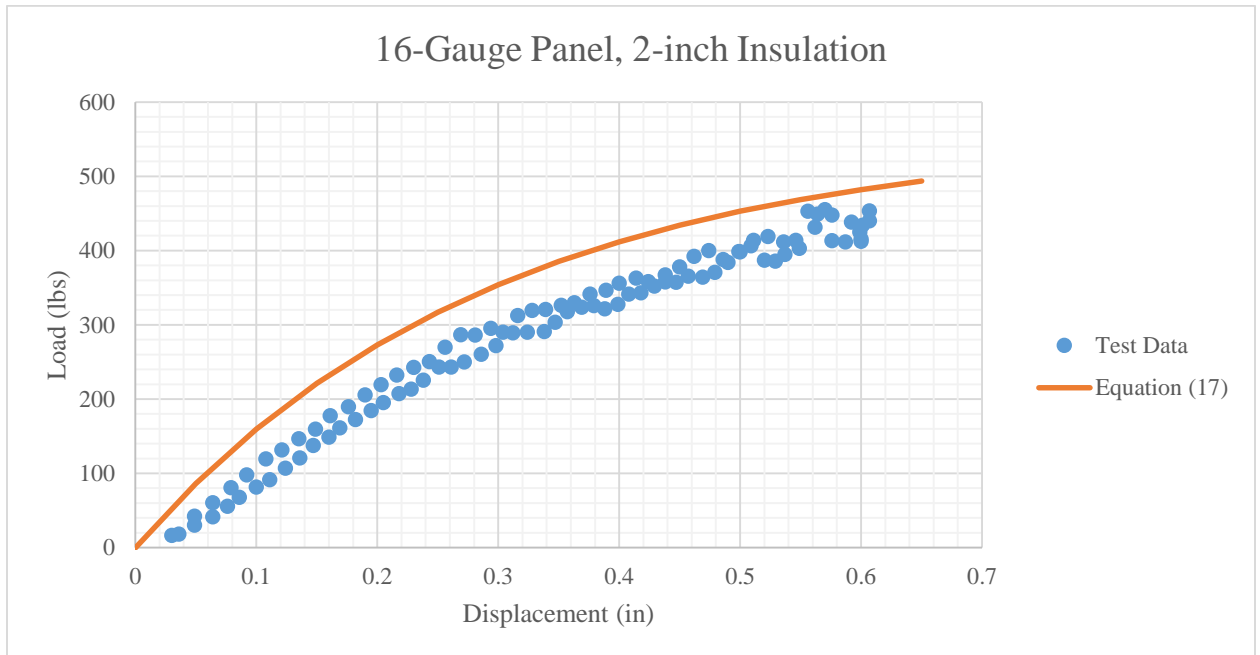


Figure 38: 16-Gauge Panel, 2-inch Insulation Load versus Displacement Plot with Exponential Curve (1.5-inch Flange).

To confirm the validity of the exponential equation, the equation was plotted on a load versus displacement plot for the 2.5-inch CFS stud. With the limited data available for the 2.5-inch CFS stud, only one panel thickness and one insulation thickness is available for comparison. In order to take into account the larger bearing area of the 2.5-inch flange, the coefficient in the exponential equation was increased by the ratio of areas between the 2.5-inch and 1.5-inch flanges. Equation (18) is the new exponential equation with the increased coefficient:

$$P = (-833 t_{\text{insul}} e^{-60 t_{\text{panel}} \Delta} + 833 t_{\text{insul}})/t_{\text{insul}}^{0.85} . \quad (18)$$

The load versus displacement plot along with the curve-fit Equation (18) can be seen in Figure 39.

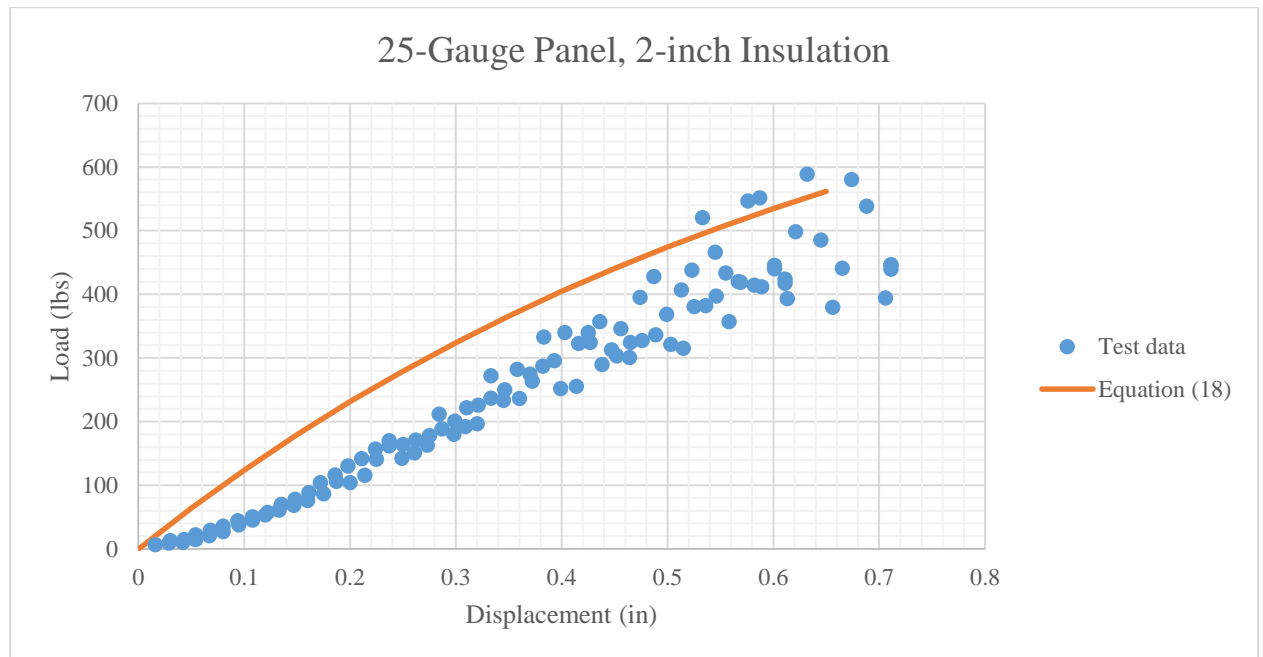


Figure 39: 25-Gauge Panel, 2-inch Insulation Load versus Displacement Plot with Exponential Curve (2.5-inch Flange).

It was decided that Equation (17) and (18) fit the test data well enough to be implemented into the finite element model. Since the CFS stud used in the study by Leonardelli had a 2-inch flange [3], a similar ratio increase to that done for the 2.5-inch flange was performed. This result can be seen in Equation (19):

$$P = (-667 t_{\text{insul}} e^{-60 t_{\text{panel}} \Delta} + 667 t_{\text{insul}})/t_{\text{insul}}^{0.85} . \quad (19)$$

The derivative of Equation (19) is the stiffness of the insulation strut. This stiffness is shown in Equation (20):

$$k = (667 t_{\text{insul}} 60 t_{\text{panel}} e^{-60 t_{\text{panel}} \Delta})/t_{\text{insul}}^{0.85} . \quad (20)$$

3.3 Mathcad Implementation

Mathcad 15 was used to implement the finite element model. There were two primary reasons for using Mathcad 15 in place of a more advanced programming language. First, the author was more familiar with Mathcad than the other languages. Second, it was known that Mathcad had the capability to model the geometric and material nonlinearities involved in the model.

Each element was input into Mathcad separately. Along with the stiffness matrix, a location vector (LV) was created for each element. The location vector identified which DOF's were supports on the element, and which were free to displace or rotate. The non-support DOF's had a number entered in the location vector, which was the label of the DOF in the nonzero displacement model. An example LV for a cantilever beam can be

seen in Figure 40. The DOF's for the end in the fixed support has all zero inputs in the LV and the free end has number inputs to match the DOF numbers in the nonzero displacement model.

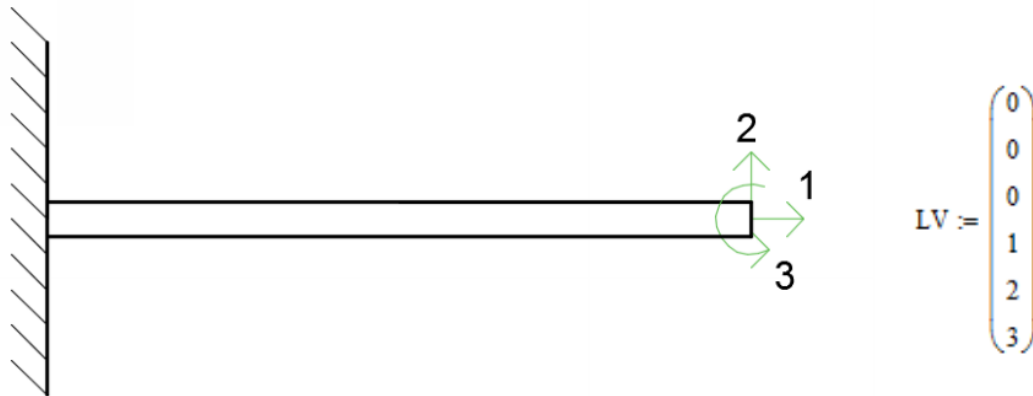


Figure 40: Cantilever Beam Location Vector Example.

A series of programmed functions were implemented into Mathcad to automate the model as much as possible. Figure 41 shows the function to create a frame element stiffness matrix based on the modulus of elasticity (E), area (A), moment of inertia (I) and length (L) of the element.

$$\text{Beam_2D}(E, A, I, L) \equiv \begin{pmatrix} \frac{A \cdot E}{L} & 0 & 0 & \frac{-A \cdot E}{L} & 0 & 0 \\ 0 & \frac{12 \cdot E \cdot I}{L^3} & \frac{6 \cdot E \cdot I}{L^2} & 0 & \frac{-12 \cdot E \cdot I}{L^3} & \frac{6 \cdot E \cdot I}{L^2} \\ 0 & \frac{6 \cdot E \cdot I}{L^2} & \frac{4 \cdot E \cdot I}{L} & 0 & \frac{-6 \cdot E \cdot I}{L^2} & \frac{2 \cdot E \cdot I}{L} \\ \frac{-A \cdot E}{L} & 0 & 0 & \frac{A \cdot E}{L} & 0 & 0 \\ 0 & \frac{-12 \cdot E \cdot I}{L^3} & \frac{-6 \cdot E \cdot I}{L^2} & 0 & \frac{12 \cdot E \cdot I}{L^3} & \frac{-6 \cdot E \cdot I}{L^2} \\ 0 & \frac{6 \cdot E \cdot I}{L^2} & \frac{2 \cdot E \cdot I}{L} & 0 & \frac{-6 \cdot E \cdot I}{L^2} & \frac{4 \cdot E \cdot I}{L} \end{pmatrix}$$

Figure 41: Frame Element Stiffness Matrix Programmed Function [12].

The next programmed function in Mathcad, seen in Figure 42, begins the process of creating a global stiffness matrix for the screw connection. The “Zero_Matrix” function creates a matrix populated with all zeroes based on the “nrow” and “ncol” inputs. The values for “nrow” and “ncol” correlate to the number of DOF’s that are free to displace or rotate when subject to an external force.

$$\text{Zero_Matrix}(\text{nrow}, \text{ncol}) \equiv \begin{array}{l} \text{for } i \in 1.. \text{nrow} \\ \quad \text{for } j \in 1.. \text{ncol} \\ \quad \quad z_{i,j} \leftarrow 0 \\ \quad z \end{array}$$

Figure 42: "Zero_Matrix" Programmed Equation [12].

Figure 43 shows the function used to assemble the global stiffness matrix by combining the element stiffness matrices. The “LV” input is the location vector for each element while “keg” is the matrix for each element.

$$\text{Assem_Matrix}(K, \text{keg}, LV) \equiv \left| \begin{array}{l} \text{for } ie \in 1..\text{rows}(\text{keg}) \\ \quad \text{for } je \in 1..\text{cols}(\text{keg}) \\ \quad \quad \text{if } (LV_{ie} \neq 0) \cdot (LV_{je} \neq 0) \\ \quad \quad \quad i \leftarrow LV_{ie} \\ \quad \quad \quad j \leftarrow LV_{je} \\ \quad \quad \quad K_{i,j} \leftarrow K_{i,j} + \text{keg}_{ie,je} \\ K \end{array} \right.$$

Figure 43: Global Matrix Assembly Programmed Function [12].

A programmed function was created to make element displacement vectors from the global displacement vector. The LV for the element tells the function which displacement to take from the global displacement vector and insert into the element displacement vector. This function can be seen in Figure 44.

$$\text{Elem_Disp}(u, LV) \equiv \left| \begin{array}{l} \text{for } ie \in 1..\text{length}(LV) \\ \quad \text{if } (LV_{ie} \neq 0) \\ \quad \quad i_g \leftarrow LV_{ie} \\ \quad \quad v_{ie} \leftarrow u_{i_g} \\ \quad v_{ie} \leftarrow 0 \text{ otherwise} \\ v \end{array} \right.$$

Figure 44: Element Displacement Vector Function [12].

The next set of programmed functions in Mathcad are used to find the internal forces in each element. Figures 45 and 46 show the programmed equation for the CFS stud and panel. These functions include the material nonlinearity found in the plate elements. Element forces are found by inputting the previous displacement of the

element, initial stiffness of the element, the ratio of initial stiffness to plastic moment “a” and the Exponential Power Factor (EPF). The initial stiffness and plastic moment are modified values from *Roark's* [11]. The EPF value is used to modify the moment-rotation relationship. See 4.1.1 for more information on the EPF adjustment. The moment equation developed from *Roark's* [11] was used to find the element forces for the plates. Only the nonzero displacement DOF has the moment equation, the DOF with zero displacement has a zero input for the element force.

$$\text{Elem_Forces1}(u,k,a,\text{EPF}) \equiv \left| \begin{array}{l} \beta \leftarrow 0 \\ \alpha \leftarrow 0 \\ \theta_1 \leftarrow u_1 \\ \Delta\theta_1 \leftarrow \theta_1 - \alpha \\ \theta_2 \leftarrow u_2 \\ \Delta\theta_2 \leftarrow \theta_2 - \alpha \\ u_e \leftarrow \begin{pmatrix} \Delta\theta_1 \\ \Delta\theta_2 \end{pmatrix} \\ M_n \leftarrow \frac{-k}{a} \cdot e^{-a \cdot |u_{e2}|} \cdot \text{EPF} + \frac{k}{a} \\ f_e \leftarrow \begin{pmatrix} 0 \\ M_n \end{pmatrix} \\ f_e \leftarrow f_e \\ f_e \end{array} \right|$$

Figure 45: Element Forces Function for the CFS Stud.


```

Elem_Forces3(u,k,a,EPF) ≡
|
β ← 0
α ← 0
θ1 ← u1
Δθ1 ← θ1 - α
θ2 ← u2
Δθ2 ← θ2 - α
ue ←  $\begin{pmatrix} \Delta\theta1 \\ \Delta\theta2 \end{pmatrix}$ 
Mn ←  $\frac{-k}{a} \cdot e^{-a \cdot |ue_1|} \cdot EPF + \frac{k}{a}$ 
fe ←  $\begin{pmatrix} M_n \\ 0 \end{pmatrix}$ 
fe ← fe
fe

```

Figure 46: Element Forces Function for the Panel.

Figure 47 shows the element force program for the insulation strut. The force in the insulation strut (P_c) is the equation found from the CFS stud insulation testing which includes the material nonlinearity. Like the plate element, an input of zero is input for the zero displacement DOF.

$$\text{Elem_Forces4}(u, le, t) \equiv \left| \begin{array}{l} le2 \leftarrow \sqrt{(u_2 + le - u_1)^2} \\ \beta_0 \leftarrow 0 \\ \alpha \leftarrow 0 \\ \Delta x1 \leftarrow 0 \\ \Delta x2 \leftarrow le2 - le \\ ue \leftarrow \begin{pmatrix} \Delta x1 \\ \Delta x2 \end{pmatrix} \\ Pc \leftarrow \frac{-667 \cdot 1e \cdot e^{-t \cdot |ue_2| \cdot .60} + 667 \cdot 1e}{1000(le^{0.85})} \\ fe \leftarrow \begin{pmatrix} 0 \\ -Pc \end{pmatrix} \\ fe \end{array} \right|$$

Figure 47: Element Forces Function for the Insulation Strut.

The final element force function is for the screw element. This function also implements the corotational formulation for the geometric nonlinearity. Because the screw does not have material nonlinearity, the force is found by multiplying the stiffness matrix by the displacement vector. Figure 48 shows the programmed function for the screw element.

$$\begin{aligned}
 \text{Elem_Forces2}(u, le, E, A, I) \equiv & \begin{aligned}
 & le2 \leftarrow \sqrt{(u_4 + le)^2 + (u_5)^2} \\
 & \beta_0 \leftarrow 0 \\
 & \beta_1 \leftarrow \arcsin\left(\frac{u_5}{le2}\right) \\
 & \alpha \leftarrow \beta_1 - \beta_0 \\
 & \theta_1 \leftarrow u_3 \\
 & \Delta\theta_1 \leftarrow \theta_1 - \alpha \\
 & \Delta x_1 \leftarrow 0 \\
 & \Delta y_1 \leftarrow 0 \\
 & \theta_2 \leftarrow u_6 \\
 & \Delta\theta_2 \leftarrow \theta_2 - \alpha \\
 & \Delta x_2 \leftarrow le2 - le \\
 & \Delta y_2 \leftarrow 0 \\
 & ue \leftarrow \begin{pmatrix} \Delta x_1 \\ \Delta y_1 \\ \Delta\theta_1 \\ \Delta x_2 \\ \Delta y_2 \\ \Delta\theta_2 \end{pmatrix} \\
 & T \leftarrow \begin{pmatrix} \cos(\beta_1) & \sin(\beta_1) & 0 & 0 & 0 & 0 \\ -\sin(\beta_1) & \cos(\beta_1) & 0 & 0 & 0 & 0 \\ 0 & 0 & 1 & 0 & 0 & 0 \\ 0 & 0 & 0 & \cos(\beta_1) & \sin(\beta_1) & 0 \\ 0 & 0 & 0 & -\sin(\beta_1) & \cos(\beta_1) & 0 \\ 0 & 0 & 0 & 0 & 0 & 1 \end{pmatrix} \\
 & ke \leftarrow \begin{pmatrix} \frac{A \cdot E}{le} & 0 & 0 & \frac{-A \cdot E}{le} & 0 & 0 \\ 0 & \frac{12 \cdot E \cdot I}{le} & \frac{6 \cdot E \cdot I}{le^2} & 0 & \frac{-12 \cdot E \cdot I}{le^3} & \frac{6 \cdot E \cdot I}{le^2} \\ 0 & \frac{6 \cdot E \cdot I}{le^2} & \frac{4 \cdot E \cdot I}{le} & 0 & \frac{-6 \cdot E \cdot I}{le^2} & \frac{2 \cdot E \cdot I}{le} \\ \frac{-A \cdot E}{le} & 0 & 0 & \frac{A \cdot E}{le} & 0 & 0 \\ 0 & \frac{-12 \cdot E \cdot I}{le^3} & \frac{-6 \cdot E \cdot I}{le^2} & 0 & \frac{12 \cdot E \cdot I}{le^3} & \frac{-6 \cdot E \cdot I}{le^2} \\ 0 & \frac{6 \cdot E \cdot I}{le^2} & \frac{2 \cdot E \cdot I}{le} & 0 & \frac{-6 \cdot E \cdot I}{le^2} & \frac{4 \cdot E \cdot I}{le} \end{pmatrix} \\
 & fe \leftarrow ke \cdot ue \\
 & fe \leftarrow T^T \cdot fe \\
 & fe
 \end{aligned}
 \end{aligned}$$

Figure 48: Element Forces Function for the Screw.

Figures 49, 50 and 51 show the element stiffness functions for the CFS stud, panel and insulation strut. These functions are similar to the functions used for the element forces. The differences include the use of the stiffness equation instead of the force equations and creating two by two matrices for the plates and insulation. Figure 52 shows the stiffness function for the screw. The screw stiffness function ignored all displacement except the rigid body rotation of the screw. The function used the rigid body rotation to transform the stiffness matrix from the element orientation to match the global orientation.

$$\text{Stiffness1}(\mathbf{u}, \mathbf{k}, \mathbf{a}, \text{EPF}) \equiv \left| \begin{array}{l} \beta \leftarrow 0 \\ \alpha \leftarrow 0 \\ \theta_1 \leftarrow \mathbf{u}_1 \\ \Delta\theta_1 \leftarrow \theta_1 - \alpha \\ \theta_2 \leftarrow \mathbf{u}_2 \\ \Delta\theta_2 \leftarrow \theta_2 - \alpha \\ \mathbf{u}_e \leftarrow \begin{pmatrix} \Delta\theta_1 \\ \Delta\theta_2 \end{pmatrix} \\ k_n \leftarrow \text{EPF} \cdot k \cdot e^{-a \cdot |\mathbf{u}_e|} \cdot \text{EPF} \\ k_e \leftarrow \begin{pmatrix} k_n & -k_n \\ -k_n & k_n \end{pmatrix} \\ \mathbf{K} \leftarrow k_e \\ \mathbf{K} \end{array} \right.$$

Figure 49: Stiffness Function for the CFS Stud.

$$\text{Stiffness3}(u, k, a, \text{EPF}) \equiv \left| \begin{array}{l} \beta \leftarrow 0 \\ \alpha \leftarrow 0 \\ \theta 1 \leftarrow u_1 \\ \Delta \theta 1 \leftarrow \theta 1 - \alpha \\ \theta 2 \leftarrow u_2 \\ \Delta \theta 2 \leftarrow \theta 2 - \alpha \\ \text{ue} \leftarrow \begin{pmatrix} \Delta \theta 1 \\ \Delta \theta 2 \end{pmatrix} \\ k_n \leftarrow \text{EPF} \cdot k \cdot e^{-a \cdot |\text{ue}_1|} \cdot \text{EPF} \\ k_e \leftarrow \begin{pmatrix} k_n & -k_n \\ -k_n & k_n \end{pmatrix} \\ K \leftarrow k_e \\ K \end{array} \right|$$

Figure 50: Stiffness Function for the Panel.

$$\text{Stiffness4}(u, l_e, t) \equiv \left| \begin{array}{l} l_{e2} \leftarrow \sqrt{(u_2 + l_e - u_1)^2} \\ \beta_o \leftarrow 0 \\ \alpha \leftarrow 0 \\ \Delta x 1 \leftarrow 0 \\ \Delta x 2 \leftarrow l_{e2} - l_e \\ \text{ue} \leftarrow \begin{pmatrix} \Delta x 1 \\ \Delta x 2 \end{pmatrix} \\ k_c \leftarrow \frac{667 \cdot l_e \cdot 60 \cdot t \cdot e^{-t \cdot |\text{ue}_2|} \cdot 60}{1000(l_e^{0.85})} \\ k_e \leftarrow \begin{pmatrix} k_c & -k_c \\ -k_c & k_c \end{pmatrix} \\ K \leftarrow k_e \\ K \end{array} \right|$$

Figure 51: Stiffness Function for the Insulation Strut.

$$\begin{aligned}
 \text{Stiffness2}(u, l_e, k_e) \equiv & \left| \begin{aligned}
 l_{e2} &\leftarrow \sqrt{(u_4 + l_e)^2 + (u_5)^2} \\
 \beta_1 &\leftarrow \text{asin}\left(\frac{u_5}{l_{e2}}\right) \\
 T &\leftarrow \begin{pmatrix} \cos(\beta_1) & \sin(\beta_1) & 0 & 0 & 0 & 0 \\ -\sin(\beta_1) & \cos(\beta_1) & 0 & 0 & 0 & 0 \\ 0 & 0 & 1 & 0 & 0 & 0 \\ 0 & 0 & 0 & \cos(\beta_1) & \sin(\beta_1) & 0 \\ 0 & 0 & 0 & -\sin(\beta_1) & \cos(\beta_1) & 0 \\ 0 & 0 & 0 & 0 & 0 & 1 \end{pmatrix} \\
 K &\leftarrow T^T \cdot k_e \cdot T \\
 K
 \end{aligned} \right.
 \end{aligned}$$

Figure 52: Stiffness Function for the Screw.

In order to determine when the model converged, two error equations were used. The first error equation -- Equation (21) -- is the square root of the internal forces squared divided by the external force squared. The second error equation -- Equation (22) -- finds the sum of the work done by the internal forces and divides it by the work done by the external force. These terms would be zero once the model converged, but in practice it was assumed that the when both error equations produced values less than 0.001, the model had sufficiently converged. The subscripts in Equation (22) are the DOF numbers:

$$\text{Error} = \sqrt{(\Delta P^2 / F^2)}, \quad (21)$$

$$\text{Error} = [\Sigma (\Delta P_i U_i) / (F U_3)]. \quad (22)$$

3.3.1 Geometric Nonlinearity Verification

Visual Analysis was used to validate the geometric nonlinear portion of the Mathcad model. Figure 53 shows the Visual Analysis model. The connection model input

in Visual Analysis followed the load-controlled model. The top model was used to verify the base iteration, while the bottom was used to verify the first iteration of geometric nonlinearity. Custom properties were input for the members in Visual Analysis to match those used in the Mathcad model. The rotational elements were input as springs in Visual Analysis. The base iteration has the external vertical force at DOF 3 in the reduced model. The first iteration applied the unbalanced forces ΔP . Displacements for both the base iteration and the first iteration matched those found in the Mathcad model.

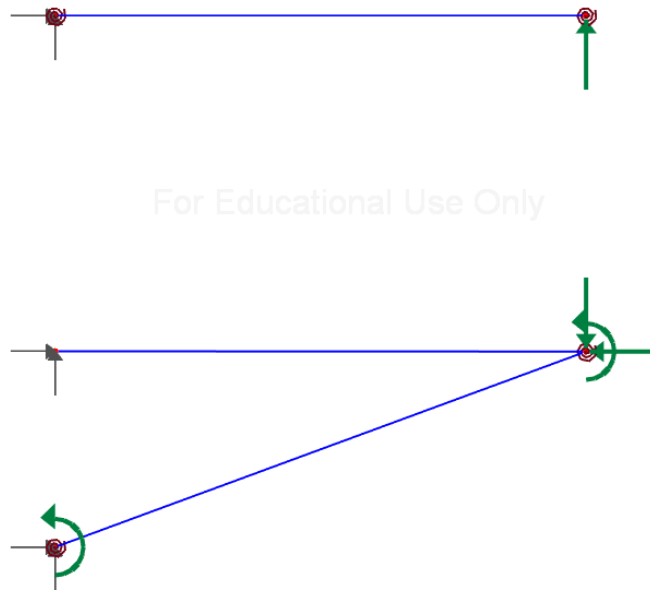


Figure 53: Visual Analysis Verification Model for the Base Iteration (Top) and the First Iteration (Bottom).

3.3.2 Load-Controlled Model

When the model was initially set up it was designed to be a load-controlled analysis. In this type of analysis, a fixed amount of external load is applied in each load-step and iterations are completed in each load step. The Newton-Raphson method, in

which the structure stiffness is updated with each iteration, is used to iterate equilibrium at each load step [13]. With each load step, a base iteration must be run in order to start the iterations. The base iteration is a traditional finite element analysis and does not take into account geometric nonlinearity. An example load versus displacement plot with three iterations for each load step can be seen in Figure 54.

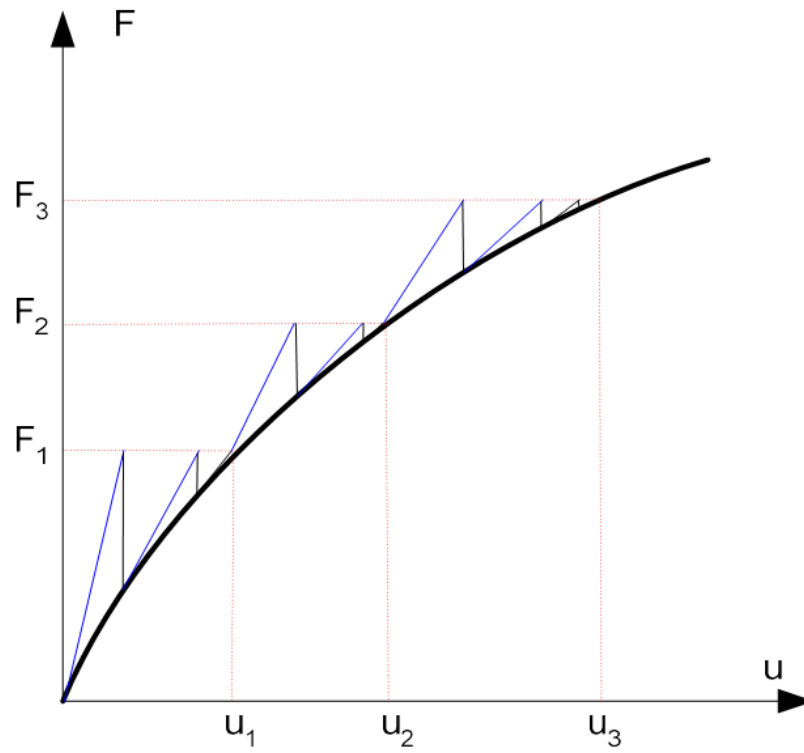


Figure 54: Load-Controlled Analysis Load versus Displacement Graph [10].

The load-controlled analysis was not able to converge when the CFS stud and panel yielded. The area of non-convergence for load-controlled analysis is circled in Figure 55. Another issue with the load-controlled analysis was the large number of iterations in each load step. Over twenty iterations were needed for the load steps to converge. For these reasons, the load-controlled analysis was not implemented into the final model.

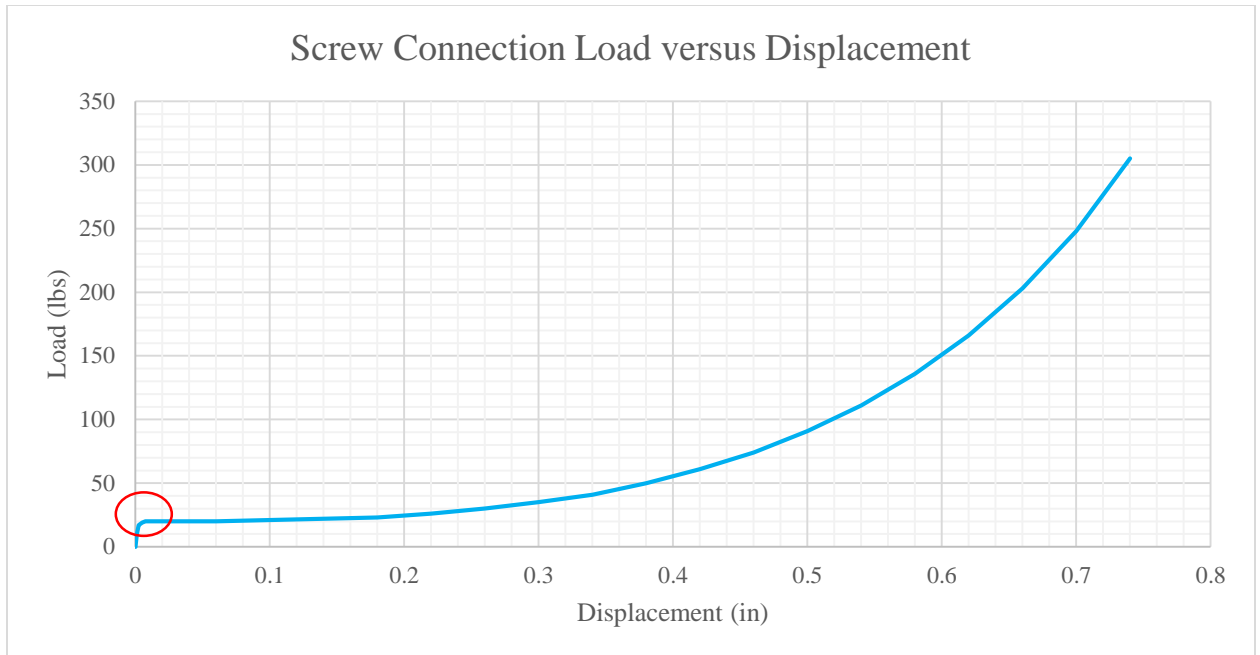


Figure 55: Load versus Displacement Graph with Area of Non-Convergence Circled.

3.3.3 Displacement-Controlled Model

The finite element model was changed to displacement-controlled analysis in order to have the model converge where plate yielding occurs. This method treats the key DOF (in this case DOF 3) as a support with a support settlement rather than a typical non-zero displacement DOF. Instead of entering a load, a displacement is entered and the iterations begin immediately without a base iteration. The advantage of the displacement-controlled analysis is that the convergence takes place with fewer iterations than the load-controlled analysis. The model still uses the Newton-Raphson method with the displacement-controlled analysis because the stiffness matrix is recalculated within each iteration. The only difference is the model is now held at a constant displacement instead of a constant force.

Section 4 - Using the Model

4.1 Calibrating the Model

Adjustments were made to the properties of the finite element model in order to make the analysis more realistic. The most significant modification made was to the thickness of the panel. Leonardelli's thickness the 16-gauge panel, 0.0565 inches [3], matched the measured thickness of the panel in this study. However, Leonardelli's thickness for the 25-gauge panel, 0.0180 inches [3], did not match the measured thickness in this study. The measured thickness for the 25-gauge panel was 0.0240 inches and this thickness was used in the finite element model. The panels used by Leonardelli were ASTM 1003 (ASTM 2013) designation ST50H ($F_y=50$ ksi, $F_u=66$ ksi).

The CFS studs used in the Leonardelli study were either ST33H (0.0451 inch; $F_y=33$ ksi, $F_u=45$ ksi) or ST50H (0.0713 inch and 0.1017 inch; $F_y=50$ ksi, $F_u=66$ ksi) [3]. The AISI designations for the CFS stud are 600S200-97, 600S200-68, and 600S200-43 [3]. Table 2 shows each connection type tested by Leonardelli with the material properties input into the finite element model.

The screws used by Leonardelli were Grabber Construction Products Hex-Head Drivall Self-Drilling screws [3]. Table 3 shows geometric properties of the different screw typed used in by Leonardelli with the maximum tension and shear load for the screw. It should be noted that Leonardelli's geometric properties of screws came from the *AISI North American Specification* Table C-E4-1 [1]. These properties do not match those published in ICC-ES evaluation report for the screw [14]. The ICC-ES evaluation is outdated and the difference in the geometric properties was small, so for those reasons the AISI North American Specification geometric properties were used. The strength

properties in the ICC-ES evaluation were the only available published strengths so those will be used in the finite element model.

Table 2: Connection Types and Material Properties.

Type	Insul. t (in.)	t₁ (in.)	F_{y1} (ksi)	F_{u1} (ksi)	t₂ (in.)	F_{y2} (ksi)	F_{u2} (ksi)	Screw
13	1	0.0451	33	45	0.0240	50	66	10
14	1	0.0451	33	45	0.0240	50	66	12
15	1	0.0451	33	45	0.0565	50	66	10
16	1	0.0451	33	45	0.0565	50	66	12
17	1	0.0713	50	66	0.0240	50	66	10
18	1	0.0713	50	66	0.0240	50	66	12
19	1	0.0713	50	66	0.0565	50	66	10
20	1	0.0713	50	66	0.0565	50	66	12
21	1	0.1017	50	66	0.0240	50	66	10
22	1	0.1017	50	66	0.0240	50	66	12
23	1	0.1017	50	66	0.0565	50	66	10
24	1	0.1017	50	66	0.0565	50	66	12
25	2	0.0451	33	45	0.0240	50	66	12
26	2	0.0451	33	45	0.0240	50	66	14
27	2	0.0451	33	45	0.0565	50	66	12
28	2	0.0451	33	45	0.0565	50	66	14
29	2	0.0713	50	66	0.0240	50	66	12
30	2	0.0713	50	66	0.0240	50	66	14
31	2	0.0713	50	66	0.0565	50	66	12
32	2	0.0713	50	66	0.0565	50	66	14
33	2	0.1017	50	66	0.0240	50	66	12
34	2	0.1017	50	66	0.0240	50	66	14
35	2	0.1017	50	66	0.0565	50	66	12
36	2	0.1017	50	66	0.0565	50	66	14
49	4	0.0451	33	45	0.0240	50	66	14
50	4	0.0451	33	45	0.0565	50	66	14
51	4	0.0713	50	66	0.0240	50	66	14
52	4	0.0713	50	66	0.0565	50	66	14
53	4	0.1017	50	66	0.0240	50	66	14
54	4	0.1017	50	66	0.0565	50	66	14

Table 3: Grabber Construction Products Screw Properties [1, 14].

Screw	Shaft diameter, d (in.)	Head diameter (in.)	Shear Strength P_{ss} (lbs)	Tension Strength P_{ss} (lbs)
10	0.190	0.413	1910	2455
12	0.216	0.433	2814	2534
14	0.250	0.520	4000	3658

4.1.1 Adjustments to *Roark's* Moment Capacity

The moment capacity and stiffness from *Roark's* were further modified in an attempt to get more accurate results. The adjustments made to the values from the *Roark's* equation can be justified in two ways. First, *Roark's* is for elastic analysis [11] and the finite element model includes inelastic behavior for the plates. Second, the selected case from *Roark's* assumes the trunnion is completely fixed to the plate. This is the most similar to the screw connection, but the screw will never be completely fixed to the plate.

The first modification factor used in the finite element model is the Rotational Plate Stiffness Factor (RPS_{factor}). This factor is a constant of 1.5 that is used to increase from the yield moment to the plastic moment of the plate. Equations (23) and (24) show the calculation of the plastic moment and stiffness. The units for the inputs in Equations (23) and (24) are ksi for E and σ_y and E , and inches for t and a . The other inputs are unitless. The units for k_o are kip-inches per radian, and kip-inches for M_p . Both the stiffness and moment capacity were multiplied by the RPS_{factor} because the stiffness is treated as the derivative of the moment-rotation equation. Figure 56 shows the effect of the RPS_{factor} on the moment-rotation relationship. Equations (23) and (24) are as follows:

$$k_o = RPS_{\text{factor}} E t^3 / \alpha, \quad (23)$$

$$M_p = RPS_{\text{factor}} \sigma_y a t^2 / \beta. \quad (24)$$

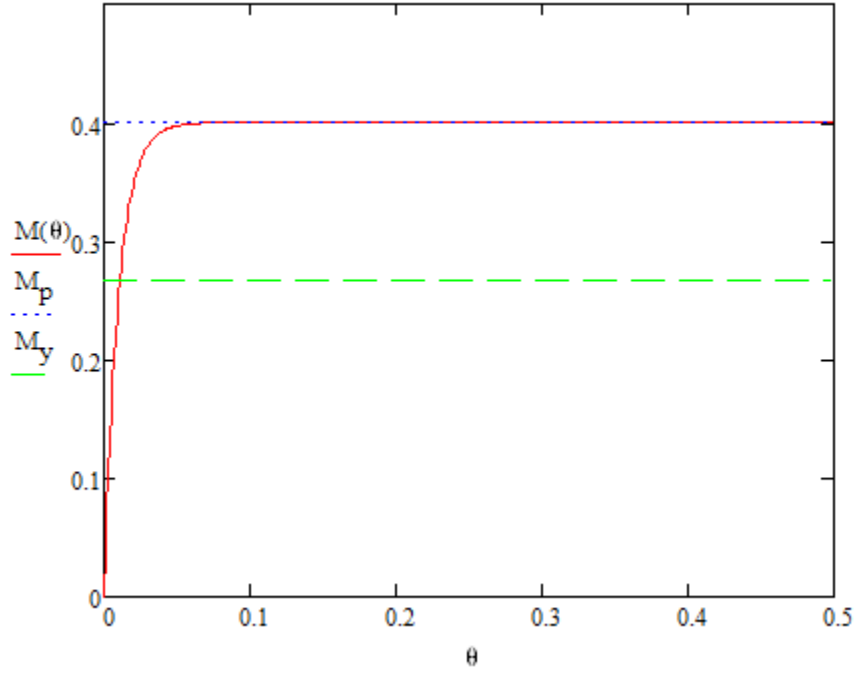


Figure 56: Moment-Rotation Relationship with RPS_{factor} .

The second modification to the moment-rotation relationship is the Exponential Power Factor (EPF). The EPF allows for the plate to reach a higher rotation before becoming fully plastic. The higher rotation is achieved by lowering the stiffness of the plate. Equations 25 and 26 show the EPF implemented into the moment-rotation equations.

$$k = EPF k_o e^{-(k_o/M_y) EPF \theta}, \quad (25)$$

$$M = -M_p * e^{-(k_o/M_y) EPF \theta} + M_p. \quad (26)$$

The EPF value was determined by finding the approximate displacement of yield in the Leonardelli load versus displacement plots. Only connections types 13, 23, 26, 30 and 52 were used to determine the EPF value. The vertical displacement was then used to find the angle of rotation of the screw, θ . This uses only rigid body rotation of the screw and ignores local rotation at each end of the screw. The EPF value was then determined for each connection type by trial and error. The angle of rotation at yield for the CFS stud and sheathing panel were estimated from the moment-rotation plots in Mathcad. A weighted average was found for the angle of rotation by including the thickness of the stud and panel as shown in Equation (27). Once the weighted average was reasonably near the angle of rotation of the screw, the EPF was recorded for the connection. The EPF value was then averaged for each of the connection types and the average value was used for the for all connection types. Table 4 shows the angle of rotations and EPF for each connection type. Equation (27) is:

$$\theta = (t_1 \theta_{t1} + t_2 \theta_{t2}) / (t_1 + t_2) . \quad (27)$$

Table 4: EPF by Connection Type.

Connection Type	Approx. Disp. at Yield (in.)	θ (rad.)	t_1 (in.)	t_2 (in.)	θ of t_1 at Yield (rad)	θ of t_2 at Yield (rad)	θ Average (rad)	EPF
13	0.015	0.015	0.0240	0.0451	0.04	0.0035	0.016	0.3
23	0.015	0.015	0.0565	0.1017	0.035	0.006	0.016	0.275
26	0.04	0.02	0.0240	0.0451	0.05	0.006	0.021	0.3
30	0.05	0.025	0.0240	0.0713	0.075	0.01	0.026	0.2
52	0.06	0.015	0.0565	0.0713	0.03	0.006	0.017	0.35
Average		0.018						0.285

Once the EPF value was determined, it was implemented into the finite element model. The original expectation for the EPF was that the plates would not become fully plastic until a displacement was reached that was large enough to activate the compression strut. This was not the actual outcome, the EPF allowed for greater rotation but the plates reached their plastic moment before the compression strut became significantly engaged. Figure 57 show load versus displacement plot with and without the EPF and RPS_{factor} .

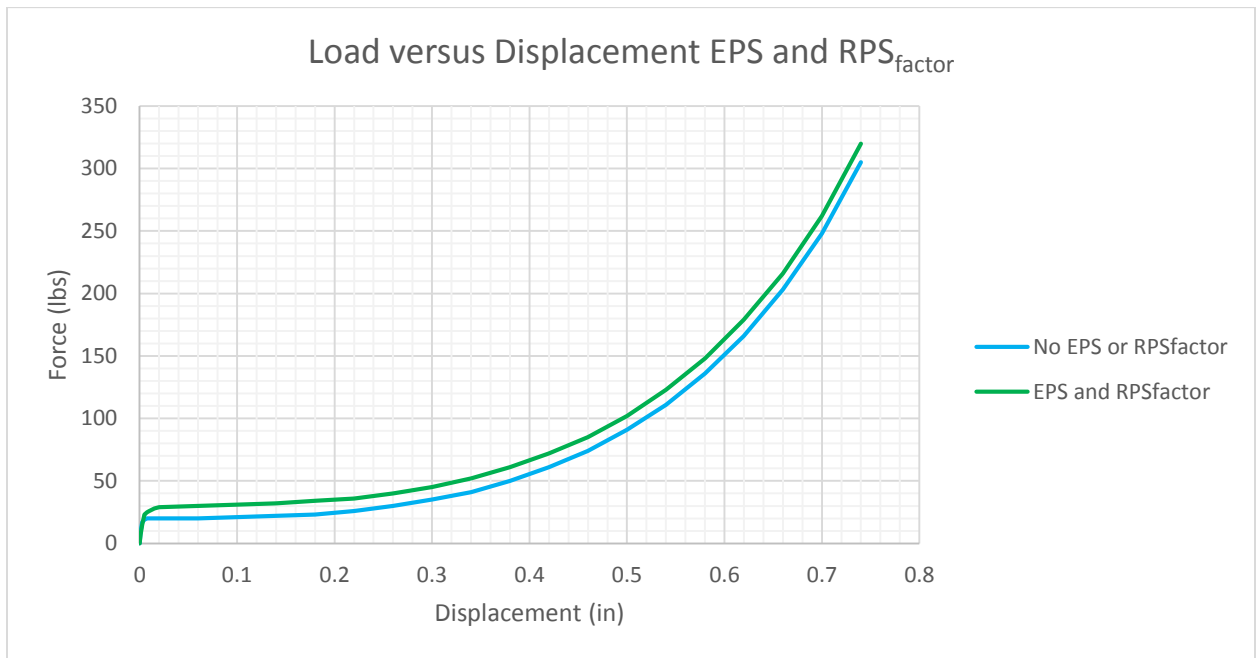


Figure 57: Load versus Displacement Plot Showing EPF and RPS_{factor} Effects.

4.2 Simulation of P-Δ Responses

To validate the model, five load versus displacement plots were created and compared to the load versus displacement plots from Leonardelli test data [3]. These plots demonstrated the different variables in the connection types. Each connection type's load versus displacement relationship was evaluated until it failed by combined shear and

pull-over, combined shear and pull-out, combined shear and tension in the screw, or combined tension and bending in the screw.

Connection type 13 had the 0.0451-inch CFS stud, 0.0240-inch panel, and the number 10 screw with a 1-inch insulation layer. The finite element model predicted failure due to combined shear and pull-out at a displacement of 0.74 inches and a force of 320 pounds. The load versus displacement plot can be seen in Figure 58.

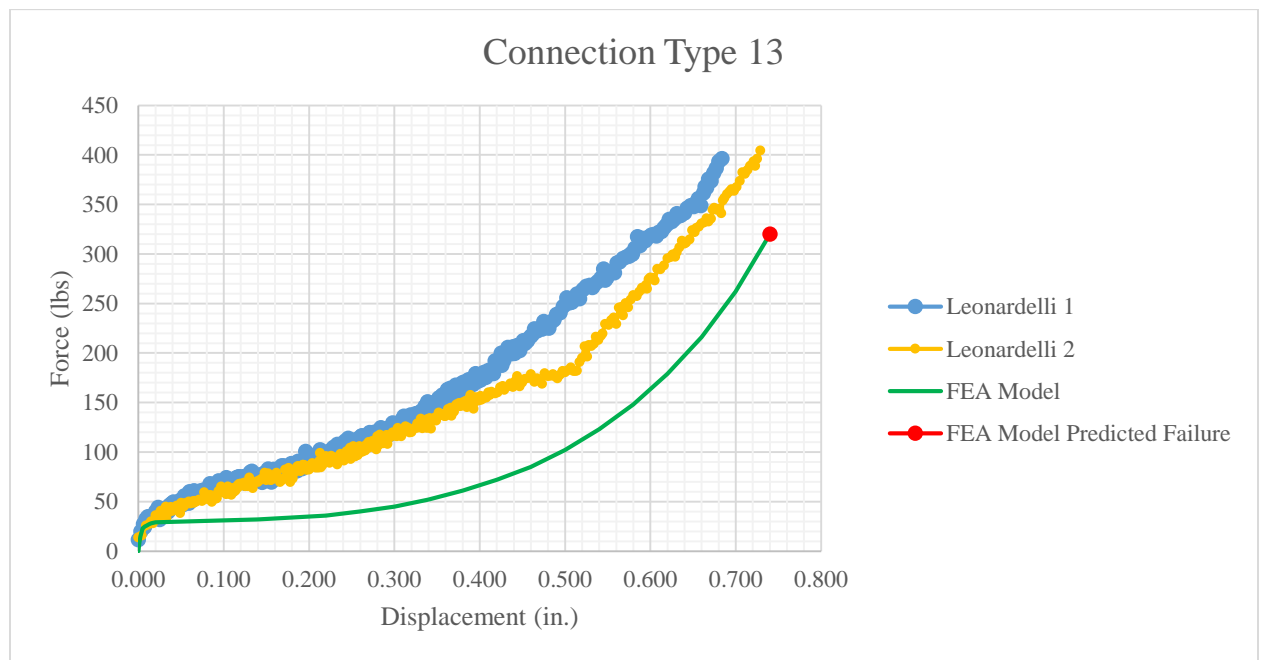


Figure 58: Load versus Displacement Plot for Connection Type 13.

Connection type 23 had the 0.1017-inch CFS stud, 0.0565-inch panel and the number 10 screw with a 1-inch insulation layer. The finite element model predicted failure due to combined tension and bending in the screw at a displacement of 0.008 inches and a force of 98 pounds. Due to the large difference in the failure load and

displacement between the model and Leonardelli's data, the simulation was continued past the failure point. The load versus displacement plot can be seen in Figure 59.

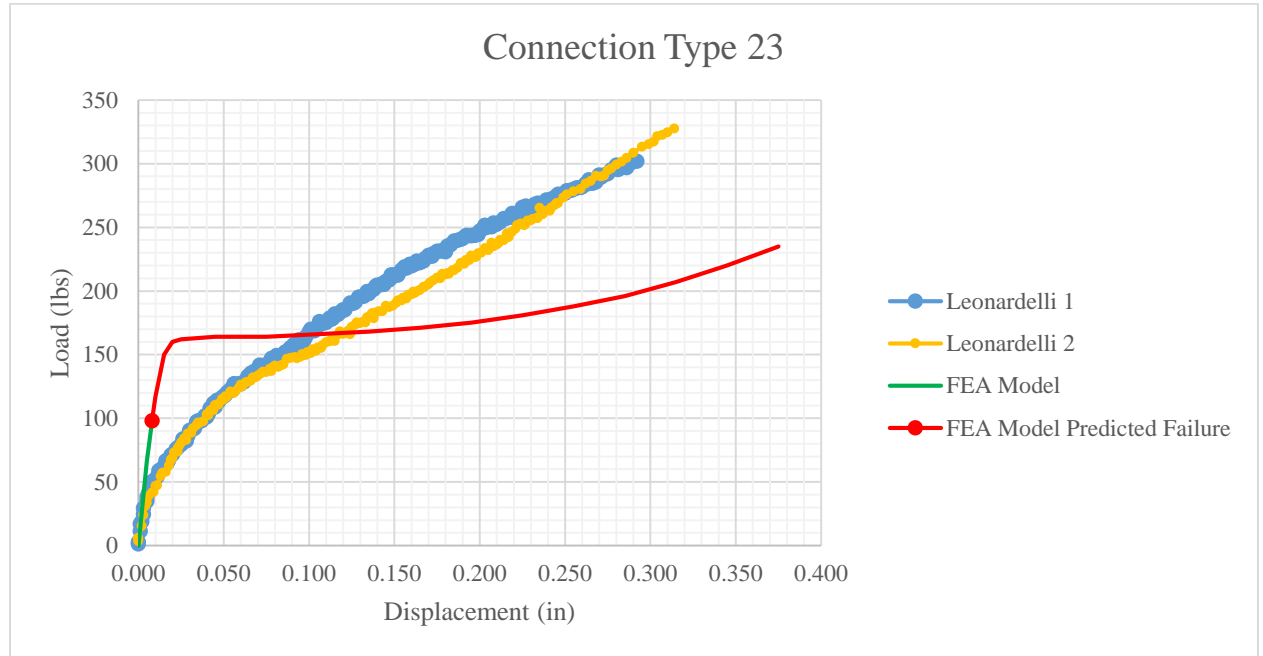


Figure 59: Load versus Displacement Plot for Connection Type 23.

Connection type 26 has the 0.0451-inch CFS stud, 0.0240-inch panel, and the number 14 screw with a 2-inch insulation layer. The finite element model predicted failure due to combined shear and pull-out at a displacement of 1.26 inches and a force of 309 pounds. The load versus displacement plot can be seen in Figure 60.

Connection type 30 has the 0.0713-inch CFS stud, 0.0240-inch panel, and the number 14 screw with a 2-inch insulation layer. The finite element model predicted failure due to combined shear and pull-over at a displacement of 1.655 inches and a force of 862 pounds. The load versus displacement plot can be seen in Figure 61.

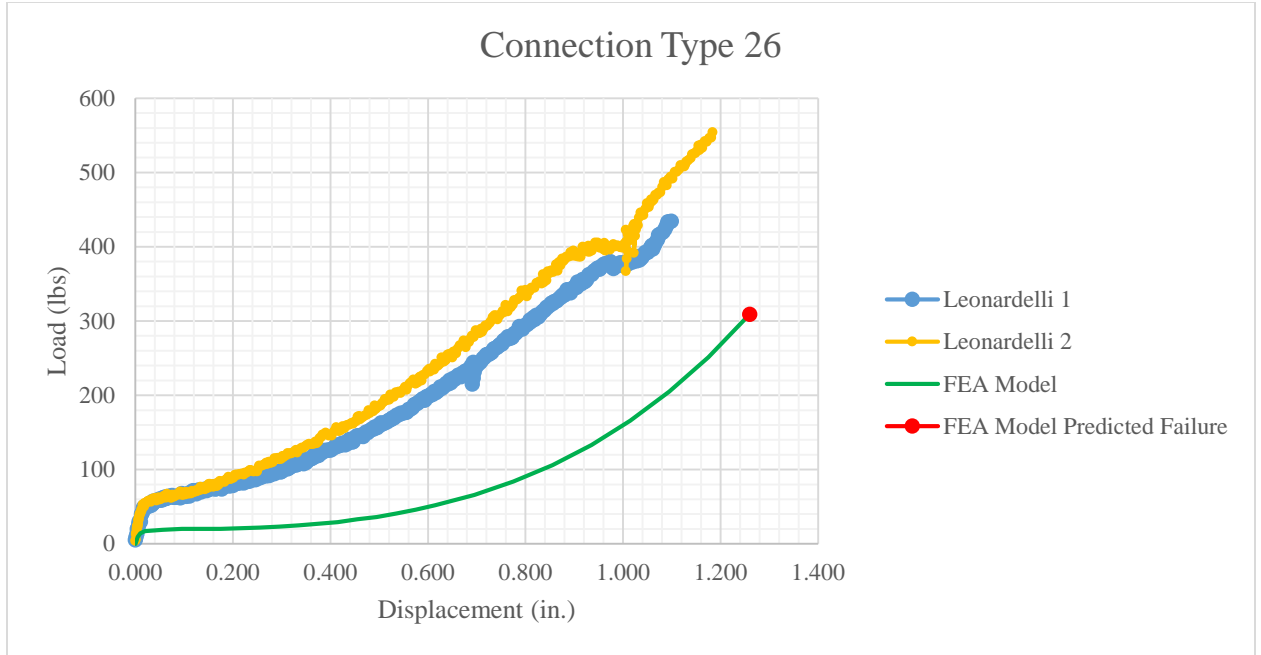


Figure 60: Load versus Displacement Plot for Connection Type 26.

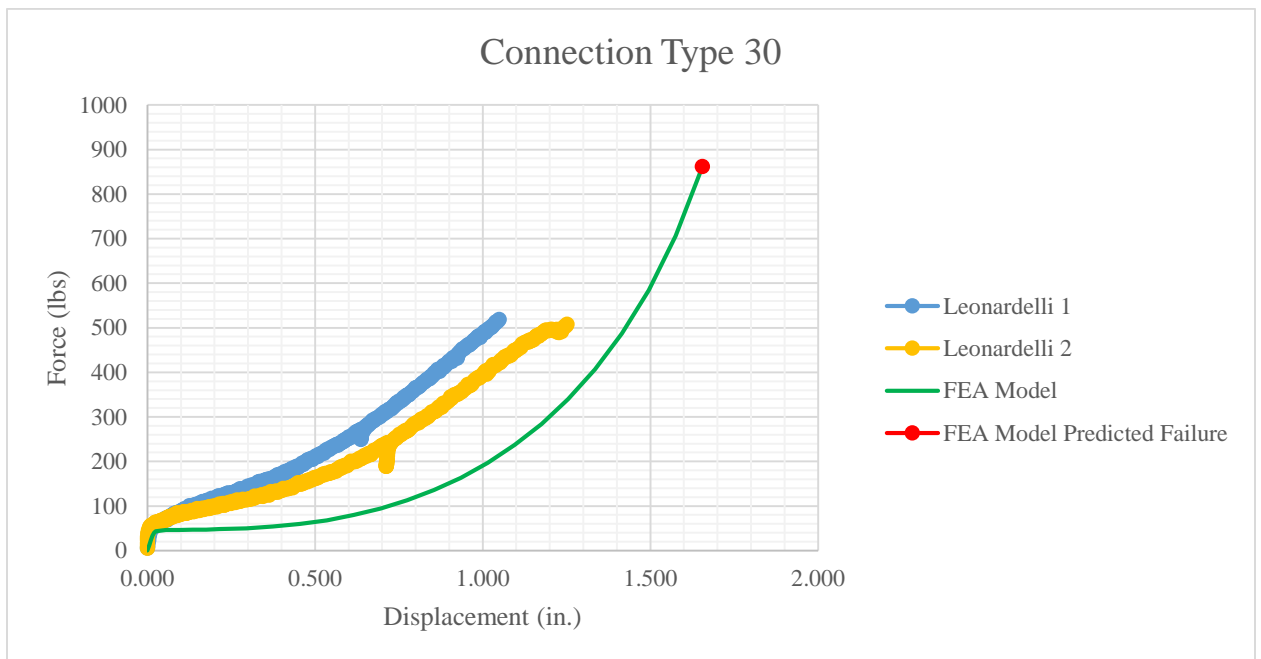


Figure 61: Load versus Displacement Plot for Connection Type 30.

Connection type 52 has the 0.0713-inch CFS stud, 0.0565-inch panel, and the number 14 screw with a 4-inch insulation layer. The finite element model predicted failure due to combined tension and bending in the screw at a displacement of 2.8 inches and a force of 840 pounds. The model continued past the point of failure to show that failure due to combined shear and pull-out occurs at a displacement of 2.9 inches. The closeness of these two failure modes suggests that the real connection type 52 could fail due to either one: combined tension and bending in the screw or combined shear and pull-out. The load versus displacement plot can be seen in Figure 62.

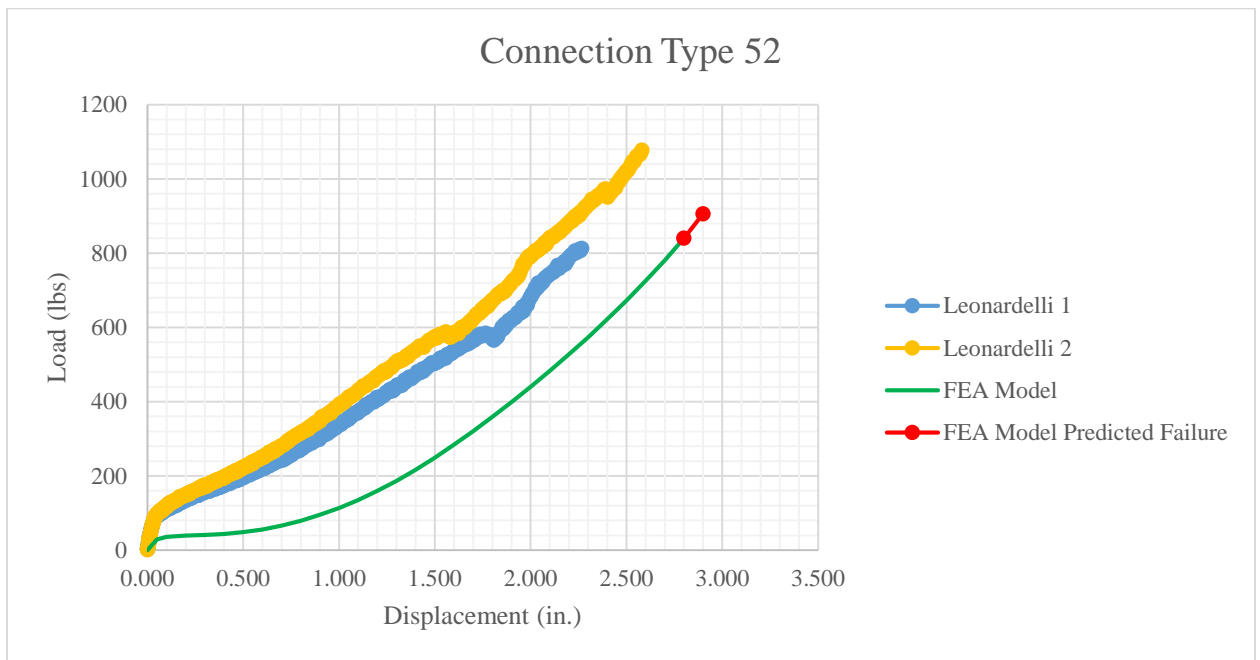


Figure 62: Load versus Displacement Plot for Connection Type 52.

4.3 Strength Prediction of Connection

Each connection type was analyzed in the finite element model to find the failure load and displacement. Each failure was then compared to the failures observed by

Leonardelli [3]. Table 5 shows the failure load, failure displacement and failure mode for each connection type. The subscripts A, B and C refer to the first, second and third trial of testing performed by Leonardelli [3].

Leonardelli used failure mode terminology from AISI S905 *Test Methods for Mechanically Fastened Cold-Formed Steel Connections* [3], as shown in Figure 5. The failure modes that occur for the connection types tested are Type II Failure (Bearing, Tearing, Piling Up), Type IV Failure (Shearing of Fastener), and Type V Failure (Tension Failure of Fastener Through Tilting, Pull-Over, and Pull-Out [6].

The model failure modes are Mode A (combined bending and tension in the screw), Mode B (combined shear and pull-over), Mode C (combined shear and pull-out), and Mode D (combined shear and tension in the screw). Modes A and B correspond to the Leonardelli's Type V failure and modes C and D correspond to the Leonardelli's Type IV failure.

The model did not account for AISI S905 Type I Failure, Type II Failure and Type III failure. Leonardelli did not observe these failure modes [3]. Table 5 compares the Leonardelli data and the data produced by the model for each connection type.

Calculation for combined shear and pull-over (Mode B) and combined shear and pull-out (Mode C) may not be accurate due to limitations on thicknesses in the *North American Specification*. Combined shear and pull-over has a minimum thickness of 0.0285 inches and a maximum of 0.0445 inches for the panel [1]. Neither panel used in the analyzed connection types meet this requirement. Combined shear and pull-out has a minimum thickness of 0.0297 inches and a maximum thickness of 0.0724 inches for the

CFS stud. The CFS stud with a thickness of 0.1017 inches does not meet that requirement.

Table 5: Failure Modes for Each Connection Type [3].

Type	P_A (lbs)	P_B (lbs)	P_C (lbs)	Δ_A (in.)	Δ_B (in.)	Δ_C (in.)	Test Mode	P_{Model} (lbs)	Δ_{Model} (in.)	Model Mode
13	396	404		0.68	0.73		V	320	0.74	C
14	349	379	462	0.65	0.76	0.75	V	368	0.765	C
15	191	251		0.29	0.31		IV	75	0.023	A
16	472	402	479	0.62	0.62	0.64	V/IV	129	0.33	A
17	482	464		0.65	0.71		V	81	0.25	A
18	569	537	615	0.80	0.76	0.79	121	123	0.41	A
19	364	296		0.38	0.37		IV	118	0.03	A
20	611	523	690	0.63	0.56	0.66	IV	167	0.30	A
21	325	300		0.43	0.38		IV	71	0.01	A
22	584	453		0.78	0.54		IV	86	0.008	A
23	302	327		0.29	0.31		IV	98	0.008	A
24	792	973		0.65	0.72		IV	108	0.006	A
25	410	470		1.17	1.33		V	257	1.19	C
26	434	554		1.10	1.18		V	309	1.26	C
27	544	557		1.19	1.19		V	45	0.18	A
28	521	520		1.08	0.98		IV	250	0.90	C
29	443	417		1.02	1.02		V	75	0.63	A
30	518	508		1.05	1.25		V	862	1.655	B
31	1269	1129		1.65	1.68		V	89	0.42	A
32	650	469		1.21	0.98		IV	1093	0.84	A
33	548	485		0.99	0.94		V	44	0.03	A
34	554	572		1.05	0.96		V	68	0.03	A
35	866	1945		1.19	1.74		IV/V	75	0.03	A
36	1076	1161		1.67	1.45		V	99	0.03	A
49	580	551		2.26	2.04		V	219	1.86	B
50	358	379		1.53	1.24		V	168	1.28	B
51	568	601		1.66	1.82		V	760	2.91	C
52	813	1007		2.27	2.58		V	840	2.8	A
53	675	581		1.91	1.90		V	34	0.11	A
54*	1422	1219		3.18	-		IV	47	0.09	A

* Leonardelli excluded displacement data for Trial B of connection type 54 due to data recording error [3].

Section 5 - Recommendations

Selected results from Table 5 along with the load versus displacement plots for a range of connection types validate the finite element model. However, the finite element model does not give accurate prediction of failure load for a significant amount of connection types. Typically these connection types use thicker CFS studs and sheathing panels and fail due to combined tension and bending in the screw. The finite element model predicts that these failures occur at very low displacement and forces. The most likely reason for this premature failure in the model is the stiffness and yield moment provided by *Roark's Formulas for Stress and Strain* is not accurate for these plates.

As the plates become thicker, the values of α and β from *Roark's Formulas for Stress and Strain* have a more significant effect on the stiffness and yield moment of the plates [7]. The values of α and β are dependent on the b/a ratio measured from the Leonardelli failure photographs [3]. Using the photographs may not be a valid way to determine the b/a ratio. One reason why this may not be valid is that there is no way to prove the CFS stud and sheathing panel are fully yielded in the photo. The photographs also show a small ring around the screw hole in the CFS stud and panel where drilling may have affected the integrity of the member. Because of these problems, it is recommended that the bending CFS stud wall and sheathing panel be investigated further.

Determining the insulation stiffness by testing with a CFS stud was not accurate for these connection types. The primary reason for this inaccuracy is that the CFS stud used for insulation testing had a flange thickness of 1.5 inches and 2.5 inches, but the flange width of the studs used by Leonardelli was 2 inches. Another issue is the insulation testing performed in this study had a limited scope of XPS insulation with

thickness of 1 inch, 2 inches and 4 inches. Other types of insulation are used with CFS systems.

The stiffness of the insulation in the model was found from limited test data and did not have a formal regression analysis performed. The stiffness equation was simply curve-fit, leading to inaccuracy in the model. It is recommended that testing be performed with multiple CFS stud flange widths, insulation thicknesses of 1 inch to 4 inches, and multiple panel types. A regression analysis should be performed on the insulation stiffness test data found in the test program in order to get a more accurate stiffness equation.

With further research, the finite element model may be able to accurately predict the maximum load and displacement of all types of the CFS screw connection.

References

- [1] American Iron and Steel Institute (AISI). 2012. *North American Specification for the Design of Cold-Formed Steel Structural Members: 2012 Edition*. AISI S100-2012. Washington, DC: American Iron and Steel Institute.

- [2] Leonardelli, Anthony, Douglas Stahl, Cristopher D. Moen. “The Effect of Rigid Board Insulation on Screw Connections in Cold-Formed Steel”. In AEI Conference. 24-27 March 2015. *AEI 2015: Birth and Life of the Integrated Building*. Milwaukee, Wisconsin: American Society of Civil Engineers, pp. 219-229.

- [3] Leonardelli, Anthony J. 2014. “The Effect of Rigid Board Insulation on Screw Connections in Cold-Formed Steel”. Master’s thesis, Milwaukee School of Engineering.

- [4] Aune, Petter; Marcia Patton-Mallory. March 1986. *Lateral Load-Bearing Capacity of Nailed Joints Based on the Yield Theory; Theoretical Development*. Technical Report FPL-469. Madison, Wisconsin: Forest Products Laboratory, Forest Service, U.S. Department of Agriculture.

- [5] Aune, Petter; Marcia Patton-Mallory. March 1986. *Lateral Load-Bearing Capacity of Nailed Joints Based on the Yield Theory; Experimental Verification*. Technical Report FPL-470. Madison, Wisconsin: Forest Products Laboratory, Forest Service, U.S. Department of Agriculture.

- [6] American Iron and Steel Institute (AISI). 2012. *Test Methods for Mechanically Fastened Cold-Formed Steel Connection: 2008 Edition with Supplement No. 1, 2011*. AISI S905-08 w/ S1-11. Washington, DC: American Iron and Steel Institute.

- [7] Gao, Tian. 2012. “Direct Strength Method for the Flexural Design of Through-Fastened Metal Building Roof and Wall Systems under Wind Uplift or Suction”. Ph. D. diss., Virginia Polytechnic Institute and State University.

- [8] Yaw, Louie L. 30 November 2009. “2D Corotational Beam Formulation”. Walla Walla University. College Place, WA.

- [9] Parente Jr., E., G.V. Nogueira, M. Meireles Neto, L.S. Moreira. October 2014. “Material and geometric nonlinear analysis of reinforced concrete frames” *Ibracon Structures and Materials Journal* Vol. 7 (5), pp 879-891.

- [10] Spring 2008. “Introduction to Nonlinear Structural Problems”. Class notes from ME-565: Advanced Finite Element Analysis. Hormoz Zareh. Portland State University, Portland, Oregon. Available from Portland State University. ADDRESS: <http://web.cecs.pdx.edu/~hormoz/me565/sp08/lectures/nonlinearity.pdf> [Accessed: 3 May 2015].
- [11] Young, Warren C., Richard G. Budynas. “Flat Plates” 7th. Ed. 2002. *Roark’s Formulas for Stress and Strain*. New York: McGraw-Hill, pp 427-524. Available from UAM Azcapotzalco. ADDRESS: http://materiales.azc.uam.mx/gjl/Clases/MA10_I/Roark%27s%20formulas%20for%20stress%20and%20strain.pdf [Accessed: 27 October 2014].
- [12] Witt, Zane. 25 September 2015. “Finite Element Library Functions.” Class notes from AE-610: Finite Element Analysis. Professor H.P. Huttelmaier. Milwaukee School of Engineering, Milwaukee, Wisconsin. Available from the author.
- [13] McGuire, William, Richard H. Gallagher, Ronald D. Ziemian. “Incremental-Iterative Methods”. 2014. *Matrix Structural Analysis*. 2nd. Ed. Available from Bucknell University. ADDRESS: <http://digitalcommons.bucknell.edu/books/7/> [Accessed: 12 April 2015].

- [14] ICC Evaluation Service. September 2013. *ICC-ES Evaluation Report: Grabber Drivall and Superdrive Self-Drilling Tapping Screws*. Whittier, CA: ICC Evaluation Service, LLC.

Appendix A: Mathcad Worksheet

MSST Screw Model

Connection Type 13

ORIGIN = 1

Adjustment Factors:

$RPS_{factor} := 1.5$

RPS_{factor} is the plate stiffness increase factor

$EPF := 0.285$

EPF lessens the rotational plate stiffness to increase displacement before yield

$$U := \begin{pmatrix} 0 \\ 0 \\ 0 \\ 0 \end{pmatrix}$$

Element #1-Stud

Properties:

$E1 := 29500$ ksi

Blue: Input values

$t1 := 0.0451$ in

Yellow: Output Values

$\sigma_{y1} := 33$ ksi

Green: Interaction Check

$\sigma_{u1} := 45$ ksi

$d_{screw} := 0.190$ in

$P_{ScrewAllow} := 2455$ lbs

$V_{ScrewAllow} := 1910$ lbs

$ba := 0.659031$ Ratio for Roark, observed from Leonardelli failure photos

$a := \frac{d_{screw}}{2 \cdot ba} = 0.144$ in Use ratio and screw diameter to find bending radius a (see Roark)

Roark:

$$\alpha1 := \left[\frac{(ba - 0.6) \cdot (0.035 - 0.084)}{(0.7 - .6)} \right] + 0.084 = 0.055$$

$$\beta1 := \left[\frac{(ba - 0.6) \cdot (0.731 - 1.067)}{(0.7 - .6)} \right] + 1.067 = 0.869$$

$$k_a := \frac{E1 \cdot t1^3}{\alpha1} \cdot RPS_{factor} = 73.704 \text{ k-in/rad} \quad \text{Yield Stiffness}$$

$$M_p := \frac{\sigma_{y1} \cdot a \cdot t1^2}{\beta1} \cdot RPS_{factor} = 0.01671 \text{ k-in} \quad \text{Yield Moment}$$

$$M := M_p$$

Material Nonlinearity:

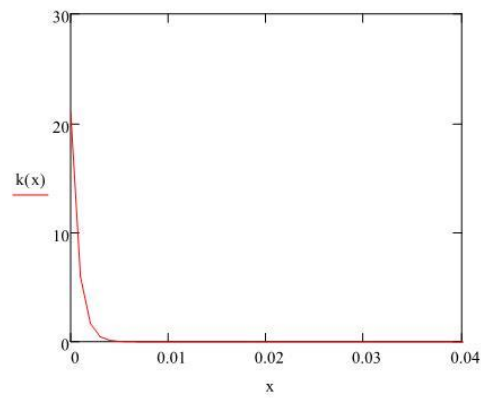
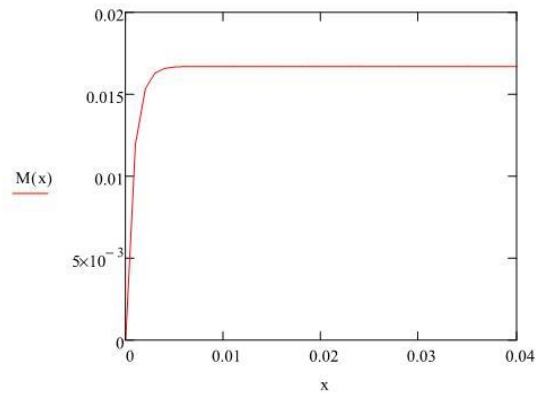
$$x := 0, .001 \dots .5$$

$$a1 := \frac{k_a}{M} \quad \text{Exponential term used in equation below}$$

$$k(x) := EPF \cdot k_a \cdot e^{-a1 \cdot x \cdot EPF} \quad \text{Stiffness - see paper for derivation}$$

$$M(x) := \left(\frac{-ka \cdot e^{-a1 \cdot x} \cdot EPF}{a1} \right) + \frac{ka}{a1} \quad \text{Moment capacity - see paper for derivation}$$

$M(100) = 0.01671$ k-in Yield moment check, should match value M



$k(U_1) = 21.006$ Stiffness at zero rotation/displacement

Element Stiffness Matrix:

$$k1 := \begin{pmatrix} ka & -ka \\ -ka & ka \end{pmatrix} \quad LV1 := \begin{pmatrix} 0 \\ 1 \end{pmatrix}$$

Element #2-ScrewProperties:

$$E2 := 29500 \text{ ksi}$$

$$Le := 1 \text{ in}$$

$$I2 := \frac{\pi \cdot \left(\frac{d_{\text{screw}}}{2} \right)^4}{4} = 6.397 \times 10^{-5} \text{ in}^4$$

$$A2 := \frac{\pi \cdot d_{\text{screw}}^2}{4} = 0.028 \text{ in}^2$$

Element Stiffness Matrix:

$$\theta2 := 0 \text{ rad} \quad \text{original angle of screw}$$

$$T2 := \text{Rot}(\cos(\theta2), \sin(\theta2))$$

$$k2 := \text{Beam_2D}(E2, A2, I2, Le)$$

$$LV2 := \begin{pmatrix} 0 \\ 0 \\ 1 \\ 2 \\ 3 \\ 4 \end{pmatrix}$$

Element #3-Sheathing/PanelProperties:

$$E3 := 29500 \text{ ksi}$$

$$t3 := 0.0240 \text{ in}$$

$$\sigma_{y3} := 50 \text{ ksi}$$

$$\sigma_{u3} := 66 \text{ ksi}$$

$$d_{\text{screwhead}} := 0.413 \text{ in}$$

$$ba := 0.584255 \quad \text{Ratio for Roark, observed from Leonardelli failure photos}$$

$$a := \frac{d_{\text{screwhead}}}{2 \cdot ba} = 0.353 \text{ in} \quad \text{Use ratio and screw diameter to find bending radius a (see Roark)}$$

Roark:

$$\alpha3 := \left[\frac{(ba - 0.5) \cdot (0.084 - 0.169)}{(0.6 - .5)} \right] + 0.169 = 0.097$$

$$\beta3 := \left[\frac{(ba - 0.5) \cdot (1.067 - 1.489)}{(0.6 - 0.5)} \right] + 1.489 = 1.133$$

$$kb := \frac{E3 \cdot t3^3}{\alpha3} \cdot RPS_{\text{factor}} = 6.281 \text{ k-in/rad} \quad \text{Yield Stiffness}$$

$$M_{p3} := \frac{\sigma_{y3} \cdot a \cdot t3^2}{\beta3} \cdot RPS_{\text{factor}} = 0.01347 \text{ k-in} \quad \text{Yield Moment}$$

$$M := M_p$$

Material Nonlinearity:

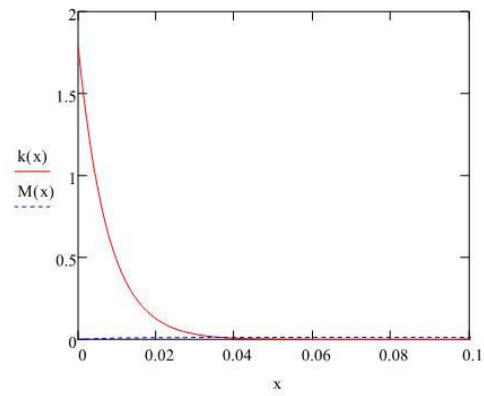
$$x := 0, .001 \dots 10$$

$$a3 := \frac{kb}{M} \quad \text{Exponential term used in equation below}$$

$$k(x) := EPF \cdot kb \cdot e^{-a3 \cdot x \cdot EPF} \quad \text{Stiffness - see paper for derivation}$$

$$M(x) := \left(\frac{-kb \cdot e^{-a3 \cdot x \cdot EPF}}{a3} \right) + \frac{kb}{a3} \quad \text{Moment capacity - see paper for derivation}$$

$$M(100) = 0.01347 \text{ k-in} \quad \text{Yield moment check, should match value M}$$



$k(U_4) = 1.79$ Stiffness at zero rotation/displacement

Element Stiffness Matrix:

$$k3 := \begin{pmatrix} kb & -kb \\ -kb & kb \end{pmatrix} \quad LV3 := \begin{pmatrix} 4 \\ 0 \end{pmatrix}$$

Element #4-Insulation Compression StrutProperties:

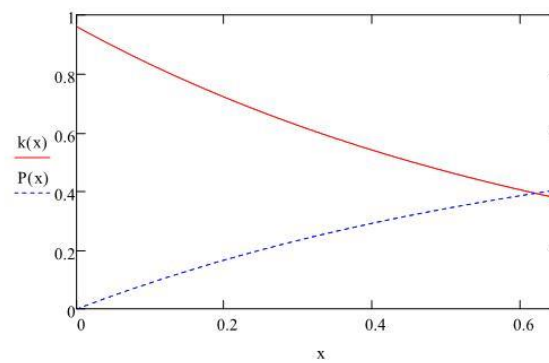
Le = insulation thickness

$$LV4 := \begin{pmatrix} 0 \\ 2 \end{pmatrix}$$

$$x := 0, .001 \dots .65$$

$$P(x) := \frac{-667 \cdot Le \cdot e^{-13 \cdot x \cdot 60} + 667 \cdot Le}{1000 Le^{0.85}}$$

$$k(x) := \frac{d}{dx} P(x) \rightarrow 0.96048 \cdot e^{-1.44 \cdot x}$$



Initial Displacement

ndof := 4

ndof tells the programmed equations how many free DOFs there are.

$$U := \begin{pmatrix} 0 \\ 0 \\ 0.74 \\ 0 \end{pmatrix}$$

First Iteration**Element #1**

u1 := Elem_Disp(U, LV1)
 fe1 := Elem_Forces1(u1, ka, a1, EPF)
 K1 := Stiffness1(u1, ka, a1, EPF)

Element #2

u2 := Elem_Disp(U, LV2)
 fe2 := Elem_Forces2(u2, Le, E2, A2, I2)
 K2 := Stiffness2(u2, Le, k2)

Element #3

u3 := Elem_Disp(U, LV3)
 fe3 := Elem_Forces3(u3, kb, a3, EPF)
 K3 := Stiffness3(u3, kb, a3, EPF)

Element #4

u4 := Elem_Disp(U, LV4)
 fe4 := Elem_Forces4(u4, Le, t3)
 K4 := Stiffness4(u4, Le, t3)

$$\Sigma fe := \begin{pmatrix} fe1_2 + fe2_3 \\ fe2_4 + fe4_2 \\ fe2_6 + fe3_1 \end{pmatrix} = \begin{pmatrix} -7.213 \\ 155.487 \\ -7.213 \end{pmatrix}$$

F := fe2_5 = 133.008

$\Delta P := -\Sigma fe$

K := Zero_Matrix(ndof, ndof)

K := Assem_Matrix(K, K1, LV1)

K := Assem_Matrix(K, K2, LV2)

K := Assem_Matrix(K, K3, LV3)

K := Assem_Matrix(K, K4, LV4)

$K_m := K_{mod}(K)$

$$\Delta U := K_m^{-1} \cdot \Delta P$$

$$\Delta U_m := \Delta U_{\text{mod}}(\Delta U)$$

$$U := U + \Delta U_m = \begin{pmatrix} 0.203 \\ -0.297 \\ 0.74 \\ 0.904 \end{pmatrix}$$

$$\text{err1} := \frac{\sqrt{\Delta P \cdot \Delta P}}{\sqrt{F \cdot F}} = 1.172$$

$$\text{err2} := \frac{\Delta P_1 \cdot U_1 + \Delta P_2 \cdot U_2 + \Delta P_3 \cdot U_4}{F \cdot U_3} = 0$$

Second Iteration

Element #1

u1 := Elem_Disp(U, LV1)
 fe1 := Elem_Forces1(u1, ka, a1, EPF)
 K1 := Stiffness1(u1, ka, a1, EPF)

Element #2

u2 := Elem_Disp(U, LV2)
 fe2 := Elem_Forces2(u2, Le, E2, A2, I2)
 K2 := Stiffness2(u2, Le, k2)

Element #3

u3 := Elem_Disp(U, LV3)
 fe3 := Elem_Forces3(u3, kb, a3, EPF)
 K3 := Stiffness3(u3, kb, a3, EPF)

Element #4

u4 := Elem_Disp(U, LV4)
 fe4 := Elem_Forces4(u4, Le, t3)
 K4 := Stiffness4(u4, Le, t3)

$$\Sigma fe := \begin{pmatrix} fe1_2 + fe2_3 \\ fe2_4 + fe4_2 \\ fe2_6 + fe3_1 \end{pmatrix} = \begin{pmatrix} -4.217 \\ 7.642 \\ -1.574 \end{pmatrix}$$

$$F := fe2_5 = 16.733$$

$$\Delta P := -\Sigma fe$$

$$K := \text{Zero_Matrix}(\text{ndof}, \text{ndof})$$

$$K := \text{Assem_Matrix}(K, K1, LV1)$$

$$K := \text{Assem_Matrix}(K, K2, LV2)$$

$$K := \text{Assem_Matrix}(K, K3, LV3)$$

$$K := \text{Assem_Matrix}(K, K4, LV4)$$

$$K_m := K_{\text{mod}}(K)$$

$$\underline{\Delta U} := K_m^{-1} \cdot \Delta P$$

$$\Delta U_m := \Delta U_{\text{mod}}(\Delta U)$$

$$U := U + \Delta U_m = \begin{pmatrix} 0.831 \\ -0.326 \\ 0.74 \\ 0.831 \end{pmatrix}$$

$$\underline{\text{err1}} := \frac{\sqrt{\Delta P \cdot \Delta P}}{\sqrt{F \cdot F}} = 0.53$$

$$\underline{\text{err2}} := \frac{\Delta P_1 \cdot U_1 + \Delta P_2 \cdot U_2 + \Delta P_3 \cdot U_4}{F \cdot U_3} = 0.367$$

Third Iteration

Element #1

$$u1 := \text{Elem_Disp}(U, LV1)$$

$$fe1 := \text{Elem_Forces1}(u1, ka, a1, EPF)$$

$$K1 := \text{Stiffness1}(u1, ka, a1, EPF)$$

Element #2

$$u2 := \text{Elem_Disp}(U, LV2)$$

$$fe2 := \text{Elem_Forces2}(u2, Le, E2, A2, I2)$$

$$\underline{K2} := \text{Stiffness2}(u2, Le, k2)$$

Element #3

$$u3 := \text{Elem_Disp}(U, LV3)$$

$$fe3 := \text{Elem_Forces3}(u3, kb, a3, EPF)$$

$$K3 := \text{Stiffness3}(u3, kb, a3, EPF)$$

Element #4

$$u4 := \text{Elem_Disp}(U, LV4)$$

$$fe4 := \text{Elem_Forces4}(u4, Le, t3)$$

$$K4 := \text{Stiffness4}(u4, Le, t3)$$

$$\Sigma fc := \begin{pmatrix} fe1_2 + fe2_3 \\ fe2_4 + fe4_2 \\ fe2_6 + fe3_1 \end{pmatrix} = \begin{pmatrix} 1.533 \times 10^{-4} \\ 0.125 \\ 1.533 \times 10^{-4} \end{pmatrix}$$

$$\underline{F} := fe2_5 = 0.456$$

$$\underline{\Delta P} := -\Sigma fc$$

$$K := \text{Zero_Matrix}(\text{ndof}, \text{ndof})$$

$$K := \text{Assem_Matrix}(K, K1, LV1)$$

$$K := \text{Assem_Matrix}(K, K2, LV2)$$

$$K := \text{Assem_Matrix}(K, K3, LV3)$$

$$K := \text{Assem_Matrix}(K, K4, LV4)$$

$$K_m := K_{\text{mod}}(K)$$

$$\Delta U_m := K_m^{-1} \cdot \Delta P$$

$$\Delta U_m := \Delta U_{\text{mod}}(\Delta U)$$

$$U := U + \Delta U_m = \begin{pmatrix} 0.831 \\ -0.327 \\ 0.74 \\ 0.832 \end{pmatrix}$$

$$\text{err1} := \frac{\sqrt{\Delta P \cdot \Delta P}}{\sqrt{F \cdot F}} = 0.274$$

$$\text{err2} := \frac{\Delta P_1 \cdot U_1 + \Delta P_2 \cdot U_2 + \Delta P_3 \cdot U_4}{F \cdot U_3} = 0.12$$

Fourth Iteration

Element #1

```
u1 := Elem_Disp(U, LV1)
fe1 := Elem_Forces1(u1, ka, a1, EPF)
K1 := Stiffness1(u1, ka, a1, EPF)
```

Element #2

```
u2 := Elem_Disp(U, LV2)
fe2 := Elem_Forces2(u2, Le, E2, A2, I2)
K2 := Stiffness2(u2, Le, k2)
```

Element #3

```
u3 := Elem_Disp(U, LV3)
fe3 := Elem_Forces3(u3, kb, a3, EPF)
K3 := Stiffness3(u3, kb, a3, EPF)
```

Element #4

```
u4 := Elem_Disp(U, LV4)
fe4 := Elem_Forces4(u4, Le, t3)
K4 := Stiffness4(u4, Le, t3)
```

$$\Sigma fe := \begin{pmatrix} fe1_2 + fe2_3 \\ fe2_4 + fe4_2 \\ fe2_6 + fe3_1 \end{pmatrix} = \begin{pmatrix} 1.331 \times 10^{-6} \\ -5.904 \times 10^{-5} \\ 1.331 \times 10^{-6} \end{pmatrix}$$

$$F := fe2_5 = 0.32$$

$$\Delta P := -\Sigma fe$$

```
K := Zero_Matrix(ndof, ndof)
```

```
K := Assem_Matrix(K, K1, LV1)
```

```
K := Assem_Matrix(K, K2, LV2)
```

```
K := Assem_Matrix(K, K3, LV3)
```

```
K := Assem_Matrix(K, K4, LV4)
```

$$K_m := K_{\text{mod}}(K)$$

$$\Delta U_m := K_m^{-1} \cdot \Delta P$$

$$\Delta U_m := \Delta U_{\text{mod}}(\Delta U)$$

$$U := U + \Delta U_m = \begin{pmatrix} 0.831 \\ -0.327 \\ 0.74 \\ 0.832 \end{pmatrix}$$

$$\text{err1} := \frac{\sqrt{\Delta P \cdot \Delta P}}{\sqrt{F \cdot F}} = 1.847 \times 10^{-4}$$

$$\text{err2} := \frac{\Delta P_1 \cdot U_1 + \Delta P_2 \cdot U_2 + \Delta P_3 \cdot U_4}{F \cdot U_3} = -9.084 \times 10^{-5}$$

Fifth Iteration

Element #1

$$u1 := \text{Elem_Disp}(U, LV1)$$

$$fe1 := \text{Elem_Forces1}(u1, ka, a1, EPF)$$

$$K1 := \text{Stiffness1}(u1, ka, a1, EPF)$$

Element #2

$$u2 := \text{Elem_Disp}(U, LV2)$$

$$fe2 := \text{Elem_Forces2}(u2, Le, E2, A2, I2)$$

$$K2 := \text{Stiffness2}(u2, Le, k2)$$

Element #3

$$u3 := \text{Elem_Disp}(U, LV3)$$

$$fe3 := \text{Elem_Forces3}(u3, kb, a3, EPF)$$

$$K3 := \text{Stiffness3}(u3, kb, a3, EPF)$$

Element #4

$$u4 := \text{Elem_Disp}(U, LV4)$$

$$fe4 := \text{Elem_Forces4}(u4, Le, t3)$$

$$K4 := \text{Stiffness4}(u4, Le, t3)$$

$$\Sigma fe := \begin{pmatrix} fe1_2 + fe2_3 \\ fe2_4 + fe4_2 \\ fe2_6 + fe3_1 \end{pmatrix} = \begin{pmatrix} -6.519 \times 10^{-10} \\ 3.707 \times 10^{-8} \\ -6.519 \times 10^{-10} \end{pmatrix}$$

$$F := fe2_5 = 0.32$$

$$\Delta P := -\Sigma fe$$

$$K := \text{Zero_Matrix}(\text{ndof}, \text{ndof})$$

$$K := \text{Assem_Matrix}(K, K1, LV1)$$

$$K := \text{Assem_Matrix}(K, K2, LV2)$$

$$K := \text{Assem_Matrix}(K, K3, LV3)$$

$$K := \text{Assem_Matrix}(K, K4, LV4)$$

$$\begin{aligned}
 K_m &:= K_{\text{mod}}(K) \\
 \Delta U_m &:= K_m^{-1} \cdot \Delta P \\
 \Delta U_m &:= \Delta U_{\text{mod}}(\Delta U) \\
 U &:= U + \Delta U_m = \begin{pmatrix} 0.831 \\ -0.327 \\ 0.74 \\ 0.832 \end{pmatrix}
 \end{aligned}
 \qquad
 \begin{aligned}
 \text{err1} &:= \frac{\sqrt{\Delta P \cdot \Delta P}}{\sqrt{F \cdot F}} = 1.159 \times 10^{-7} \\
 \text{err2} &:= \frac{\Delta P_1 \cdot U_1 + \Delta P_2 \cdot U_2 + \Delta P_3 \cdot U_4}{F \cdot U_3} = 5.573 \times 10^{-8}
 \end{aligned}$$

Sixth Iteration

Element #1

$u1 := \text{Elem_Disp}(U, LV1)$
 $fe1 := \text{Elem_Forces1}(u1, ka, a1, EPF)$
 $K1 := \text{Stiffness1}(u1, ka, a1, EPF)$

Element #2

$u2 := \text{Elem_Disp}(U, LV2)$
 $fe2 := \text{Elem_Forces2}(u2, Le, E2, A2, I2)$
 $K2 := \text{Stiffness2}(u2, Le, k2)$

Element #3

$u3 := \text{Elem_Disp}(U, LV3)$
 $fe3 := \text{Elem_Forces3}(u3, kb, a3, EPF)$
 $K3 := \text{Stiffness3}(u3, kb, a3, EPF)$

Element #4

$u4 := \text{Elem_Disp}(U, LV4)$
 $fe4 := \text{Elem_Forces4}(u4, Le, t3)$
 $K4 := \text{Stiffness4}(u4, Le, t3)$

$$\Sigma fe := \begin{pmatrix} fe1_2 + fe2_3 \\ fe2_4 + fe4_2 \\ fe2_6 + fe3_1 \end{pmatrix} = \begin{pmatrix} 4.056 \times 10^{-13} \\ -2.311 \times 10^{-11} \\ 4.056 \times 10^{-13} \end{pmatrix}$$

$$F_s := fe2_5 = 0.32$$

$$\Delta P_s := -\Sigma fe$$

$$K := \text{Zero_Matrix}(\text{ndof}, \text{ndof})$$

$$K := \text{Assem_Matrix}(K, K1, LV1)$$

$$K := \text{Assem_Matrix}(K, K2, LV2)$$

$$K := \text{Assem_Matrix}(K, K3, LV3)$$

$$K := \text{Assem_Matrix}(K, K4, LV4)$$

$$K_m := K_{\text{mod}}(K)$$

$$\Delta U := K_m^{-1} \cdot \Delta P$$

$$\Delta U_m := \Delta U_{\text{mod}}(\Delta U)$$

$$U := U + \Delta U_m = \begin{pmatrix} 0.831 \\ -0.327 \\ 0.74 \\ 0.832 \end{pmatrix}$$

$$\text{err1} := \frac{\sqrt{\Delta P \cdot \Delta P}}{\sqrt{F \cdot F}} = 7.226 \times 10^{-11}$$

$$\text{err2} := \frac{\Delta P_1 \cdot U_1 + \Delta P_2 \cdot U_2 + \Delta P_3 \cdot U_4}{F \cdot U_3} = -3.474 \times 10^{-11}$$

Failure Prediction Equations

Tension + Bending

$$u2 := \text{Elem_Disp}(U, LV2)$$

$$fe2 := \text{Elem_Forces2}(u2, Le, E2, A2, I2)$$

$$fe2_L := \text{Local_Forces2}(u2, Le, E2, A2, I2)$$

$$\text{ScrewForce} := fe2_{L_4} = 0.405 \quad \text{k}$$

$$\text{ScrewShear} := fe2_{L_5} = 0.03 \quad \text{k}$$

$$\text{GlobalTension} := fe2_4 = 0.25 \quad \text{k}$$

$$\text{GlobalShear} := fe2_5 = 0.32 \quad \text{k}$$

$$\text{ScrewMoment} := \max(|fe2_3|, |fe2_6|) = 0.017 \quad \text{k-in}$$

$$y2 := \frac{d_{\text{screw}}}{2} = 0.095 \quad \text{in}$$

$$\sigma_{\text{screw}} := \frac{\text{ScrewForce}}{A2} + \frac{\text{ScrewMoment} \cdot y2}{I2} = 39.099 \quad \text{ksi}$$

$$\sigma_{\text{allow}} := \frac{P_{\text{ScrewAllow}}}{1000 \cdot A2} = 86.587 \quad \text{ksi}$$

$$\text{ScrewCheck} := \begin{cases} \text{"Fail"} & \text{if } \sigma_{\text{allow}} < \sigma_{\text{screw}} \\ \text{"OK"} & \text{otherwise} \end{cases}$$

$$\text{ScrewCheck} = \text{"OK"}$$

AISI Limit Equations

$$t_1 := t3 = 0.024 \quad \text{in} \quad F_{u1} := \sigma_{u3} = 66 \quad \text{ksi}$$

$$t_2 := t1 = 0.045 \quad \text{in} \quad F_{u2} := \sigma_{u1} = 45 \quad \text{ksi}$$

$$\frac{t_2}{t_1} = 1.879$$

Combined Shear and Pullover

$$T := \text{GlobalTension}$$

$$V := \text{GlobalShear}$$

$$P_{nv} := 2.7 \cdot t_1 \cdot d_{\text{screw}} \cdot F_{u1} = 0.813 \quad \text{k} \quad \text{Nominal shear strength (E4.5.1)}$$

$$P_{nov} := 1.5 \cdot t_1 \cdot d_{\text{screwhead}} \cdot F_{u1} = 0.981 \quad \text{k} \quad \text{Nominal pull-over strength (E4.5.1)}$$

$$\text{Interaction} := \frac{V}{P_{nv}} + \frac{0.71 \cdot T}{P_{nov}} = 0.575$$

$$\text{Pullover} := \begin{cases} \text{"Fail"} & \text{if } \text{Interaction} > 1.1 \\ \text{"OK"} & \text{otherwise} \end{cases}$$

$$\text{Pullover} = \text{"OK"}$$

Combined Shear and Pullout

$$P_{nv} := 4.2 \cdot \left(t_2^3 \cdot d_{\text{screw}} \right)^{\frac{1}{2}} \cdot F_{u2} = 0.789 \quad \text{k} \quad \text{Nominal shear strength (E4.5.2)}$$

$$P_{nov} := 0.85 \cdot t_2 \cdot d_{\text{screw}} \cdot F_{u2} = 0.328 \quad \text{k} \quad \text{Nominal pull-over strength (E4.5.1)}$$

$$\text{Interaction} := \frac{V}{P_{nv}} + \frac{T}{P_{nov}} = 1.169$$

$$\text{Pullout} := \begin{cases} \text{"Fail"} & \text{if Interaction} > 1.15 \\ \text{"OK"} & \text{otherwise} \end{cases}$$

Pullout = "Fail"

Combined Shear and Tension

$$P_{nts} := \frac{P_{\text{ScrewAllow}}}{1000} = 2.455 \quad \text{k} \quad \text{Screw tension strength (E4.5.3)}$$

$$P_{nvs} := \frac{V_{\text{ScrewAllow}}}{1000} = 1.91 \quad \text{k} \quad \text{Screw shear strength (E4.5.3)}$$

$$\text{Interaction} := \frac{\text{ScrewShear}}{P_{nvs}} + \frac{\text{ScrewForce}}{P_{nts}} = 0.181$$

$$\text{Combined} := \begin{cases} \text{"Fail"} & \text{if Interaction} > 1.3 \\ \text{"OK"} & \text{otherwise} \end{cases}$$

Pullover = "OK"

Roark Ratios:Panels/Sheathing:

$$t=0.0180" \quad ba=0.584255$$

$$t=0.0565" \quad ba=0.452125$$

Studs:

$$t=0.0451" \quad ba=0.659031$$

$$t=0.0713" \quad ba=0.668559$$

$$t=0.1017" \quad ba=0.712415$$

Screw Shear Strengths:

$$\#10 \quad 1910 \text{ lbs}$$

$$\#12 \quad 2814 \text{ lbs}$$

$$\#14 \quad 4000 \text{ lbs}$$

Screw Tension Strengths:

$$\#10 \quad 2455 \text{ lbs}$$

$$\#12 \quad 2534 \text{ lbs}$$

$$\#14 \quad 3658 \text{ lbs}$$

Programmed Functions

This function is used to transform a local element matrix into global coordinates

$$\text{Rot}(C, S) \equiv \begin{pmatrix} C & S & 0 & 0 & 0 & 0 \\ -S & C & 0 & 0 & 0 & 0 \\ 0 & 0 & 1 & 0 & 0 & 0 \\ 0 & 0 & 0 & C & S & 0 \\ 0 & 0 & 0 & -S & C & 0 \\ 0 & 0 & 0 & 0 & 0 & 1 \end{pmatrix}$$

This function is used for the screw element matrix. It is a beam-column stiffness matrix.

$$\text{Beam_2D}(E, A, I, L) \equiv \begin{pmatrix} \frac{A \cdot E}{L} & 0 & 0 & -\frac{A \cdot E}{L} & 0 & 0 \\ 0 & \frac{12 \cdot E \cdot I}{L^3} & \frac{6 \cdot E \cdot I}{L^2} & 0 & -\frac{12 \cdot E \cdot I}{L^3} & \frac{6 \cdot E \cdot I}{L^2} \\ 0 & \frac{6 \cdot E \cdot I}{L^2} & \frac{4 \cdot E \cdot I}{L} & 0 & -\frac{6 \cdot E \cdot I}{L^2} & \frac{2 \cdot E \cdot I}{L} \\ -\frac{A \cdot E}{L} & 0 & 0 & \frac{A \cdot E}{L} & 0 & 0 \\ 0 & -\frac{12 \cdot E \cdot I}{L^3} & \frac{6 \cdot E \cdot I}{L^2} & 0 & \frac{12 \cdot E \cdot I}{L^3} & -\frac{6 \cdot E \cdot I}{L^2} \\ 0 & \frac{6 \cdot E \cdot I}{L^2} & \frac{2 \cdot E \cdot I}{L} & 0 & -\frac{6 \cdot E \cdot I}{L^2} & \frac{4 \cdot E \cdot I}{L} \end{pmatrix}$$

The function below creates a $n \times n$ zero matrix. It is the first step used when assembling the element matrices into the global stiffness matrix.

$$\text{Zero_Matrix}(\text{nrow}, \text{ncol}) \equiv \begin{cases} \text{for } i \in 1.. \text{nrow} \\ \quad \text{for } j \in 1.. \text{ncol} \\ \quad \quad z_{i,j} \leftarrow 0 \end{cases}$$

This function assembles the global stiffness matrix. The LV terms are the location vectors which eliminate the supports and leave only the free DOFs in the matrix.

$$\text{Assem_Matrix}(K, \text{keg}, \text{LV}) \equiv \left| \begin{array}{l} \text{for } ie \in 1 \dots \text{rows}(\text{keg}) \\ \quad \text{for } je \in 1 \dots \text{cols}(\text{keg}) \\ \quad \quad \text{if } (LV_{ie} \neq 0) \cdot (LV_{je} \neq 0) \\ \quad \quad \quad i \leftarrow LV_{ie} \\ \quad \quad \quad j \leftarrow LV_{je} \\ \quad \quad \quad K_{i,j} \leftarrow K_{i,j} + \text{keg}_{ie,je} \end{array} \right| K$$

The function below gives element displacements based on the element's location vector.

$$\text{Elem_Disp}(u, \text{LV}) \equiv \left| \begin{array}{l} \text{for } ie \in 1 \dots \text{length}(\text{LV}) \\ \quad \text{if } (LV_{ie} \neq 0) \\ \quad \quad ig \leftarrow LV_{ie} \\ \quad \quad v_{ie} \leftarrow u_{ig} \\ \quad v_{ie} \leftarrow 0 \text{ otherwise} \end{array} \right| v$$

The next four functions find the element forces in each iteration. To find the element forces the function use the geometric and material nonlinearities.

$$\text{Elem_ForcesI}(u, k, a, \text{EPF}) \equiv \left| \begin{array}{l} \beta \leftarrow 0 \\ \alpha \leftarrow 0 \\ \theta 1 \leftarrow u_1 \\ \Delta \theta 1 \leftarrow \theta 1 - \alpha \\ \theta 2 \leftarrow u_2 \\ \Delta \theta 2 \leftarrow \theta 2 - \alpha \\ ue \leftarrow \begin{pmatrix} \Delta \theta 1 \\ \Delta \theta 2 \end{pmatrix} \\ M_n \leftarrow \frac{-k}{a} \cdot e^{-a \cdot |ue_2|} \cdot \text{EPF} + \frac{k}{a} \\ fe \leftarrow \begin{pmatrix} 0 \\ M_n \end{pmatrix} \\ fe \leftarrow fe \end{array} \right| fe$$

$$\text{Elem_Forces2}(u, le, E, A, I) \equiv \left| \begin{array}{l} le2 \leftarrow \sqrt{(u_4 + le)^2 + (u_5)^2} \\ \beta_0 \leftarrow 0 \\ \beta_1 \leftarrow \arcsin\left(\frac{u_5}{le2}\right) \\ \alpha \leftarrow \beta_1 - \beta_0 \\ \theta_1 \leftarrow u_3 \\ \Delta\theta_1 \leftarrow \theta_1 - \alpha \\ \Delta x_1 \leftarrow 0 \\ \Delta y_1 \leftarrow 0 \\ \theta_2 \leftarrow u_6 \\ \Delta\theta_2 \leftarrow \theta_2 - \alpha \\ \Delta x_2 \leftarrow le2 - le \\ \Delta y_2 \leftarrow 0 \\ ue \leftarrow \begin{pmatrix} \Delta x_1 \\ \Delta y_1 \\ \Delta\theta_1 \\ \Delta x_2 \\ \Delta y_2 \\ \Delta\theta_2 \end{pmatrix} \\ T \leftarrow \begin{pmatrix} \cos(\beta_1) & \sin(\beta_1) & 0 & 0 & 0 & 0 \\ -\sin(\beta_1) & \cos(\beta_1) & 0 & 0 & 0 & 0 \\ 0 & 0 & 1 & 0 & 0 & 0 \\ 0 & 0 & 0 & \cos(\beta_1) & \sin(\beta_1) & 0 \\ 0 & 0 & 0 & -\sin(\beta_1) & \cos(\beta_1) & 0 \\ 0 & 0 & 0 & 0 & 0 & 1 \end{pmatrix} \\ ke \leftarrow \begin{pmatrix} \frac{A \cdot E}{le} & 0 & 0 & \frac{-A \cdot E}{le} & 0 & 0 \\ 0 & \frac{12 \cdot E \cdot I}{le} & \frac{6 \cdot E \cdot I}{le^2} & 0 & \frac{-12 \cdot E \cdot I}{le^3} & \frac{6 \cdot E \cdot I}{le^2} \\ 0 & \frac{6 \cdot E \cdot I}{le^2} & \frac{4 \cdot E \cdot I}{le} & 0 & \frac{-6 \cdot E \cdot I}{le^2} & \frac{2 \cdot E \cdot I}{le} \\ \frac{-A \cdot E}{le} & 0 & 0 & \frac{A \cdot E}{le} & 0 & 0 \\ 0 & \frac{-12 \cdot E \cdot I}{le^3} & \frac{-6 \cdot E \cdot I}{le^2} & 0 & \frac{12 \cdot E \cdot I}{le^3} & \frac{-6 \cdot E \cdot I}{le^2} \end{pmatrix} \end{array} \right|$$

$$\begin{array}{l}
 \left(\begin{array}{cccccc}
 0 & \frac{6 \cdot E \cdot I}{l_e^2} & \frac{2 \cdot E \cdot I}{l_e} & 0 & \frac{-6 \cdot E \cdot I}{l_e^2} & \frac{4 \cdot E \cdot I}{l_e}
 \end{array} \right) \\
 f_e \leftarrow k_e \cdot u_e \\
 f_e \leftarrow T^T \cdot f_e \\
 f_e
 \end{array}$$

$$\begin{array}{l}
 \text{Elem_Forces3}(u, k, a, EPF) \equiv \begin{array}{l}
 \beta \leftarrow 0 \\
 \alpha \leftarrow 0 \\
 \theta_1 \leftarrow u_1 \\
 \Delta\theta_1 \leftarrow \theta_1 - \alpha \\
 \theta_2 \leftarrow u_2 \\
 \Delta\theta_2 \leftarrow \theta_2 - \alpha \\
 u_e \leftarrow \begin{pmatrix} \Delta\theta_1 \\ \Delta\theta_2 \end{pmatrix} \\
 M_n \leftarrow \frac{-k}{a} \cdot e^{-a \cdot |u_{e1}|} \cdot EPF + \frac{k}{a} \\
 f_e \leftarrow \begin{pmatrix} M_n \\ 0 \end{pmatrix} \\
 f_e \leftarrow f_e \\
 f_e
 \end{array}
 \end{array}$$

$$\begin{array}{l}
 \text{Elem_Forces4}(u, l_e, t) \equiv \begin{array}{l}
 l_{e2} \leftarrow \sqrt{(u_2 + l_e - u_1)^2} \\
 \beta_o \leftarrow 0 \\
 \alpha \leftarrow 0 \\
 \Delta x_1 \leftarrow 0 \\
 \Delta x_2 \leftarrow l_{e2} - l_e \\
 u_e \leftarrow \begin{pmatrix} \Delta x_1 \\ \Delta x_2 \end{pmatrix} \\
 P_c \leftarrow \frac{-667 \cdot l_e \cdot e^{-t \cdot |u_{e2}|} \cdot 60 + 667 \cdot l_e}{1000(l_e^{0.85})} \\
 f_e \leftarrow \begin{pmatrix} P_c \\ -P_c \end{pmatrix} \\
 f_e
 \end{array}
 \end{array}$$

The next four functions find the element stiffness matrices at each iteration. The transformation matrix is built into the functions where needed. Geometric and material nonlinearity are also used in these equations.

$$\text{Stiffness1}(u, k, a, \text{EPF}) \equiv \left| \begin{array}{l} \beta \leftarrow 0 \\ \alpha \leftarrow 0 \\ \theta 1 \leftarrow u_1 \\ \Delta \theta 1 \leftarrow \theta 1 - \alpha \\ \theta 2 \leftarrow u_2 \\ \Delta \theta 2 \leftarrow \theta 2 - \alpha \\ u_e \leftarrow \begin{pmatrix} \Delta \theta 1 \\ \Delta \theta 2 \end{pmatrix} \\ k_n \leftarrow \text{EPF} \cdot k \cdot e^{-a \cdot |u_{e2}|} \cdot \text{EPF} \\ k_e \leftarrow \begin{pmatrix} k_n & -k_n \\ -k_n & k_n \end{pmatrix} \\ K \leftarrow k_e \\ K \end{array} \right|$$

$$\text{Stiffness2}(u, l_e, k_e) \equiv \left| \begin{array}{l} l_{e2} \leftarrow \sqrt{(u_4 + l_e)^2 + (u_5)^2} \\ \beta 1 \leftarrow \text{asin}\left(\frac{u_5}{l_{e2}}\right) \\ T \leftarrow \begin{pmatrix} \cos(\beta 1) & \sin(\beta 1) & 0 & 0 & 0 & 0 \\ -\sin(\beta 1) & \cos(\beta 1) & 0 & 0 & 0 & 0 \\ 0 & 0 & 1 & 0 & 0 & 0 \\ 0 & 0 & 0 & \cos(\beta 1) & \sin(\beta 1) & 0 \\ 0 & 0 & 0 & -\sin(\beta 1) & \cos(\beta 1) & 0 \\ 0 & 0 & 0 & 0 & 0 & 1 \end{pmatrix} \\ K \leftarrow T^T \cdot k_e \cdot T \\ K \end{array} \right|$$

$$\text{Stiffness3}(u, k, a, \text{EPF}) \equiv \left| \begin{array}{l} \beta \leftarrow 0 \\ \alpha \leftarrow 0 \\ \theta 1 \leftarrow u_1 \\ \Delta \theta 1 \leftarrow \theta 1 - \alpha \\ \theta 2 \leftarrow u_2 \\ \Delta \theta 2 \leftarrow \theta 2 - \alpha \\ \text{ue} \leftarrow \begin{pmatrix} \Delta \theta 1 \\ \Delta \theta 2 \end{pmatrix} \\ k_n \leftarrow \text{EPF} \cdot k \cdot e^{-a \cdot |\text{ue}_1|} \cdot \text{EPF} \\ k_e \leftarrow \begin{pmatrix} k_n & -k_n \\ -k_n & k_n \end{pmatrix} \\ K \leftarrow k_e \\ K \end{array} \right|$$

$$\text{Stiffness4}(u, l_e, t) \equiv \left| \begin{array}{l} l_e 2 \leftarrow \sqrt{(u_2 + l_e - u_1)^2} \\ \beta_0 \leftarrow 0 \\ \alpha \leftarrow 0 \\ \Delta x 1 \leftarrow 0 \\ \Delta x 2 \leftarrow l_e 2 - l_e \\ \text{ue} \leftarrow \begin{pmatrix} \Delta x 1 \\ \Delta x 2 \end{pmatrix} \\ k_c \leftarrow \frac{667 \cdot l_e \cdot 60 \cdot t \cdot e^{-t \cdot |\text{ue}_2|} \cdot 60}{1000(l_e^{0.85})} \\ k_e \leftarrow \begin{pmatrix} k_c & -k_c \\ -k_c & k_c \end{pmatrix} \\ K \leftarrow k_e \\ K \end{array} \right|$$

The next two functions are used to reduce the nonzero displacement DOF that is being treated as a support out of the analysis.

$$K_{\text{mod}}(K) \equiv \left| \begin{array}{c} K_{\text{mod}} \leftarrow \begin{pmatrix} K_{1,1} & K_{1,2} & K_{1,4} \\ K_{2,1} & K_{2,2} & K_{2,4} \\ K_{4,1} & K_{4,2} & K_{4,4} \end{pmatrix} \\ K_{\text{mod}} \end{array} \right|$$

$$\Delta U_{\text{mod}}(\Delta U) \equiv \left| \begin{array}{c} \Delta U_{\text{mod}} \leftarrow \begin{pmatrix} \Delta U_1 \\ \Delta U_2 \\ 0 \\ \Delta U_3 \end{pmatrix} \\ \Delta U_{\text{mod}} \end{array} \right|$$

The final function is used in the failure prediction calculations. It finds the element forces of the screw in local coordinates.

$$\text{Local_Forces2}(u, lc, E, A, I) \equiv \left| \begin{array}{l} lc2 \leftarrow \sqrt{(u_4 + lc)^2 + (u_5)^2} \\ \beta_0 \leftarrow 0 \\ \beta_1 \leftarrow \arcsin\left(\frac{u_5}{lc2}\right) \\ \alpha \leftarrow \beta_1 - \beta_0 \\ \theta_1 \leftarrow u_3 \\ \Delta\theta_1 \leftarrow \theta_1 - \alpha \\ \Delta x_1 \leftarrow 0 \\ \Delta y_1 \leftarrow 0 \\ \theta_2 \leftarrow u_6 \\ \Delta\theta_2 \leftarrow \theta_2 - \alpha \\ \Delta x_2 \leftarrow lc2 - lc \\ \Delta y_2 \leftarrow 0 \\ ue \leftarrow \begin{pmatrix} \Delta x_1 \\ \Delta y_1 \\ \Delta\theta_1 \\ \Delta x_2 \\ \Delta y_2 \end{pmatrix} \end{array} \right|$$

$$\begin{aligned}
 & \left(\Delta \theta_2 \right) \\
 T \leftarrow & \begin{pmatrix} \cos(\beta_1) & \sin(\beta_1) & 0 & 0 & 0 & 0 \\ -\sin(\beta_1) & \cos(\beta_1) & 0 & 0 & 0 & 0 \\ 0 & 0 & 1 & 0 & 0 & 0 \\ 0 & 0 & 0 & \cos(\beta_1) & \sin(\beta_1) & 0 \\ 0 & 0 & 0 & -\sin(\beta_1) & \cos(\beta_1) & 0 \\ 0 & 0 & 0 & 0 & 0 & 1 \end{pmatrix} \\
 ke \leftarrow & \begin{pmatrix} \frac{A \cdot E}{le} & 0 & 0 & \frac{-A \cdot E}{le} & 0 & 0 \\ 0 & \frac{12 \cdot E \cdot I}{le} & \frac{6 \cdot E \cdot I}{le^2} & 0 & \frac{-12 \cdot E \cdot I}{le^3} & \frac{6 \cdot E \cdot I}{le^2} \\ 0 & \frac{6 \cdot E \cdot I}{le^2} & \frac{4 \cdot E \cdot I}{le} & 0 & \frac{-6 \cdot E \cdot I}{le^2} & \frac{2 \cdot E \cdot I}{le} \\ \frac{-A \cdot E}{le} & 0 & 0 & \frac{A \cdot E}{le} & 0 & 0 \\ 0 & \frac{-12 \cdot E \cdot I}{le^3} & \frac{-6 \cdot E \cdot I}{le^2} & 0 & \frac{12 \cdot E \cdot I}{le^3} & \frac{-6 \cdot E \cdot I}{le^2} \\ 0 & \frac{6 \cdot E \cdot I}{le^2} & \frac{2 \cdot E \cdot I}{le} & 0 & \frac{-6 \cdot E \cdot I}{le^2} & \frac{4 \cdot E \cdot I}{le} \end{pmatrix} \\
 & fe \leftarrow ke \cdot ue \\
 & fe \leftarrow fe \\
 & fe
 \end{aligned}$$

Structural Engineering**Capstone Report Approval Form****Master of Science in Structural Engineering – MSST****Milwaukee School of Engineering**

This capstone report, entitled “Modeling Cold-Formed Steel Screw Connections with an Insulation Layer Using Finite Element Analysis” submitted by the student Zane F. Witt, has been approved by the following committee:

Faculty Advisor: _____

Date: _____

Dr. Douglas Stahl

Faculty Advisor: _____

Date: _____

Dr. Hans-Peter Huttelmaier

Faculty Advisor: _____

Date: _____

Dr. Todd Davis